CONTROLLING A PASSIVE HAPTIC MASTER DURING BILATERAL TELEOPERATION

A Dissertation
Presented to
The Academic Faculty

by

Benjamin Andrew Black

In Partial Fulfillment
of the Requirements for the Degree
Doctor of Philosophy in the
G.W. Woodruff School of Mechanical Engineering

Georgia Institute of Technology
December 2007

CONTROLLING A PASSIVE HAPTIC MASTER DURING BILATERAL TELEOPERATION

Approved by:

Professor Wayne J. Book,
Committee Chair
G.W. Woodruff School of Mechanical Engineering
Georgia Institute of Technology

Professor Julie Jacko
Biomedical Engineering
Georgia Institute of Technology

Professor Aldo A. Ferri
G.W. Woodruff School of Mechanical Engineering
Georgia Institute of Technology

Professor Lena Ting
Biomedical Engineering
Georgia Institute of Technology

Professor Kok-Meng Lee
G.W. Woodruff School of Mechanical Engineering
Georgia Institute of Technology

Dr Jeannie Falcon
Academic Relations
School of Mechanical Engineering
National Instruments
Univ. of Texas

Date Approved: August 8 2007

To Amanda, who has lovingly and patiently been my girlfriend, fiancé & wife throughout this work and without whom I wouldn't be sane,

and to my parents without the support of whom I woldn't be who I am today nor would I have found the success with which I have been blessed.

ACKNOWLEDGEMENTS

I want to thank my advisor and the rest of my committee for their help in this long process. Without their input the research would not have been possible nor successful.

I want to especially thank Dr. Jeannie Falcon and the Academic Relations group at National Instruments whose support over the past four years has made my research possible.

I would like to thank the students in the IMDL whose research in passive haptics paved the way for mine, especially Davin Swanson and Matt Reed. I would like to thank JD Huggins, Carwyn Jones, the helpful people in the machine and electronics shops and everyone else who made hardware changes run smoothly.

Finally, I would like to thank my wife, Amanda, my family and all of my friends who have been supportive of me over my four years at Georgia Institute of Technology.

TABLE OF CONTENTS

LIST OF TABLES

LIST OF FIGURES

SUMMARY

The field of haptic robotics revolves around creation and control of devices that allow a human user to physically interact with either a virtual or a remote environment. The root of the word "haptic" comes from the greek word meaning "touch," and subsequently haptic devices provide a sense of touch to the man-machine interface.

An extensive list of applications can be generated for haptic devices, including fields as far apart as surgery and video gaming. However, all of the devices allow the user to physically interact with and remotely control some physical device or environment, be it virtual or real. In that sense, the origin of all haptics can be traced back to early research in teleoperation, an academic term for "remote control." The research presented here will focus on that category of haptic use.

A natural classification of haptic devices has developed based on the energetic nature of their actuators, either "active" or "passive." Active haptic devices utilize active components that give the device the ability to add energy to the man-machine system. Conversely, passive haptic devices utilize passive actuators such as brakes, clutches or similar components that can add no energy, either keeping the energy of the man-machine system constant or dissipating it. The research presented here focuses on the use of such passive devices, specifically the ones that dissipate energy.

Dissipative passive haptic devices have a few benefits that will be explored in greater detail in the introduction and background. Briefly, they are inherently safe. The inability to add energy to the human-machine system means that the device can never become unstable. Furthermore, the device can never output more power than

the human applies to it, and without mechanical advantage the device can create no more than a reaction force to what the human applies. When in motion, the device can only provide a force to resist motion.

While guaranteeing safety, passive devices present an interesting control problem. Unlike an active device, the passive device cannot generate arbitrary forces, only forces that oppose motion (or input force in the static state). This leads to the question of how to provide haptic feedback with this inherently smaller subset of possible feedback forces.

After looking at the background of the project, the research presented here will develop the underlying the control problem and will propose three control algorithms for generating haptic forces, two relatively simple algorithms and one more complex. The final goal of the research involves human testing, however along the way to a final test of the control algorithms, the research explores some side topics. The first of these tests explores network latency within the local subnet and then extends the test to include a cross-country test, looking at both TCP/IP and UDP/IP communications protocols. The second test uses simulated human input to partially validate the controllers and actuation scehems. The final side project experimentally evaluates the human perception of force direction and shows that the subjects could resolve force no finer than 67.5 ° range.

The research culminates with a final human-factors test that explores shape identification and point-to-point motion tasks both with a passive and an active haptic device in teleopertation. The results show that with the passive device, the users were able to identify large detail of shapes nearly as well with the passive device as with the active device, while identification of finer detail was much more difficult with the passive device. Furthermore, the results show the passive device with a dynamic compensating control to perform nearly as well as the active device in point-to-point motion tasks. These results show encouraging indications that the passive device not

only can provide useful feedback but that it performs nearly as well an active device at certain tasks.

CHAPTER I

INTRODUCTION

In a very general sense, haptic devices are designed to provide a human user with the ability to physically interact with either a virtual or remote environment. The word "haptic" comes from the greek word *haphe* and refers to the sense of touch. As such a haptic robotic device augments a user's sensory feedback by providing tactile physical sensory information in the form of forces, vibrations, motions or a combination of the three.

Hayward compares the development of haptic devices to the development of the computer monitor [36]. A blank piece of paper provides very little sensory information other than the physical fact that it is a piece of paper with a fixed shape, thickness and color. When encoded with information in the form of black or colored marks, the paper can display information that is interpreted as text, language, images, ideas, etc. However a printed sheet of paper typically can display only one fixed set of information at a time. In comparison, a computer monitor encodes information no differently than a piece of paper but allows that information to be changed dynamically to represent a changing set information.

Similar to a piece of paper, a traditional computer input device such as a mouse displays little physical information to the user other than size, shape, inertia, some friction, etc. Furthermore, none of that information acts as an output from the computer. However, much like a computer monitor, a haptic devices allow the physical sensory information being returned to the user to be programmed, controlled and changed dynamically. Simple commercial haptic devices include mice that vibrate or bounce to let the user know that the cursor has rolled across an icon on the desktop or

video game controllers that vibrate to let the player know that he has been attacked or driven off the virtual road. A haptic device typically behaves as both an input and an output device, for instance allowing the user to control a cursor in a virtual environment (input) while simultaneously allowing the user to feel objects within that environment (output).

An interesting multi-modal device has been dubbed "digital clay" and acts both as a physical and visual output, changing shape to represent three-dimensional objects. However at the same time, the digital clay device also provides haptic feedback to the user allowing him to feel the physical properties of the object being displayed [88]. Haptic devices have found a long list of useful applications due primarily to the power of the sense of touch. They extend in size from micro-scale [9] to the workspace of automobile assembly [70], and their scope covers applications from surgery assistance [87][72][50] to handling of hazardous materials [69]. In a subset of the possible tasks utilizing haptic feedback, an operator can use a haptic device in teleoperation, or remote control or a second device or robot. In this, a remote, or "slave" device is controlled by a haptic "master" device. The user interacts with the remote environment through the master and the slave devices. Forces from the remote system are transmitted to the human user through the actuation of the haptic master device.

Looking specifically at classification of haptic devices, they can be categorized by the energetic nature of their actuators, either active or passive. Active devices comprise the larger portion of existing haptic interfaces and are actuated by active components such as electric motors, hydraulic or pneumatic actuators, etc. Active devices can produce a large range of forces, limited by the maximum output of their actuators as well as their kinematics; however due to their active nature, they can also potentially have stability and therefore safety issues.

A much less common group, passive haptic devices are actuated with components such a brakes, clutches or Continuously Variable Transmissions (CVTs) that either

dissipate or redirect the energy that the operator supplies to the system. Devices using CVTs redirect energy and are energetically neutral, while devices that use clutches and brakes have the ability to dissipate energy through friction and are subsequently deemed dissipative passive haptic devices [85]. Realistically all devices dissipate some energy, but dissipative passive devices control and use dissipation to produce haptic forces. All passive haptic devices share the trait that they can only redirect or dissipate a user's motion and therefore cannot generate arbitrary haptic feedback. However, unlike an active device, passive haptic devices are inherently stable and safe.

1.1 Research Overview

The research presented here begins from the standpoint that a dissipative passive haptic device must be controlled differently from its active counterpart due to its inherent differences in force generation. As compared to an active device, it can only produce a small subset of possible endpoint forces at any given time. When moving, the dissipative passive device can only produce forces that oppose the motion of the user. If the device is stopped, it can only generate a reaction force to the user.

The research further focuses on using the dissipative passive haptic device in a teleoperation scenario, producing haptic feedback based only on the knowledge of the positions of the master and slave devices. As opposed to interacting with a virtual environment, when operating in teleoperation the control system needs to be able to generate feedback without much knowledge of the remote environment. In an exploration task, the environment is completely unknown and the controller must produce haptic feedback based only on the known states of the master and slave devices. Furthermore, true teleoperation (as opposed to a virtual experiment or a simulation) involves the real details of network-based communication as well as the true dynamics of the slave device. Each of these components adds to the complexity of

the teleoperation task, yet the topic merits exploration due to the obvious important applications of teleoperation.

In a very general sense, the research attempts to answer the following three central questions:

- Can a passive haptic device produce usable feedback when used in teleoperation?
- Does the passive haptic device provide as effective feedback as an active device in teleoperation?
- In what tasks do the differences between the feedback provided by the passive and active devices become negligible?

To answer these questions requires a true human-factors test comparing the performance of subjects using both an active and a passive haptic device. However, along the path to the end goal, three mini-projects developed that helped to shape the final control algorithm.

The first of these side projects evaluates the network communications protocols available in the LabVIEW system, comparing TCP/IP and UDP/IP communication blocks over various portions of the local network and the internet. The results surprisingly show little difference between the protocols, especially on the local network used for the research.

The second of the smaller projects used in building the final controller attempts to simulate human input to the haptic system using various systems attached to the haptic master device. While the tests help validate the proper functioning of the control system, it quickly becomes clear that simulation of human input provides very little usable information on the haptic system.

In the most interesting of the early experiments, a group of test subjects help define the resolution of a human operator with respect to direction. The results show that the subjects are able to resolve force direction no better than $67.5\,^{\circ}$. These

early results provide encouragement that the passive haptic system will provide useful feedback even though the device cannot generate arbitrary forces. The human operator cannot resolve the difference between an "accurate" force and something that's slightly different.

Out of the results of the early tests, development of an algorithm follows that uses only the position of the master and slave devices to produce useful haptic feedback. The algorithm operates under the constraints imposed by the passive actuators and compensates for the dynamics of the master device when possible.

In the final phase of the research, the full control algorithm is tested alongside a simpler version of the controller that uses information from a force sensor in the handle of the master to close the force loop and a third controller that uses only a simple virtual coupling between the master and slave. The human-factors testing includes a teleoperation shape identification task where the subject explores a shape in the workspace of the slave device, a task that simulates a point-to-point move around an obstacle in the remote device's workspace and a peg-in-hole task in the remote environment. The subjects also complete the same three tasks with a commercially available active haptic device. While the best test possible would use two devices whose only differences involved the active versus passive nature of their actuators, the tests instead provide a comparison between two specific haptic devices. However, larger more broadly acceptable conclusions can be abstracted from the results.

Results from the testing show an expected difference between the active and passive devices; however, the results also show encouraging trends. They illustrate that the passive device approaches the active device's ability to represent large surface features in teleoperation. Similar positive results suggest that the control algorithm developed in this research provides nearly as effective feedback in tasks involving moving from point to point as the active device.

1.2 Contributions of This Research

Very briefly, the research presented here provides the following contributions to the field of robotic control and specifically haptics. These contributions will be discussed fully in the final chapter.

1. Evaluation of a passive haptic device in teleoperation.

2. Quantification of the effectiveness of a passive haptic device in arbitrary force generation.

3. Creation and evaluation of a dynamic compensating controller for passive haptic devices.

4. Quantification of human perception with respect to resolution of force direction specifically on a passive haptic device.

5. Comparison of performance enhancement gained by the use of a passive and an active haptic device.

6. Identification of tasks in which the passive haptic device provides performance improvements similar to those provided by an active device.

CHAPTER II

BACKGROUND

Loomis & Lederman [57] defined a haptic system as "a perceptual system which is composed of the following subsystems: a tactile system that processes cutaneous information (pressure, vibration, and thermal inputs), and a kinesthetic system that registers position and movement from muscles, tendons and joints." Starting from that understanding, the haptic "system" includes not only the physical device being designed and controlled but also its complex interaction with the human user. To gain a full understanding of the background of the passive haptic research presented here, it is important to look at a number of the components that have gone into the research. The following section will begin with teleoperation (the birthplace of haptics) and will include a look at current passive haptic devices, passivity-based control, similar control topics and will conclude with a discussion of human perception, a very brief background of how haptic devices interact with the human.

2.1 Teleoperation & Haptics

Modern haptic devices can be used to remotely control a second robotic device in teleoperation or can function only as an interface to a computer or virtual environment. Either way, the haptic device controls a second device (either virtual or real) and as such the origins of haptic devices can be traced to early research of Goertz in the mid 1950s [31] [32]. As referenced by Hayward [36], the lineage of the modern teleoperator can be followed back to the electro-mechanical teleoperators built by Goertz to handle radioactive material. These devices represent the first designs of a master-slave pair connected only by electrical components. The devices allowed a user to effectively handle the dangerous materials without being in any danger themselves.

Similar manipulators of the era used a direct coupling either mechanically or hydraulically from the master to the slave device [38]. Until the development of the modern computer and subsequently the microprocessor, teleoperation systems involved direct joint coupling either physically or electrically between the master and the slave (in other words joint A on robot 1 follows directly with joint A on robot 2) due to the fact that the inverse kinematics involved in translating between workspaces requires a large amount of computational power. With the introduction of the processing power that early computers and then the microprocessor represented, the complex mathematical transformations between master and slave workspace became trivial [4].

Early research in the field of specifically haptic devices gained momentum around 1980. Bejczy of the Jet Propulsion Lab writes about the kinesthetic coupling between the human user and a mechanical man-machine interface as one of the three focus areas of future research in man-machine interfaces [4]. At the time, the state of the art devices involved a real-time controller generating a force-reflection algorithm with an update rate of 50Hz, but even with that low level of feedback, Bejczy realized the importance of force reflection in man-machine interaction.

At this early stage of haptics research, the work of people like Klatzky [46], Jones [41] and Gandevia [28] that focused on the perception of forces and their impact on human perception drove the design and implementation of improved haptic devices. A full section will follow discussing the role of human perception in haptics research; however very briefly, these researchers focused on the importance of tactile information in human interaction with the surrounding world. The research showed that humans rely heavily on tactile feedback, and with that in mind the addition of haptic feedback can greatly improve the man-machine interface.

Looking at the state of the art, haptic devices have found an interesting niche in the field of medical instrumentation. In addition to the typical training devices, haptic devices are now being applied to surgical procedures. These applications include cases

where the devices allow a surgeon to perform remote surgeries as well as surgical procedures in which the doctor shares control of the tool with the robotic device, haptically enhanced surgeries. Quaid applies a haptic device as a surgical assistance during bone sculpting in orthopedic surgery [72]. Similarly, Rossi & Boschetti, explore the use of haptic devices to assist during neurosurgery and spine surgery [76][8]. Clanton demonstrates the uses of a novel interface for workspace scaling and its application to microsurgery [18]. In all of these cases, the active device used provides assistance to the human surgeon by sharing control of the tool. A passive device might perform equally as well in such applications, but due to the nature of its actuators there would never be any question about whether or not the doctor were in control of the system.

2.2 Passive Haptics

Typically the first question about passive haptic hardware that one hears is "why?" A simple answer is that the devices are guaranteed to be safe. Passivity of the actuators guarantees the device's inability to become unstable. In a system that utilizes no mechanical advantage, the forces produced by definition will never be greater than a reaction force to the input applied by the human operator. However, safety really only represents the simplest answer to the question of "why?"

In a theoretical sense, a passive actuator can produce more force per unit of volume or per unit mass than an active actuator. The typical automobile provides a good example of this. The car's active components (engine, drive-train, axles, wheels and tires) make up a very large portion of the vehicle's mass and volume while the braking system is comparatively very small. However, even though they are small and relatively light weight the brakes are designed to dissipate energy more quickly than the motor can create it; by design vehicles decelerate more quickly than they accelerate.

With respect to energy, passive actuators can also produce much larger forces and torques than active actuators with the same input energy. A friction brake requires very little energy to actuate it, but it can produce very large torques. The low power requirements make a passive device especially well suited for mobile applications.

Finally in a more esoteric sense, the most effective haptic devices of the future will likely be hybrid devices, using both passive and active actuators. However, to understand the fundamental issues in such devices it will be important to understand the strengths and weaknesses of both portions of the device separately. A large amount of research has focused on active devices, and the research presented here attempts to help broaden the comparatively small field of research using passive devices. The field of hybrid passive devices has also not yet been given much research attention, however work at Georgia Tech by Tognetti [83] and preliminary publications from Hayward [14] show a growing interest in the devices.

2.2.1 Passive Control

With respect to the control of haptic devices, possibly most relevant to the work to date is the haptic control concept of passivity and its use in guaranteeing stability of the human-machine interface [43][59]. Hannaford and Ryu first developed a haptic control law that specifically addresses passivity [35]. An adaptation of impedance control, the software implementation of passivity can guarantee stability of the haptic device and thus the safety of the human user by never allowing the output energy of the device to be positive. Ryu further extended time-domain passivity to teleoperation systems by injecting damping into the haptic device to insure that it only dissipates energy [77]. Similar approaches for stability and safety have been developed by Lee and Li [52][53][54][55] who produced a control law that relaxes the required knowledge about the remote system model and moves toward a more robust control

system, insuring that the device remains stable in spite of possible mismatches between the actual dynamics of the system and the model used by the control scheme. In all of these cases, the passivity of the controller forces the device to interact with the human operator in a stable manner, guaranteeing the operator's safety, but all of this assumes no glitches in sensor information or in the hardware or software of the control system. For very critical applications, this level of fault tolerance might not be enough.

The idea of passivity has also been extended to teleoperation as an attempt to handle network delay. Instead of communicating in terms of force and velocity, a system using wave variables applies passivity theory by transforming the input and outputs of the system in a way such that control variables become energy terms. Passivity is then insured if the power in is more than or equal to the power out. Anderson and Spong introduced the use of wave variables to handle network time-delay in haptic teleoperation [3]. Niemeyer and Slotine extend this research slightly and present theories on adaptive control of haptic devices making the original wave variable approach more stable [67] [68]. Recent research at Georgia Tech. extends upon these basics by adding predictors and the final human testing produced favorable results [15]. In all cases, the variable transform produces a safe operating environment for the human user and helps produce a usable system for teleoperation with time delay.

In the above examples of passivity-based control, the energetic nature of the device is enforced through software. The control schema attempt to ensure that an active haptic system can be forced to remain passive by reading sensor values and calculating output such that no energy is generated by the device. In contrast, haptic devices with passive actuators insure passivity through the physical constraints of their hardware and are therefore more fault-tolerant.

2.2.2 CVT-Based Passive Hardware

As previously mentioned, passive haptic systems include both energetically neutral and energetically dissipative devices. Colgate et. al have explored the use of energetically neutral haptic devices that use continuously variable transmissions (CVTs) as actuators that neither dissipate energy from nor add energy to the system [70][71][63][64]. The devices are capable of producing very stiff virtual surfaces, one method for judging a haptic device [24]; however, in free motion, they require processing and actuation that can introduce lag into the system.

Colgate's lab has produced multiple generations of devices, beginning with the unicycle cobot [85]. The 2 DOF device shown in Fig. 2.1 uses a roller blade wheel on a smooth surface to constrain the user's motion to a single DOF path. The angle of the wheel with respect to the human input changes the direction of force that the user feels. Over the following years, the principles of the unicycle cobot have been extended to full 6 DOF haptic devices [65]. In all cases, the devices use small active actuators to control and redirect the flow of energy. While the devices all use active actuators, none of the actuators actually applies forces directly or indirectly to the user and thus the devices can still be considered truly passive.

2.2.3 Dissipative Passive Hardware

Dissipative devices produce forces by resisting user motion and dissipating energy. Compared to the devices built around CVT actuators, dissipative devices have more difficulty producing stiff virtual surfaces, but perform much better in free motion. The actuation of a cobot causes a physical motion that in turn effects the output force, possibly yielding slower response times than a system such that actuates a brake.

Cho's analysis of dissipative devices produced the concept of the Force Manipulability Ellipsoid as a description of a haptic device's capabilities within the workspace [16].

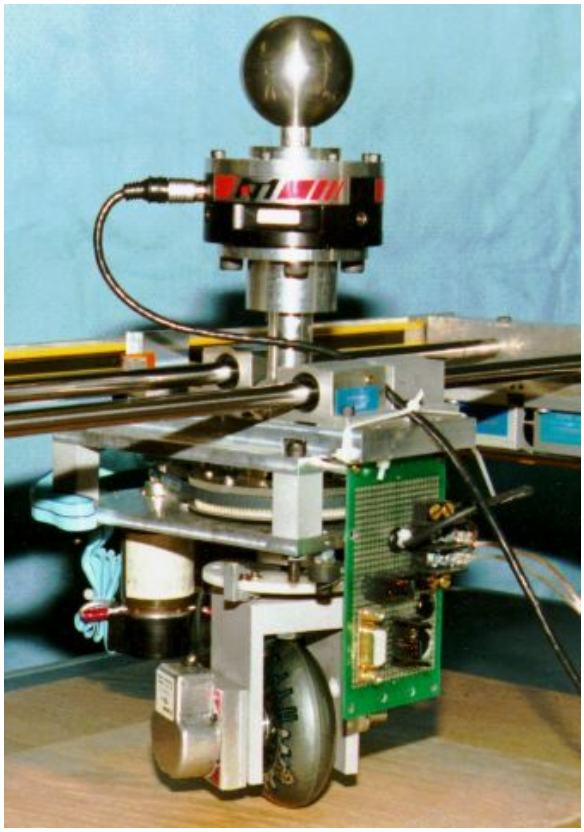

Figure 2.1: Single DOF cobot used by Colgate

The shape and size of the ellipsoid at a given point in the device's workspace describe the possible output of the device at that point. Gao and Book extended this idea and developed the concept of steerability, a passive haptic device's ability to redirect motion[30][29]. A "fully steerable" haptic device can produce forces that push the user either to the left or right of an arbitrary trajectory. Gao's analysis illustrated regions of the workspace of a haptic device in which it is fully steerable, and as such a user would want to stay within those regions so that the haptic device can produce its full range of feedback.

Compared to the field of active haptic devices, few dissipative passive devices currently exist. Other than the two devices developed through previous research at Georgia Tech (to be discussed shortly), fewer than half of a dozen have published research. Sakaguchi developed a planar device using electro-rheological (ER) brakes

and a belt / pulley system to increase their force output but have produced only a short list of publications none of which include human-factors testing [79] [27]. Matsuoka has developed the only 3-DOF device with published research, a large-workspace device intended to guarantee user-safety [60]. However, recently the lab has also produced a 6-DOF device using brakes to actuate three of the axes. The device was introduced and a short paper has been published, but again no human factors testing has been done [86]. Sing and Cho who developed the concept of the force-manipulability ellipsoid have also recently published results using a 2DOF passive haptic device. The device uses a tendon and brake drum combination to increase the device's endpoint force output of the 2-link manipulator [17]. Finally, Wannasuphoprasit has presented a design for a planar passive device using linear pneumatic cylinders (like controllable car shocks) but nothing has been published about its completion or research using it [84].

At Georgia Tech, two dissipative devices have been used for research, both developed under Book. Charles developed the first device, PTER (Passive Trajectory Enhancing Robot), that used friction brakes and clutches as actuation at its joints [19]. Impedance control of the device was explored by Gomes [33] as well as Swanson, who also developed a velocity field control used in path following haptic experiments and robust human-factors testing [81]. The research produced with each of these devices focused on haptic interaction with a virtual environment and specifically on controlling the user's velocity to provide stable assistance in path following applications. Reed improved the hardware by developing MR PTER (Magneto-Rheological Passive Trajectory Enhancing Robot), a re-configurable planar device using magneto-rheological brakes for actuation [73]. The MR brakes produce smaller joint torques and endpoint forces, but have a much faster response time and avoid some of the problems associated with friction brakes and clutches. Reed then applied the velocity field path following control to MR PTER and showed the improvements of the device

over past versions through a short human-factors test [74].

The research presented here extends the previous passive haptic research to explore the use of a passive master in teleoperation tasks. All passive haptic research thus far has been focused on using the device to interact with a virtual or previously defined environment [81]. The difficulty of a teleoperation task centers around the fact that no *a priori* knowledge of the remote environment exists. The research presented here will focus on producing haptic feedback generated based only on the knowledge of the positions of the master and of the slave devices.

2.3 Other Similar Research

The research presented here also shows some similarity in a control sense to the research of Bonivento and Melchiorri [7][61][62] whose current projects involve producing haptic feedback using a wire actuated manipulator; however unlike other wire-driven devices, the wires are not implemented in balancing pairs. Therefore at any point in the workspace, only single-directional discrete forces can be generated by each wire. Melchiorri and Bonivento demonstrated the abilities of this style of a device as a portable haptic interface that looks like a backpack with wires that come over the shoulder and between the elbow and side. The wires attach to a finger gimball with which the operator interfaces. The device is capable of producing stiff surfaces that produce reaction forces in a direction pointed toward the user. Figure 2.2 shows a line drawing of their portable device and the way in which the human interacts with it.

Possibly the most interesting application of the magnetorheological fluid currently being pursued involves the work of Sgambulleri *et al* and their fully immersive device. The user interacts with a pool of magneto-rheological fluid in which controllable magnetic fields can produce shapes and surfaces in the liquid. With some increase in resolution, the device could feasibly produce very interesting results in the future [80].

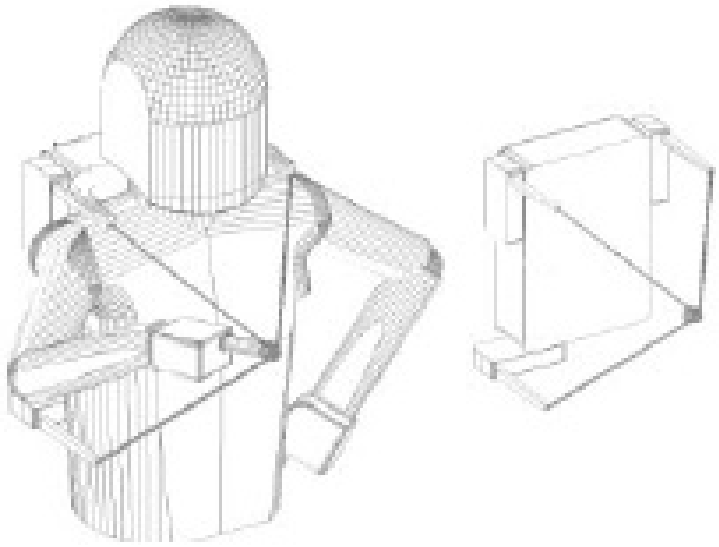

Figure 2.2: Wire-driven Haptic Device

The industry-driven research using magneto-rheological devices has developed mainly around the field of suspension systems both in automobiles and in mountain bikes [10]. The Lord Corporation, the current leading supplier of magneto-rheological devices, sees semi-active auto suspension systems as their main market [34] and currently supplies GM, Audi and Ferrari with components to improve ride quality.

Outside of the commercial applications, research involving MR dampers has be extensively explored in vibration isolation for buildings and road structures. Both Dyke and Carlson (former lab mates at Notre Dame, now at Washington University and Lord respectively) have explored the use of MR devices for seismic protection [20] [21] [40]. Their research focuses on using acceleration feedback to effectively damp out seismic vibrations with semi-active magneto-rheological systems.

Both in suspension systems and in seismic control systems, the controller assumes an oscillatory disturbance to be damped out, and the control system only applies control effort when the desired direction of applied force counters the velocity (as is required by the passive nature of the system, the details of which will be discussed at length in the following sections). While these semi-active applications seem at

first glance to share a good deal with the research presented here, the differences become apparent after closer investigation. The haptic interface rarely encounters an oscillatory input. Furthermore, much like the control approach that will be presented shortly, the semi-active control systems do nothing to insure that the device operates in the "controllable" range, only applying control effort when the velocity opposed the direction of desired force.

2.4 Human Perception

Originally in the field of haptics, a large portion of the published research came from the fields of psychology and human-computer interaction. It currently seems that much of the focus has shifted toward the development and control of the electro-mechanical systems, but it remains important to pay close attention to the human element. Discussion of haptic feedback really only makes sense when understood in conjunction with an understanding of how the user perceives the haptic stimuli.

Some of the earliest human factors testing came from Fitts in the early 1950's. Not only did he establish the theories that still drive user interface design [25], he also looked at the human behavioral response to stimuli [26], the basis of the understanding of how to influence a human user with haptic feedback.

In the more recent past, the idea of human cognitive modeling has impacted the field of human-computer interaction research. Lochart and Murdock applied principles of signal detection theory to look at decision making based on stimuli [56]. The early 80's saw the introduction of the Human Model Processor (HMP) [13] out of which the study of human cognitive architecture was born. The theories that developed out of the HMP attempted to fit the structure of human cognition into a block diagram form to mimic the architecture of a computer. In a sense, this architecture creates a limited human model that produces an output action or performance given an input set of conditions. The ACT architecture developed by Anderson [2]

and extended by Byrne [12] as well as the EPIC architecture developed by Kieras & Meyer [44] represent the most widely accepted cognitive models. Realistically, the inclusion of a human cognition model into a haptic control scheme makes very practical sense, but lies well out of the scope of the research presented here. Instead, the background research focuses more specifically on understanding how humans interpret physical stimuli.

Specifically with respect to perception in haptics, understanding of the role of tactile feedback remains central to developing an algorithm for generating force feedback. Klatzky *et al* performed rigorous experiments to determine the human's ability to recognize known shapes by touch alone [46], finding that the subjects were able to correctly identify the objects with roughly 96% accuracy (or 99% accuracy with a slighly more relaxed scoring system). The authors warned that that the results apply specifically to well-known shapes, but the research showed that with training, a human user can gain immense amounts of information about their surroundings from tactile feedback alone.

Klatzky next extended this research by adding a robotic manipulator into the system. Her research in the late 1980s explored the interaction between visual and haptic feedback and concluded that the increase in modes of feedback subsequently increased speed of object recognition [45]. If each sense behaves approximately as a separate information channel (as is proposed by most of the HMP models), Klatzky's conclusions should not be surprising. Increasing the number of information channels subsequently increases the amount of information that the user can effectively process at any given point in time.

The logical next question in this line of discovery focus on the ability of a human to perceive difference in force information, effectively attempting to define the perceptual resolution of the human. Research exploring the concept of "just noticeable differences" (JND) attempts to answer this question.

As early as the mid 1830's, Webber found that for a human to perceive a difference, a 10% change was required in the weight of a rougly 32 oz. object being lifted by the hand and arm [75]. In more recent research, Brodie & Ross experimentally determined similar JNDs in a task where the subject was asked to lift 2 oz. weights [11]. In an experiment somewhat similar to the perceptual testing that will be presented later, Jones reported force matching in the upper arm with a JND in the range of 5-9% [42]. Research in the field even extends to looking at a person's specific JND threshold and using that information as an early warning for disease and its implications on rehabilitation [1].

All of these experimental procedures explore the JND with respect to magnitude of force in full arm motion; however, very little previous research looks at force as a vector quantity. Hurmuzulu reports a very simple test done to validate a newly developed haptic device [39]. The results show poor performance in judging force direction but the authors attribute it (possibly incorrectly) to poor haptic interface performance. A more recent study by Tan specifically explores JND with respect to angle of force and finds the threshold of human perception to be on the order of 25-33° [82]. These results in turn lead to an existential question of haptics research, namely whether or not a haptic device should attempt to replicate remote or virtual forces with complete accuracy. If not how should forces be replicated, and what are the key components to producing useful feedback? The perceptual results should also justify the use of a passive device that can only display a certain subset of all possible forces.

CHAPTER III

CONTROLLER

This chapter uses the device MR PTER as a visual example to facilitate the communication of the control theory; however, the equations and concepts presented here apply to any dissipative passive device that can be divided into one or more two-link serial robots connecting the base to the handle with which the human interacts. Furthermore, an extension to longer serial robots only requires minimal extra effort. The following should show that the feedback generated by the device improves as the number of non-redundant actuators in it increases

Passive haptic devices present the somewhat unique control difficulty that they cannot produce arbitrary forces to be displayed to the user. They can only produce forces that oppose motion of a user or oppose the input force of a user when the velocities of the actuated joints reach zero. It is important to understand the differences between an active device and a passive device and to understand the the details of the passive system's force generation to be able to understand and develop a control scheme. The following section will begin by presenting the simplest actuation scheme, an on-off scheme that fully actuates a single joint at a time. The discussion will then move to a scheme that actuates multiple brakes at a time in an attempt to generate a force in an arbitrary direction.

The second portion of this chapter discusses the actual haptic force to be displayed to the user during a teleoperation task. Three control schemes are presented defining three different ways to determine what force should be output. The first scheme represents a simple application of a typical teleoperation virtual coupling between master and slave and will be the basis for the other two schemes. The second scheme

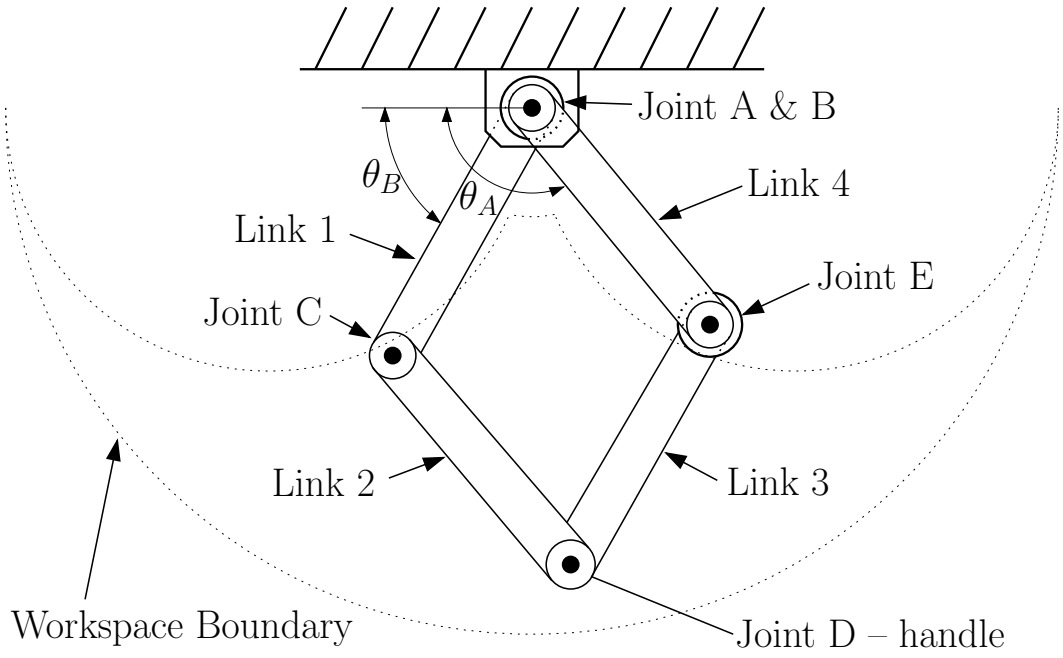

Figure 3.1: Line-drawing of MR PTER

uses feedback from a force sensor in the human-interface handle to close the loop on the force controller. The final scheme uses the dynamics of the system as a component of the force being displayed and in doing so will compensate for certain components of the dynamic forces felt by the user

3.1 Force Generation

Completely locking a brake of the passive device will force the device to move along a single degree of freedom circular path (effectively simplifying the device from a two-link, 2 DOF device to a one-link single DOF device). At any point in the workspace of the device there exists one such single DOF path for each non-redundant passive actuator, and for every non-singular point in the workspace these paths are unique.

As an illustrative example, begin by looking at the configuration of MR PTER shown in Fig. 3.1. MR PTER is a planar parallelogram-shaped manipulator (re-configurable such that the base joints are not coaxial) with brakes actuating base joints A & B as well as the "elbow" joint E (in the configuration with non-coaxial

base joints, another brake is located at joint C). The base angles θ_A and θ_B, are measured using encoders. The human interfaces with the device through a handle and a 6-DOF force / torque sensor at joint D, and the handle is allowed to freely rotate.

Using the example of MR PTER, each point in the workspace has three unique paths that correspond to locking each of the brakes, the directions of which are shown in Fig. 3.2 for a specific configuration. The directions are labeled $\vec{p_A}$, $\vec{p_B}$ & $\vec{p_E}$ to represent the paths created by locking brakes A, B & E, and the directions are guaranteed to be unique as long as the device does not enter a singular configuration.

At any given point in the workspace, the force produced by a specific brake is perpendicular to the single DOF path that would be generated by locking that brake. Locking a joint allows the device to rotate freely along the single DOF path as if the device were a single link, thus it conceptually follows that the device can only produce forces that are in line with that single equivalent member. The force can point either toward the center of rotation or away from the center of rotation depending on the endpoint velocity. Figure 3.3 shows the direction of forces at the same configuration of MR PTER as shown in Fig. 3.2. The forces are labeled $\vec{f_A}$, $\vec{f_B}$ & $\vec{f_E}$ in the negative and positive direction to represent all possible directions of force that can be generated by the individual brakes A, B & E.

The forces generated at the endpoint of the manipulator cannot have a component in the direction of the endpoint velocity. Doing so would increase the endpoint velocity and would therefore violate the inherent passivity die to the fact that a force component in the direction of motion would increase the system's energy. With the endpoint velocity shown in Fig. 3.3, the dashed vectors represent forces that cannot be generated. The region of $\vec{v}$ $\pm\frac{\pi}{2}$ defines the region of un-producible forces. This region is visible in Figs. 3.3 & 3.4 as the vertical line through the endpoint.

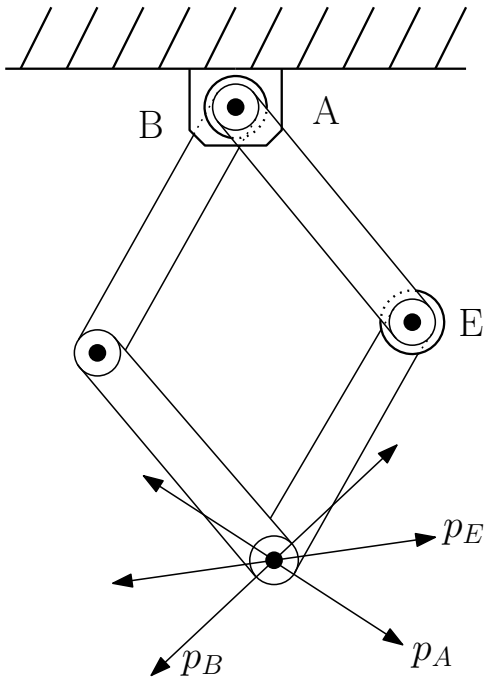

Figure 3.2: Single DOF path lines

From here forward, the discussion will deal with forces only when the input direction is known, and will be labeled only as $\vec{f_A}$, $\vec{f_B}$ & $\vec{f_E}$ to represent the forces generated by actuating brakes A, B & E. Furthermore, from here forward it will be assumed that the force to be displayed to the user is called $\vec{f_h}$, the haptic force. The calculation of $\vec{f_h}$ will be discussed in the next section. Actuation schemes only apply if $\vec{f_h}$ is at least $\frac{\pi}{2}$ radians from the direction of $\vec{v}$.

3.1.1 On-Off Actuation

In the simplest actuation scheme, the brake that produces a force closest in direction to $\vec{f_h}$ is actuated. In Fig. 3.4, brake A would be actuated for the haptic force direction $\vec{f_{h1}}$, and brake B would be actuated for force direction $\vec{f_{h2}}$. The difference in the actuated force $\vec{f_A}$ and the desired force $\vec{f_{h1}}$ will be called the angular error or θ_{error}. Work has been done exploring the achievable results using this control scheme in a simple test [5]. The results of this experiment will be discussed further in the following

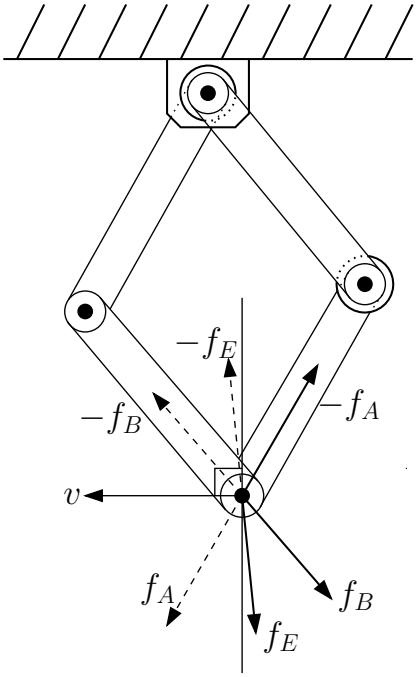

Figure 3.3: Single DOF Forces

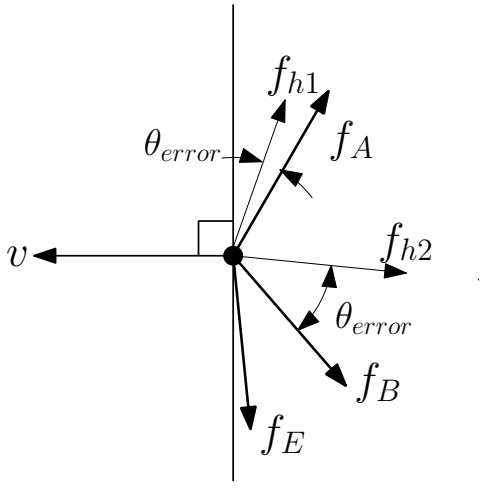

Figure 3.4: Brake forces with a defined velocity

sections.

This single brake actuation scheme can only produce forces in unique directions, effectively discretizing the force generation to the number of actuators. In the case of MR PTER, the actuation can produce force in three discrete directions, but if MR PTER's base joints were moved so that they were not co-axial a brake at joint C would be non-redundant and would produce a fourth discrete brake force.

Assuming that the direction of $\vec{f_h}$ and the direction of the endpoint velocity are completely arbitrary at any point in the workspace, it is possible to compute the average of the difference between the direction of the commanded force $\vec{f_h}$ and the direction of the actuated force. This will be referred to as the "average angle error" or $Avg(\theta_{error})$ from now on. Since both velocity and haptic force direction are considered random variables in the sense that they can be in any direction, the average angle error is actually an average over both variables.

At a given point in the workspace, each brake of an n-brake device produces a force along a line, and these force lines divide the workspace into 2*n regions as shown in Fig. 3.5. The regions are symmetric about a line between the force directions labeled e_n and e_1, so the analysis will look at n regions. The average angle error can be calculated by multiplying the probability that the velocity lies within a certain region by the average angle error within the region and summing over all regions. Equation 3.1 shows this relationship somewhat explicitly in a form reminiscent of an entropy function from information theory or a variance function from statistics.

$$Avg\left(\theta_{error}\right) = \sum P\left(region\right) * \left(AverageValue\right) \tag{3.1}$$

Since the velocity direction is assumed to be an unknown random variable, it's equally as likely for it to be at any position within the possible π range. Therefore, the probability of having an input velocity within a certain region equals the size of the region divided by π:

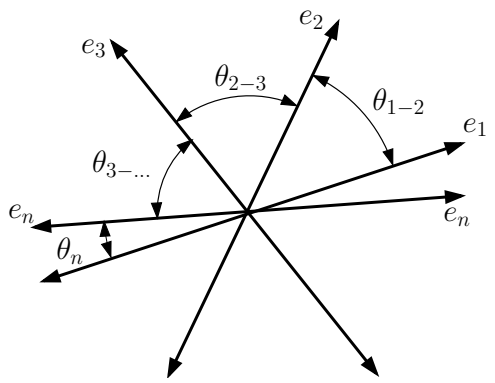

Figure 3.5: Lines of brake force at a specific configuration

$$P\left(region\right) = \frac{RegionSize}{\pi} \tag{3.2}$$

The direction of velocity defines the region of Figs. 3.5 & 3.6 in which the control operates. More explicitly, the line perpendicular to the velocity defines the region because forces can only be generated that are greater than or less than $\frac{\pi}{2}$ radians away from the velocity. Figure 3.6 shows a specific velocity and position within the workspace of MR PTER, and the dotted line defines the region of producible forces. Figure 3.7 shows the angular error as the commanded force ranges over all possible values for the configuration in Fig. 3.6. The average angle error can be understood graphically by dividing the area under the line in Fig. 3.7 by the range (in this case π), essentially integrating the error over all possible values of θ_f and dividing by the range.

The velocity direction must also range over the full extent of the region. This motion is shown in Fig. 3.8 as the velocity moves through the range of the region (as the perpendicular to the velocity moves between e_2 & e_3. In doing so, the bracketed part of the graph shown in Fig. 3.9 shifts in the direction of the arrow as the velocity direction shifts.

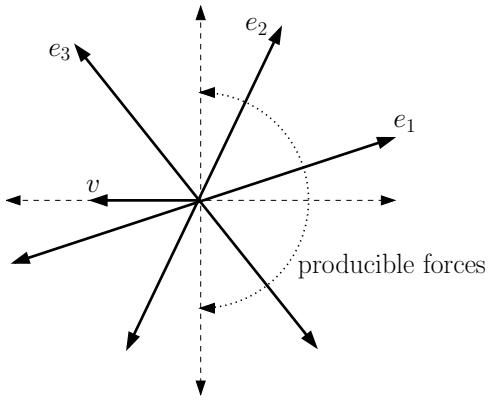

Figure 3.6: Brake forces at a specific configuration and velocity

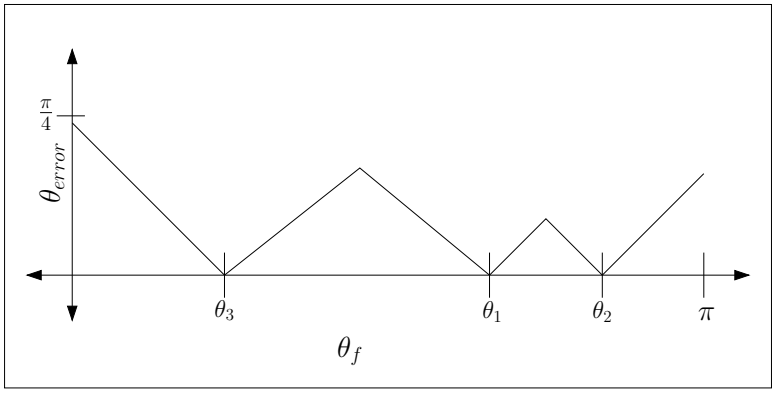

Figure 3.7: Average angle error calculation

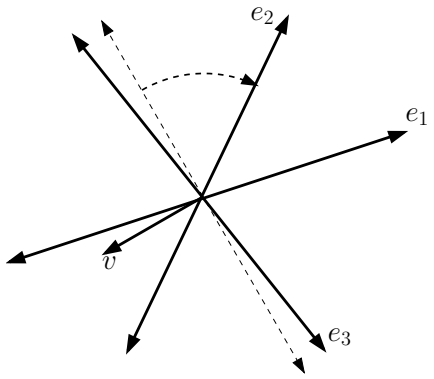

Figure 3.8: Varying of the velocity direction through a region

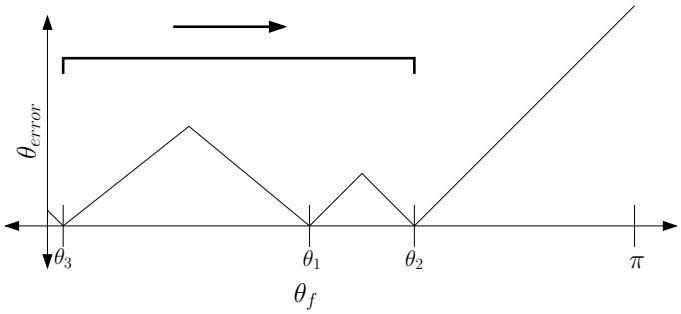

Figure 3.9: Angle error corresponding to varying the velocity direction

Using MR PTER, the average angle error for each region with a specific configuration and velocity can be evaluated yielding Eqn. 3.3:

$$Avg\left(\theta_{error}\right) = \frac{2\left(\theta_3^2 + \left(\pi - \theta_2\right)^2\right) + \left(\left(\theta_1 - \theta_3\right)^2 + \left(\theta_2 - \theta_1\right)^2\right)}{4\pi} \tag{3.3}$$

The $Avg(\theta_A)$ at any point in the workspace can then be found by combining Eqns. 3.1, 3.2 & 3.3. This complex equation takes the form of a double integral, the evaluation of which can then be plotted over the entire workspace of the device to provide a visualization of the ability of the device to produce an arbitrary force at a given point. Figure 3.11 shows a surface plot of $Avg\left(\theta_{error}\right)$ in the joint space of MR PTER.

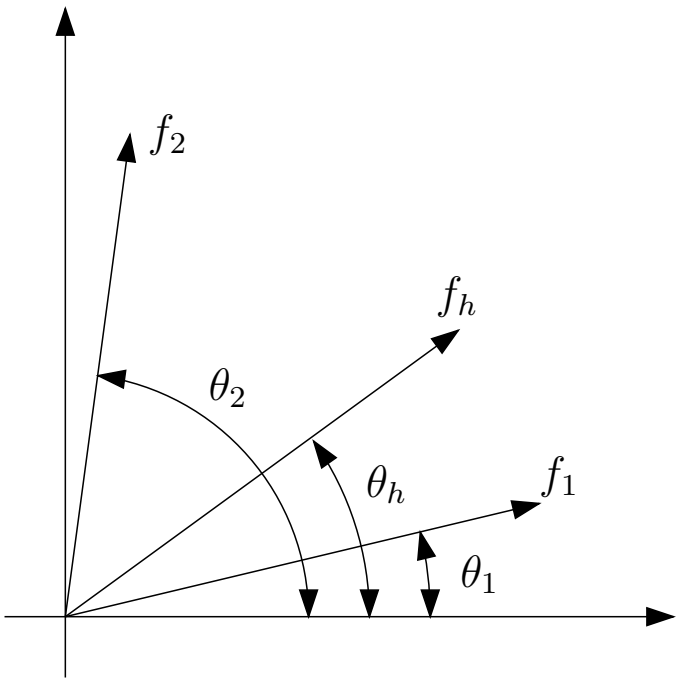

Figure 3.10: Multi-brake actuation variables

3.1.2 Multi-Brake Actuation

A more complex actuation scheme involves simultaneously using multiple brakes. If the force to be generated, $\vec{f_h}$, lies between two brake forces, they can be actuated in unison to produce an output force that matches the direction of $\vec{f_h}$. In Fig. 3.4 $\vec{f_{h2}}$ would represent one such force. However if $\vec{f_h}$ does not lie between two brake forces as is the case with $\vec{f_{h1}}$ in Fig. 3.7 the nearest brake would be the only possible actuation

For calculation of this actuation scheme, the discussion uses the variables shown in Fig. 3.10. Assume $\vec{f_h}$ lies between two brake forces, shown in this figure as $\vec{f_1}$ and $\vec{f_2}$. These forces are the resultant of a unit actuation of a brake, and are therefore a function of both endpoint velocity and kinematics and are calculated similar to Eqn. 3.4. Since there are more brakes and therefore more input torques than degrees of freedom, the Jacobian of the system is non-square. To calculate the endpoint forces, a square (2x2) sub-matrix of the Jacobian is used that corresponds to the two input torques as in Eqn. 3.4. In this equation, the subscripts of the Jacobian components

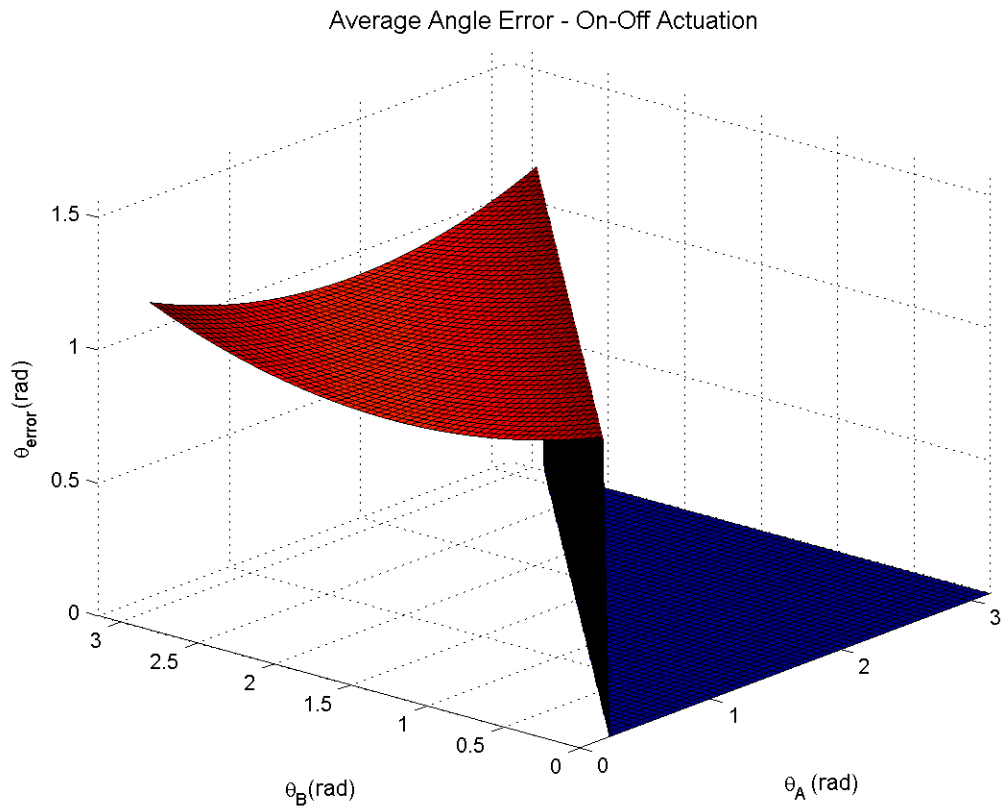

Figure 3.11: Single brake average angle error

represent the relationship between the cartesian and joint space variables. A similar equation can be derived to relate the torques at any pair of joints to the endpoint forces for a given device.

$$\begin{bmatrix} f_x & f_y \end{bmatrix}^T = \begin{bmatrix} \tau_A & \tau_B \end{bmatrix}^T \begin{bmatrix} J_{ABx} & J_{BAx} \\ J_{ABy} & J_{BAy} \end{bmatrix}^{-1} \tag{3.4}$$

The force generated by a unit brake actuation can be found by sequentially setting each brake torque to a unit strength and the other three torques to zero, then calculating the endpoint force. In this case, the angle of the two brake forces on either side of $\vec{f_h}$ is denoted by θ_1 or θ_2. The variable $\vec{f_1}$ denotes the force generated by a unit

torque of joint 1, and $\vec{f_2}$ is the result of a unit torque of joint 2. The variable θ_h defines the direction of $\vec{f_h}$. The brakes are actuated so that the resultant endpoint force matches the direction of $\vec{f_h}$. To assure this, the tangent of the linear combination of $\vec{f_1}$ and $\vec{f_2}$ in Eqn. 3.5 must match the tangent of $\vec{f_h}$. This yields Eqn. 3.6

$$f_{output} = af_1 + bf_2 \tag{3.5}$$

$$\frac{sin(\theta_h)}{cos(\theta_h)} = \frac{af_1 sin(\theta_1) + bf_2 sin(\theta_2)}{af_1 cos(\theta_1) + bf_2 cos(\theta_2)} \tag{3.6}$$

Solving for a and b yields Eqns. 3.7 & 3.8.

$$a = \frac{cos(\theta_h)sin(\theta_2) - sin(\theta_h)cos(\theta_2)}{f_1(cos(\theta_1)sin(\theta_2) - sin(\theta_1)cos(\theta_2))} \tag{3.7}$$

$$b = \frac{sin(\theta_h)cos(\theta_1) - cos(\theta_h)sin(\theta_1)}{f_2(cos(\theta_1)sin(\theta_2) - sin(\theta_1)cos(\theta_2))} \tag{3.8}$$

The output force will match the direction of $\vec{f_h}$, if the ratio of brake actuation, defined as variables V_1 & V_2 assuming that the output torque is proportional to the command voltage, matches the ratio of a to b. All of this can be normalized to match the magnitude of the commanded force, $\vec{f_h}$ bounded only by the maximum output of the actuators.

$$\frac{a}{b} = \frac{V_1}{V_2} \tag{3.9}$$

$$\sqrt{V_1^2 + V_2^2} = |f_h| \tag{3.10}$$

The following brake actuation would result:

$$V_1 = \frac{a * |f_h|}{\sqrt{a^2 + b^2}} \tag{3.11}$$

$$V_2 = \frac{b * |f_h|}{\sqrt{a^2 + b^2}} \tag{3.12}$$

Similar to the discussion of angle error with the single-brake actuation, an average angle error can be found throughout the workspace with this multi-brake actuation

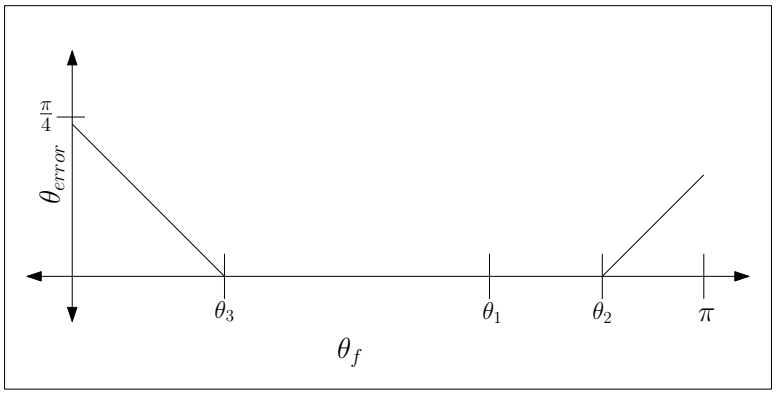

Figure 3.12: Angle error at a specific point and endpoint velocity

as well. In this case, if the desired output force lies between two brake forces, in theory θ_{error} goes to zero. Note that this analysis assumes a quasi-static case since the dynamics are currently ignored. Figure 3.12 depicts this relationship graphically. Therefore for the same configuration and known endpoint velocity that was used in looking at the single-brake actuation, the average angle error is defined by Eqn. 3.13 and corresponds to Eqn 3.11. Throughout the workspace, this equation is integrated and averaged over both velocity and desired force, the result of which is graphed in Fig. 3.13. Note that the maximum values are the same for the two actuation schemes for $\theta_A = \theta_B$; however, when the two are not equal, $Avg(\theta_{error})$ decreases with multi-brake actuation.

$$Avg\left(\theta_{error}\right) = \frac{\left(\theta_3^2 + \left(\pi - \theta_2\right)^2\right)}{\pi} \tag{3.13}$$

3.1.3 Discussion

The idea of matching force direction follows in line with the previous research done by Gao [30]; however his path-following theories do not directly apply to teleoperation. The idea of matching the direction of an arbitrary force is far more important in a sense than the ability to steer to the left or right. Furthermore, test results presented

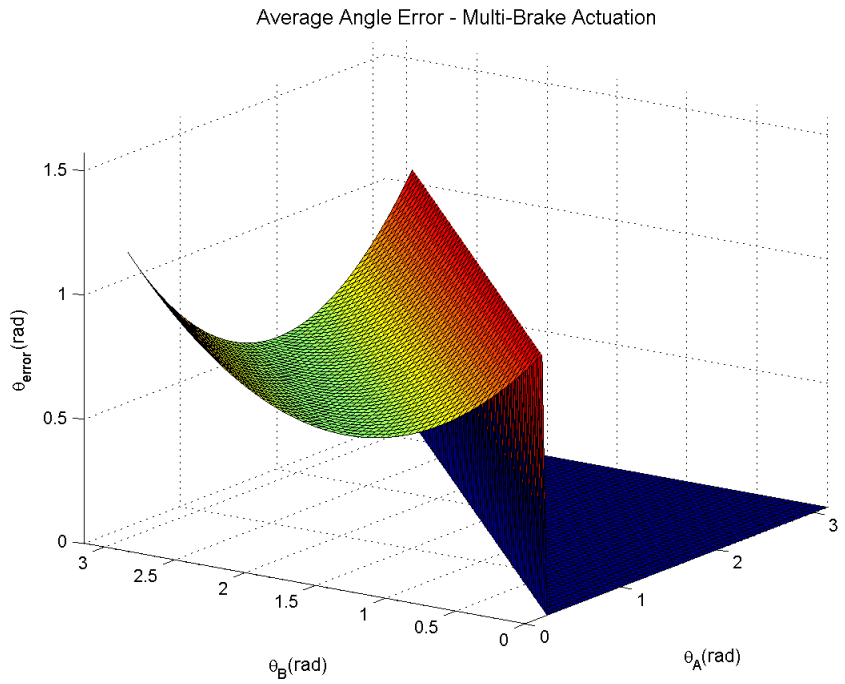

Figure 3.13: Average angle error using multi-brake actuation

in following chapters will define a human perceptive resolution as 67.5 ° or roughly $\frac{\pi}{3}$ radians. Applying this to the idea of $Avg(\theta_{error})$, if the device operates in a region where $Avg(\theta_{error})$ is lower than the perceptive threshold, on average the passive device will be able to produce a force that the human perceives to be the same as the desired haptic force. Much like the concept of "fully steerable," a device whose entire workspace has an $Avg(\theta_{error})$ smaller than $\frac{\pi}{3}$ would perform very well at arbitrary force generation. The human perceptive threshold creates a very real guideline that quantifies the quality of a passive haptic device in teleoperation.

The magnitude of the output force also plays a central role in the ability to reproduce forces. The preceding definitions and discussion have neglected this portion of the passive device's force generation capabilities. Assuming that the passive actuators have a maximum torque τ_{max} and again using the Jacobian defined in Eqn. 3.4, by

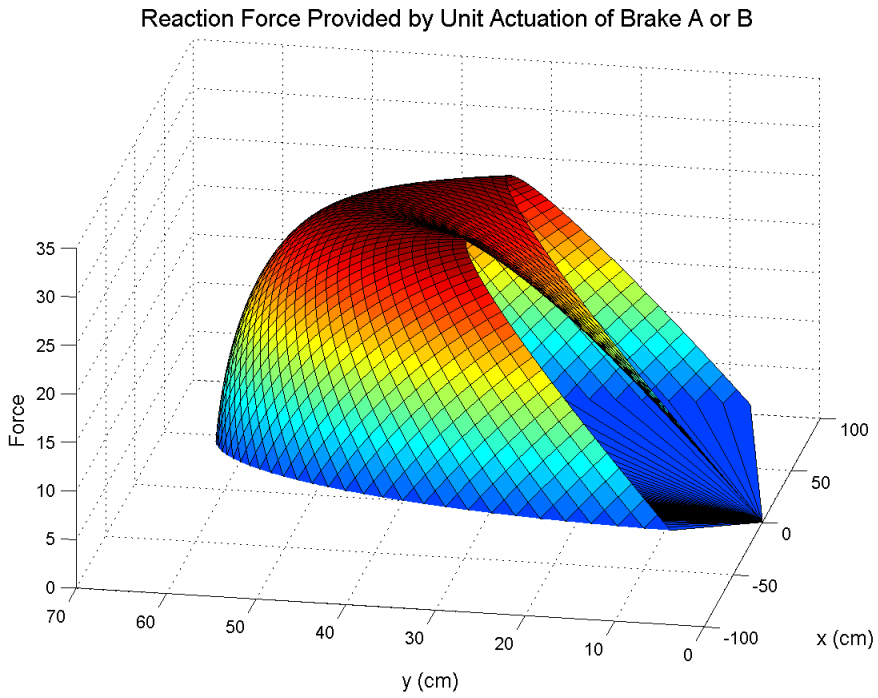

Figure 3.14: Minimum force to overcome actuation of brake A or B

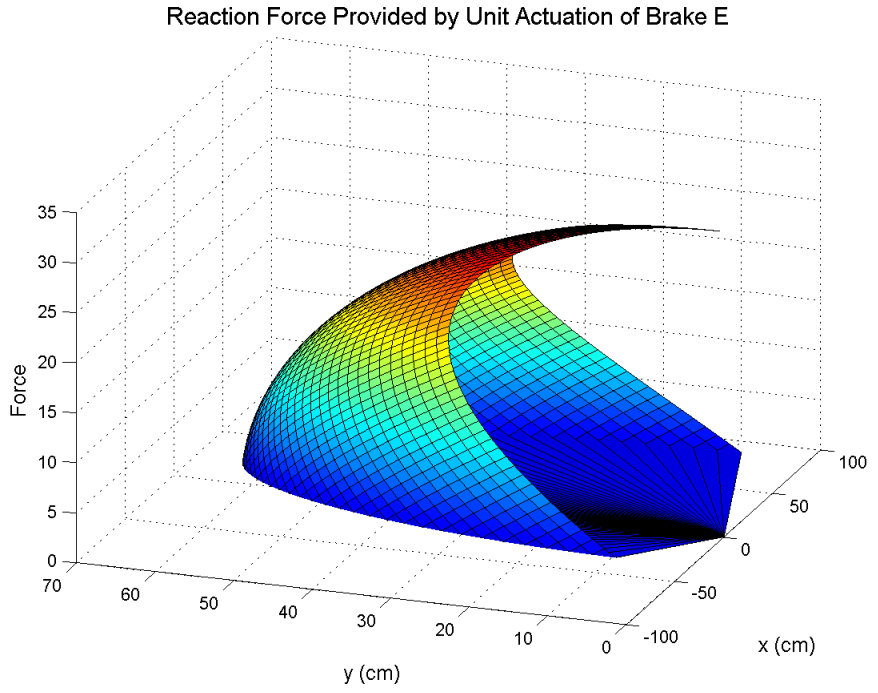

Figure 3.15: Minimum force to overcome actuation of brake E

sequentially setting one joint torque to τ_{max} and the others to zero, minimum force required to overcome τ_{max} can be found across the workspace. For instance, if operating toward the outer edge of the workspace, τ_{max} at brake A or B can only resist a very small endpoint force as seen in Fig. 3.14 which shows the force production of those two brakes over the workspace for a given actuation. Similarly, Figure 3.15 shows a plot of the endpoint force produced by a given actuation of brake E. Note that these plots do not have units on the force axis, because in reality the units mean very little except in an absolute sense. The analysis focuses more on relative force throughout the workspace, and a "better" device would have a flatter three-dimensional curve over its workspace.

Looking at the system as a whole, it makes further sense to judge the device using a combined understanding of all brakes in the device. At a specific point in the workspace, one actuator might be able to resist very large forces while the others might not. Unless the control intends to utilize the actuator capable of producing the high force, very little force will be able to be generated. Figure 3.16 illustrates the minimum force to overcome any actuator over the workspace of MR PTER. Again, better devices will have larger sections of their workspace with a flat portion of this plot.

These two metrics, θ_{error} & F_{max} have been chosen for analyzing the quality of a given passive haptic device; however they by no means represent the ideal metrics to judge a device. They provide a very physical starting point from which analysis can build. Still, these metrics make little sense without some grasp of the psycho-physical understanding of the human-device interface. Results presented later in this research regarding the perception ability of a human operator will show the need for using different metrics to judge the effectiveness of a passive haptic device.

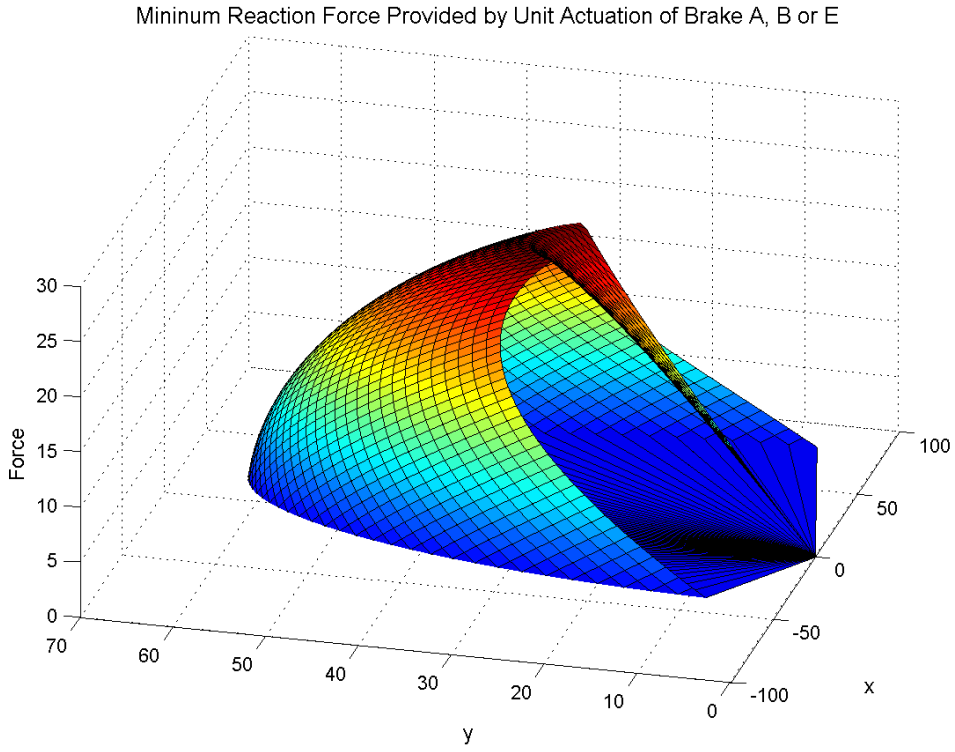

Figure 3.16: Minimum force generated by brake A, B and E

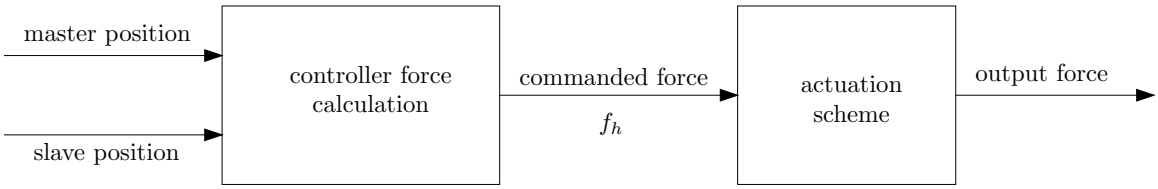

Figure 3.17: Controller diagram

3.2 Controller Force Calculation

To understand the control of a passive system, one must first understand the way in which the device can generate force. However as in any haptic system, attention must be paid to the force being displayed to the human user. In an attempt to provide useful haptic feedback, two simple schemes have been developed to determine what force should be displayed to the user (a simple virtual coupling and a closed loop method) as well as one more complicated method. The following sections will present the three haptic force algorithms. In all cases, the control system for the master device needs only to know the position information from the slave device to calculate the force to be displayed. Figure 3.17 shows a block diagram of the system.

3.2.1 Virtual Coupling Feedback

Traditionally in a simple teleoperation scheme, the force displayed to the user is proportional to the difference in position between the endpoint of the master and the slave, a virtual coupling is developed between the two devices. In this scheme, the slave follows the master, and the human interacting with the master feels as if a virtual spring connects the master to the slave. In such a scheme, Eqn. 3.14 defines K as the virtual spring constant that sets the strength of the haptic coupling. Equation 3.15 represents the haptic force $\vec{f_h}$ as a magnitude in the direction of the unit vector $\vec{e_h}$.

$$\vec{f_h} = \vec{f}_{coupling} = K * (p_s - p_m) \tag{3.14}$$

$$\vec{f}_{coupling} = K * |p_s - p_m| \, \vec{e_h} \tag{3.15}$$

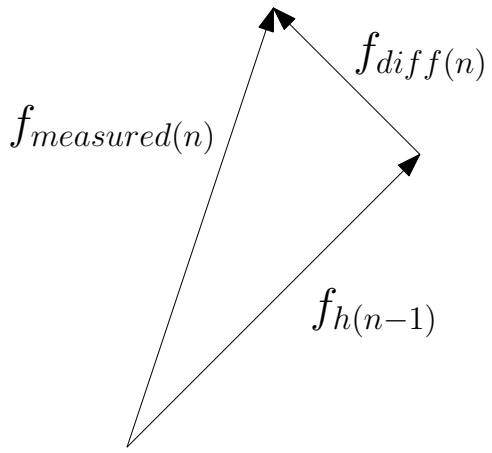

Figure 3.18: Error between commanded force and output force

This is the simplest of the three actuation schemes presented here, but it will be used as the base for the following two. In all three, the force felt by the user will be represented as a virtual spring, but the closed-loop and dynamic compensating control schemes will include an extra term.

3.2.2 Closed-Loop

Not much more complicated than the basic feedback, the closed-loop scheme uses the measured input force to close the loop with respect to force generation. In time step n, the commanded force $\vec{f}_h$ from time step $n-1$ which will be called $\vec{f}_{h(n-1)}$ is compared to the actual force measured at the handle, called $\vec{f}_{measured(n)}$ or $\{F_x, F_y\}$. The difference in the two, $\vec{f}_{diff}$ is then subtracted from the desired $\vec{f}_{coupling}$ for time step n and the corrected force is displayed to the user. The coupling force $\vec{f}_{coupling}\}$ is still defined as before by Eqns. 3.14 and 3.15. Equations 3.16 and 3.17 rigorously define these relationships and Figs. 3.18 and 3.19 show it in vector form.

$$\vec{f}_{diff(n)} = \vec{f}_{measured(n)} - \vec{f}_{h(n-1)} \tag{3.16}$$

$$\vec{f}_{h(n)} = \vec{f}_{coupling(n)} - \vec{f}_{diff(n)} \tag{3.17}$$

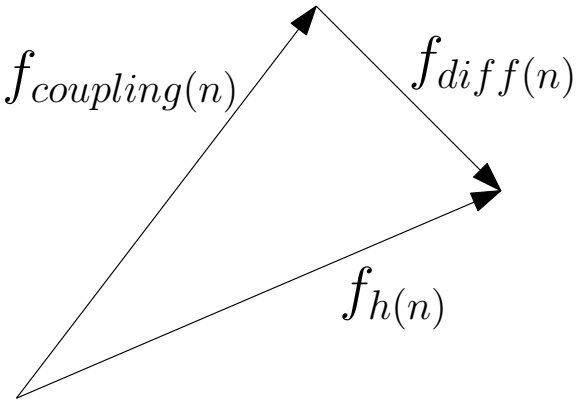

Figure 3.19: Corrected commanded force

In theory, this simple closing of the loop will compensate for any imperfections in the system. The assumption remains that the difference between $\vec{f}_h$ and $\vec{f}_{h(n-1)}$ is relatively small and that the state of the system (both velocity and position) has not changed significantly between time step $n-1$ and n. Under these assumptions, the simple error feedback will be able to compensate for friction in the system, as well as the system dynamics and any other non-ideal system behavior with minimal cost to the system. The simple calculations add basically no extra load to the control system.

3.2.3 Dynamic Compensating Controller

Most active haptic devices use some form of dynamic compensation to increase the transparency of the system. The control system can actively negate the dynamics of the master device within certain ranges of input allowing the user to feel only the forces from the virtual or remote environment, effectively making the master transparent.

Passive devices do not have this luxury over a broad range of states due to the fact that they cannot violate their own hardware-enforced passivity. Figure 3.20 shows a two link device. If a constant endpoint velocity lies anywhere within the region labeled "passive dynamic compensation possible," it is possible for a passive actuator at the

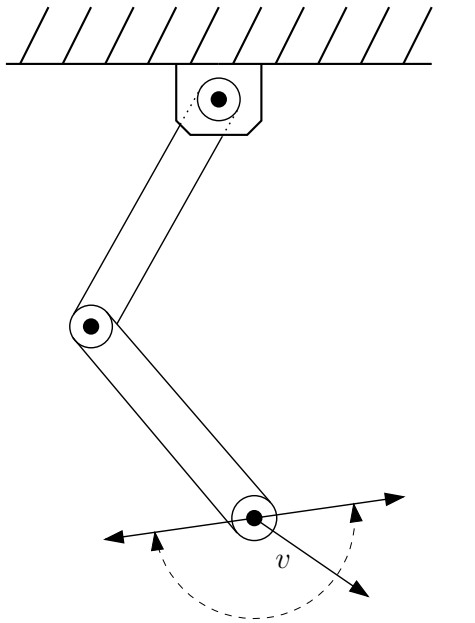

Figure 3.20: Passive dynamic compensation

elbow joint to produce a torque that compensates for the centripetal component of the dynamic forces generated by the second link.

Using the principal of transparency as a basis, a component is included in the calculation of the haptic force to be displayed to the user that compensates for a portion of the dynamics of the device. Effectively, the commanded force would be using the dynamic forces felt by the user as part of the haptic force to be displayed. If the calculated dynamic force is a good approximation of the dynamics of the device, by subtracting the dynamic force from the coupling force the user then feels a force that is actually closer to what the coupling force would be without the master dynamics. This in turn increases the transparency of the device, making it more able to display forces without the user feeling its dynamics.

A human user interacting with a haptic device has a bandwidth with a maximum of approximately 5Hz. Furthermore, a stiff passive device tends to have a good amount of mass. Therefore, for the calculation of the dynamic forces felt by the user,

an assumption has been made that the dynamic forces can be well approximated by assuming that the known velocity is constant. In an implementation sense, this allows the dynamics to be calculated as a simple algebraic equation without having to run an online, real-time simulation.

The constant velocity assumption is valid for two main reasons. First, estimation of the velocity yields a somewhat noisy signal; however estimation of acceleration yields a very noisy signal, unacceptable for use in control calculations. Furthermore, the assumption of constant velocity focuses the control calculations on coriolis and centripetal forces, the less intuitive components of the dynamic forces. As a user interacts with a haptic device, he or she expects to feel the inertia. However, coriolis and centripetal forces tend to be more difficult to intuitively understand. These justifications led to the assumptions of constant velocity for the control calculation.

Typically, the system of dynamic equations for a device would take the form of Eqn. 3.18. The term q represents the generalized coordinates of the system, M represents the equivalent mass or inertial matrix, V represents the non-linear terms and terms that are a function of the derivatives of q such as the coriolis and viscous damping, G represents forces based only on the configuration of the device such as gravity, and Q represents the generalized forces or inputs to the system.

$$M(q)\,\ddot{q} + V(q,\dot{q}) + G(q) = Q \tag{3.18}$$

For a device having more generalized coordinates than independent degrees of freedom, an appropriate derivation of the dynamics would include constraint equations and Lagrange multipliers. Assuming that the dynamics are in the form of Eqn. 3.19 where A & $\dot{A}$ come from the constraint equations, and λ are the Lagrange multipliers.

$$\begin{bmatrix} M(q) & -A^T(q,\dot{q}) \\ -A(q,\dot{q}) & [0] \end{bmatrix} \begin{bmatrix} \ddot{q} \\ \lambda \end{bmatrix} = \begin{bmatrix} Q - V(q,\dot{q}) - G(q) \\ \dot{A}(q,\dot{q})\,\dot{q} \end{bmatrix} \tag{3.19}$$

Rearranging the system of equations yields Eqn. 3.20.

$$\begin{bmatrix} \ddot{q} \\ \lambda \end{bmatrix} = \begin{bmatrix} M(q) & -A^T(q,\dot{q}) \\ -A(q,\dot{q}) & [0] \end{bmatrix}^{-1} \begin{bmatrix} Q - V(q,\dot{q}) \\ \dot{A}(q,\dot{q})\,\dot{q} \end{bmatrix} \tag{3.20}$$

In an implementation sense, the independent generalized coordinates will be measured, and the dependent generalized coordinates can be calculated using the constraint equations. Approximating the $\dot{q}$ terms, assuming no torques at the joints of a system, and assuming a constant cartesian velocity $\dot{x}, \dot{y}$, the system of equations can be solved for an endpoint force F_x, F_y. This force will be referred to as $\vec{f}_{dynamic}$.

Using $\vec{f}_{dynamic}$, the control can compensate for the dynamics of the system just as $\vec{f}_{diff}$ is used in the closed loop controller. Combining this with Eqns. 3.14 and 3.15 gives the new definition of $\vec{f}_h$ shown in Eqns. 3.21 and 3.22.

$$\vec{f}_h = K * (p_s - p_m) - \vec{f}_{dynamic} \tag{3.21}$$

$$\vec{f}_h = \vec{f}_{coupling} - \vec{f}_{dynamic} \tag{3.22}$$

The preceding equations and control systems will be applied to MR PTER and implemented in the testbed described in the following chapters and appendices.

CHAPTER IV

TESTBED

While the preceding section used MR PTER as an example to discuss the control schema developed for providing haptic feedback with a passive master, this section will more specifically address the the entire testbed (including MR PTER) and the systems used to evaluate the controllers.

4.1 Master Device

While the research focuses on passive haptic devices, the question will invariably arise as to how the passive device compares to an active device. Therefore as part of the testbed used in this research, there will be a second master device, a commercially available active device. This section will begin by fully discussing the passive master and will then briefly discuss the active device.

4.1.1 MR PTER

Figure 4.1 again shows a line drawing that illustrates the two degree of freedom (DOF) 5-link manipulator developed in previous research by Reed & Book [73] [74]. The current configuration of the device has joints A & B fixed to the base of the device so that they are co-axial, making the 5-link device have one link of length zero. As previously stated, this device will be used as the haptic master to test the control algorithms developed in the preceding chapter.

The two base joints, A & B as well as joint E are actuated using LORD magneto-rheological brakes (MRB-2107-3). Figure 4.1 illustrates the brakes as larger circles at the joints. Note that the device is reconfigurable and moving joints A & B so that they are no longer co-axial would allow for the addition of a fourth MR brake at joint

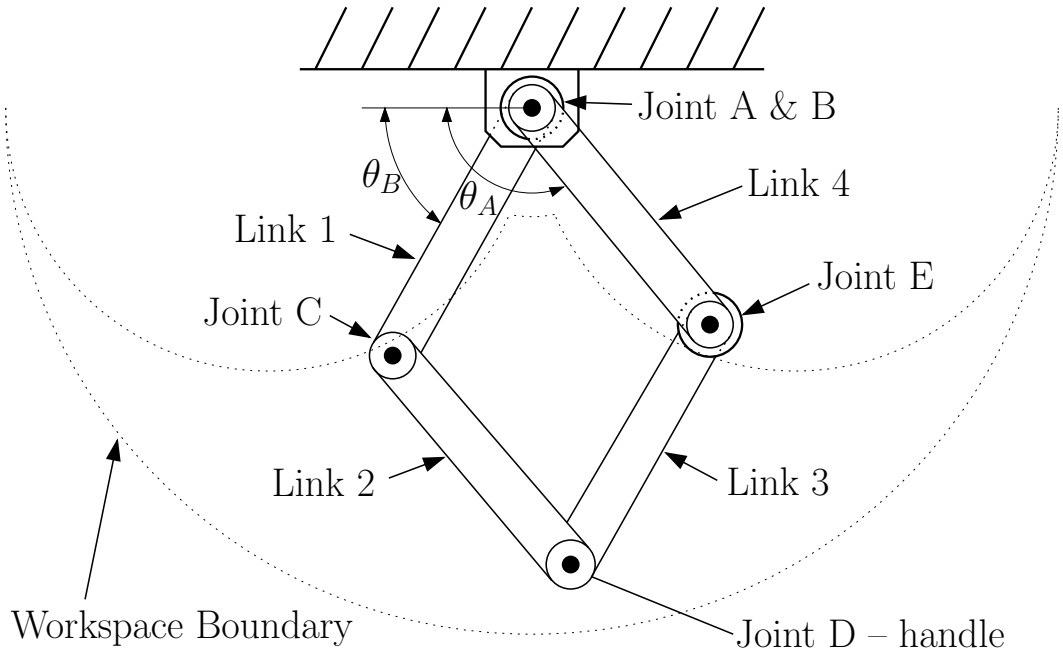

Figure 4.1: Line-drawing of MR PTER

C. In the setup used for this research, the brake at joint C has been replaced by an aluminum spacer, an axle and bearings to maintain the shape of the device and to minimize the friction at the un-actuated joint. Similarly, joint D and the handle have bearings installed to minimize friction. In his previous research, Reed spent a good amount of effort characterizing the MR brakes used in the device. He found the rise time of the brakes to be in the range of 5ms [73] [74].

Position feedback of the system is provided by two Dynamics Research Corporation HS30C176B15M5000 Quadrature Optical Encoders, one located at each of the joints A & B. The resolution approaches 50,000 counts through the angular region of the workspace. The encoders measure the angles shown in the figure as θ_A and θ_B.

Force information is obtained by using an ATI Gamma Force/Torque sensor that connects between the endpoint of the device and the handle. The force sensor interfaces with the control system through the analog output of its amplifier box. The PXI hardware reads the analog values for the two planar directions of force within

each iteration of the control loop.

As discussed in the control chapter, the passive actuators cannot compensate for the majority of the dynamic forces. Therefore to try to compensate physically for some of the dynamics, MR PTER has been significantly lightened by machining out large volumes of each link. A simple model of the device was used to calculate a maximum deflection of $\frac{1}{8}$ when loaded with 30lbs. The links were then machined out to look like an I-beam with a $\frac{1}{4}$in fillet where the $\frac{3}{16}$in web meets the $\frac{3}{8}$in flange of the I-beam. The final mass and inertia properties of the links used in the controller can be found in Table A.1.

4.1.1.1 Kinematics

Using MR PTER with co-axial base joints as in Fig. 4.1 with equal link lengths greatly simplifies the kinematic equations of the device. With these constraints, the translation between joint space and cartesian space takes the relatively simple form or Eqns. 4.1 and 4.2.

$$x = Lcos(\theta_A) + Lcos(\theta_B) \tag{4.1}$$

$$y = Lsin(\theta_A) + Lsin(\theta_B) \tag{4.2}$$

Differentiation of the relationship between cartesian and joint space yields the relationship between the cartesian velocity of the endpoint and the joint velocities shown in Eqns. 4.3 and 4.4.

$$\dot{x} = -Lsin(\theta_A)\dot{\theta}_A - Lsin(\theta_B)\dot{\theta}_B \tag{4.3}$$

$$\dot{y} = Lcos(\theta_A)\dot{\theta}_A + Lcos(\theta_B)\dot{\theta}_B \tag{4.4}$$

Substituting the relationship between θ_A, θ_B & θ_E from Eqn. 4.5 yields a relationship between each of the joint velocities and the cartesian endpoint velocity. Using that, the Jacobian can be developed in the form of Eqn. 4.6.

$$2\pi = \theta_A - \theta_B + \theta_E \tag{4.5}$$

$$\dot{x} = J\dot{\theta} \tag{4.6}$$

The non-square Jacobian for MR PTER (non-square due to the fact that there are more joints than degrees of freedom), is broken into two square Jacobian matrices shown in Eqns. 4.7 & 4.8, the elements and complete derivations of which can be found in Appendix A.

$$\begin{bmatrix} \dot{x} \\ \dot{y} \end{bmatrix} = [J_{AB}] \begin{bmatrix} \dot{\theta_A} \\ \dot{\theta_B} \end{bmatrix} = \begin{bmatrix} J_{ABx} & J_{BAx} \\ J_{ABx} & J_{BAy} \end{bmatrix} \begin{bmatrix} \dot{\theta_A} \\ \dot{\theta_B} \end{bmatrix} \tag{4.7}$$

$$\begin{bmatrix} \dot{x} \\ \dot{y} \end{bmatrix} = [J_{AE}] \begin{bmatrix} \dot{\theta_A} \\ \dot{\theta_E} \end{bmatrix} = \begin{bmatrix} J_{AEx} & J_{EAx} \\ J_{AEx} & J_{EAy} \end{bmatrix} \begin{bmatrix} \dot{\theta_A} \\ \dot{\theta_E} \end{bmatrix} \tag{4.8}$$

4.1.1.2 Dynamics

Previous research using MR PTER defined the system using 10 generalized coordinates [74]. So as to simplify the controller calculations, the system has been redefined using 5 generalized coordinates shown in Fig. 4.2 and Eqn. 4.9 and one input to the system for each generalized coordinate as represented by the generalized forces in Eqn. 4.10. This still leaves an over-constrained system having 2 independent generalized coordinates and 3 dependent generalized coordinates. Three constraint equations, Eqns. 4.11, 4.12 & 4.13, define the relationships between the 5 generalized coordinates.

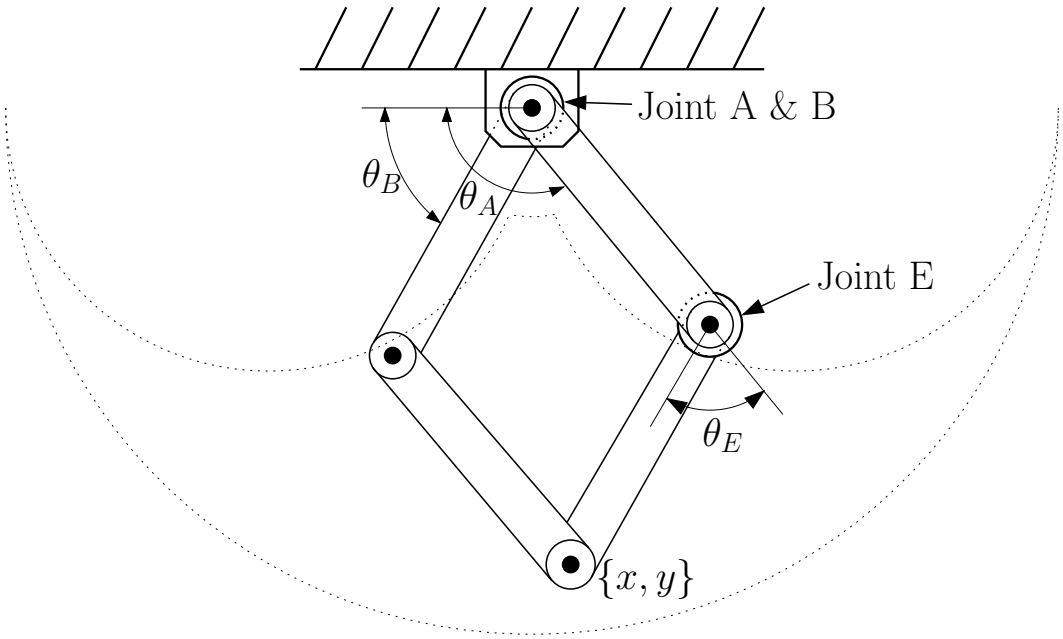

Figure 4.2: Generalized coordinates of MR PTER

$$q = \{x, y, \theta_A, \theta_B, \theta_E\} \tag{4.9}$$

$$Q = \{F_x, F_y, \tau_A, \tau_B, \tau_E\} \tag{4.10}$$

$$C_1 \Rightarrow Lcos(\theta_A) + Lcos(\theta_B) - x = 0 \tag{4.11}$$

$$C_2 \Rightarrow Lsin(\theta_A) + Lsin(\theta_B) - x = 0 \tag{4.12}$$

$$C_3 \Rightarrow 2\pi - \theta_A + \theta_B - \theta_E = 0 \tag{4.13}$$

The dynamics will be defined using the form of Eqn. 4.14 which is developed by using the Lagrange approach with constraint equations, the derivation of which can be found in Appendix A.

$$\begin{bmatrix} M(q) & -A^T(q,\dot{q}) \\ -A(q,\dot{q}) & [0] \end{bmatrix} \begin{bmatrix} \ddot{q} \\ \lambda \end{bmatrix} = \begin{bmatrix} Q - V(q,\dot{q}) - G(q) \\ \dot{A}(q,\dot{q})\,\dot{q} \end{bmatrix} \tag{4.14}$$

The equivalent mass matrix M is a function of the generalized coordinates. The matrix A and its derivative $\dot{A}$ come from the constraint equations using Eqn. 4.15. All of the non-linear terms and terms not multiplied by $\ddot{q}$ are grouped into V, and since there are no gravity terms, G can be neglected.

$$A_{ij} = \frac{\partial C_i}{\partial q_j} \tag{4.15}$$

All of these matrices can be evaluated relatively easily at each step of the control system. For a complete derivation of the dynamic equations as well as the values of each of the matrices, please see Appendix A.

4.1.1.3 Simulation

A full simulation of the system that included human, master dynamics, master-slave communication, slave dynamics, slave-master communication and force feedback was begun; however after a good amount of work, the full simulation was abandoned. Simulation of the communication provided the first sticking point and was originally modeled as a simple one time step delay, but that was an over simplification. The human-master interaction provided the final section that led to the abandonment of a full simulation.

As reported by Tognetti who collected a list of human dynamic models for his thesis [83], there exists a broad range of ways to model the human driver in a haptic system. In his research he also presented and validated a new model significantly different from the others he reported; a summary of this can be found in Table 5.1. All of these models assume that the human is either trying to move in a specific way or that the operator is trying to resist motions of the haptic system. Either of these approaches neglects the cognition of the human operator.

Producing a fully robust model of the entire system would require a model of human cognition. When the operator feels the feedback from the master device the human response depends on the task, prior training, the operator's mood, fatigue level and many other variables. This difficulty is especially important for a passive device because if the haptic master is being controlled based on position (as is the control scheme being presented here), the human closes the loop and provides the motion of the master device.

All of this said, portions of the system definitely need to be simulated to validate the controller before implementing it in a human-factors test. The behavior of the slave device can easily be verified by observing its motion and response to known inputs. The communication delays which will be directly addressed in a subsequent section are assumed to be constant and smaller than the period of the control loop. However, the dynamic model of the system requires validation before implementation. Developed using the preceding approach and implementing the physical parameters in Table A.1 in the full equations of motion listed Appendix A, the dynamic equations take the form of a system of differential algebraic equation (DAEs).

LabVIEW's Simulation Toolkit combined with the LabVIEW MathScript feature allows for an easy simulation of the DAEs. The code used for the simulation can be seen in Appendix B. Note that the simulation uses both graphical and text-based coding of the equations. Also note that the code calculates the initial conditions of the dependent generalized coordinates based on the independent generalized coordinates.

4.1.1.4 Control System

The system is controlled using a National Instruments (NI) PXI compact, ruggedized computer. The PXI-8175 controller being used operates under LabVIEW Real Time OS and runs on a Pentium III 866MHz processor with 512MB of RAM. Certain portions of the results were gathered while the system was not running in real-time.

For those tests, similar code was running under WindowsXP and was programmed using LabVIEW 7.1.

Analog and Digital I/Os are run through a PXI-6070E DAQ card, and the encoder signals are pre-processed using a US Digital LS7084. The chip eases the processing of the encoder signal by decoding the encoder channel A and channel B signals. It then sends a direction and step signal to a dedicated counter channel on the PXI-6070E card. The three MR brakes require the use of an extra analog output card, PXI-6711, and external Advanced Motion Controls 12A8 PWM amplifiers powered by an Advanced Motion Controls PS4X300W Power Supply.

The event-based control of the master is achieved using LabVIEW RT. A prioritized, asynchronous multi-threaded control structure has been developed to separate the communications threads from the threads that control the system. This provides a more stable real-time application. The same architecture was developed both under LabVIEW RT and under LabVIEW for WindowsXP; however the application running under LabVIEW RT produces more deterministic results than one running under WindowsXP.

4.1.2 Application of Control Algorithms

Possibly the most important section of the testbed discussion with regard to the research presented here focuses on the application of the control principles developed in the previous section specifically to the hardware of MR PTER. The overall flow of information can be seen in Fig. 4.3. The forces measured by the ATI sensor are represented as F_1 and F_2. A transformation matrix takes the force value as well as the angles of the base joints θ_A & θ_B and shifts those variables into the cartesian workspace fixed to the base yielding F_x, F_y, x & y. An estimator calculates a value for the endpoint velocities $\dot{x}$ & $\dot{y}$. The controller takes these values as well as the position information from the slave, x_s & y_s, and calculates a brake actuation V_1,

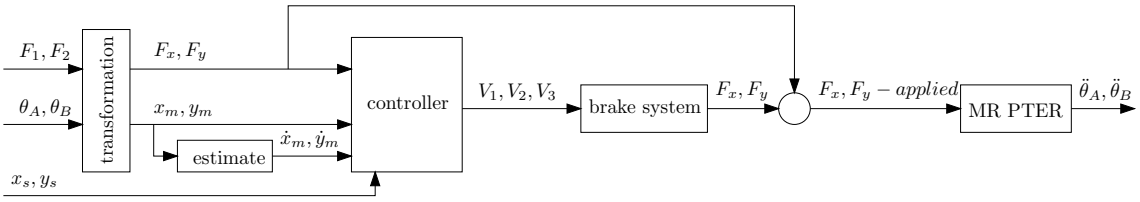

Figure 4.3: Controller information flow

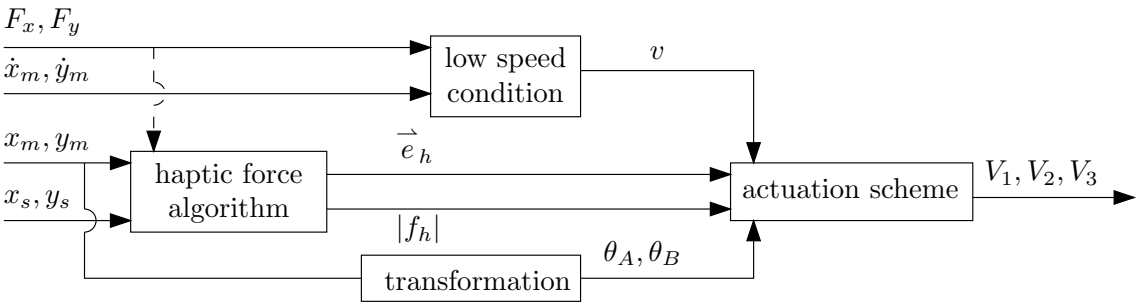

Figure 4.4: Expanded view of the controller

V_2 & V_3 that represent voltages applied to the MR brake controllers. The resultant forces of the actuation as well as the user input are applied to MR PTER and an acceleration of the system results.

An expanded portion of the controller can be seen in Fig. 4.4. The block labeled "haptic force algorithm" has the responsibility of calculating the haptic force and is dependent on the position of the master and the slave ($\{x_m, y_m\}$ and $\{x_s, y_s\}$) and the estimated velocity of the master $\{\dot{x}_m, \dot{y}_m\}$. Also, if using the dynamic compensating controller, the input force, $\{F_x, F_y\}$ becomes an input when calculating the force to be displayed $\vec{f_h}$, hence the dashed line. To facilitate the calculations of the actuation scheme, the controller breaks vector quantity $\vec{f_h}$ into its magnitude $|f_h|$ and its direction $\vec{e}_h$.

After some of the early testing, the "low speed condition" block was added to the controller. Before that, the control system became indeterminate when the endpoint velocity approached zero. Looking back to the controller section and specifically

the definition of the forces produced by each brake, as the velocity in Fig. 3.3 approaches zero, the control scheme can no longer discriminate between producible and non-producible forces. When the velocity drops below a specified threshold, the controller from using the endpoint velocity and uses the direction of the input force to approximate velocity.

Looking at the device as a static system, the force at the handle functions in the controller just as the velocity would in a dynamic system. The passive nature of the device means that it can only provide a reaction force to the input of the user. Exactly as if the device were resisting motion, the direction of the input force defines the direction of force that each of the brakes can produce.

4.1.2.1 Virtual Coupling

To insure that the workspace of the master (variables denoted by a subscript "m") and the slave (variables denoted by a subscript "s") match, the control system has to scale and shift either the workspace of the master or the slave. However, to facilitate the calculation of the force to be displayed, the shifting and scaling follow Eqns. 4.16 & 4.17 where the "bar" values shift the axes and the s scales between the workspaces. Note that the x & y values are scaled by the same amount so that the aspect ratio of coordinate systems remain the same.

$$\hat{x}_s = s * (x_s + \bar{x}) \tag{4.16}$$

$$\hat{y}_s = s * (y_s + \bar{y}) \tag{4.17}$$

After shifting and scaling the coordinate systems, the magnitude of the haptic force $|f_h|$ is proportional to the difference between the position of the master and the slave and can be calculated from Eqn. 4.18.

$$|f_h| = |f_{coupling}| = K * \sqrt{(x_m - \hat{x}_s)^2 + (y_m - \hat{y}_s)^2} \tag{4.18}$$

The direction of the haptic force to be generated, $\vec{e}_h$ gets calculated in the control algorithm using Eqn. 4.19.

$$\vec{e}_h = \vec{e}_{coupling} = \arctan \frac{y_m - \hat{y}_s}{x_m - \hat{x}_s} \tag{4.19}$$

As in the chapter about the theory of the controller, the next two controllers are based on a virtual coupling with an added term.

4.1.2.2 Closed Loop

When closing the loop in the haptic force calculation with respect to the input of the force sensor, the displayed haptic force takes the form from Eqn. 3.17. In practice, the magnitude of the virtual coupling force takes the form of Eqn. 4.20 and the direction $\vec{e}_h$ takes the form of Eqn. 4.21.

$$|f_h| = \sqrt{(|f_{coupling}| - |f_{diff}| cos(\vec{e}_{diff} - \vec{e}_h))^2 + (sin(\vec{e}_{diff} - \vec{e}_h))^2} \tag{4.20}$$

$$\vec{e}_h = \vec{e}_{coupling} - \arctan \left(\frac{|f_{diff}| sin(\vec{e}_{diff} + \vec{e}_{coupling})}{|f_{coupling}| - cos(\vec{e}_{diff} - \vec{e}_{coupling})} \right) \tag{4.21}$$

4.1.2.3 Dynamic Compensating

Like the closed loop controller applied in the previous section, the dynamic compensating controller starts with the basic coupling force $\vec{e}_{coupling}$ and following with Eqn. 3.14 & 3.15. However instead of compensating with a feedback term, the dynamic compensating controller subtracts a calculated dynamic force from the coupling force. The system of equations takes the previous form of Eqn. 3.19.

In practice the dynamic compensation controller makes the assumptions of Eqn. 4.22. Therefore in the dynamic equations shown in Eqn. 3.20 the only unknowns are $\left\{\ddot{\theta}_A, \ddot{\theta}_B, \ddot{\theta}_E, F_x, F_y\right\}$, the state velocities $\{\dot{q}\}$, and the Lagrange multipliers $\{\lambda_1, \lambda_2, \lambda_3\}$.

However estimation of the derivatives of the independent variables $\dot{x}$ & $\dot{y}$ in the controller makes it possible to also calculate the values of $\dot{\theta}_A$, $\dot{\theta}_B$ & $\dot{\theta}_E$. This leaves a solvable algebraic system of equations and unknowns.

$$\ddot{x} = \ddot{y} = \tau_A = \tau_B = \tau_E = 0 \tag{4.22}$$

Rearranging the dynamic equations yields an equation for $\{F_{x-D}, F_{y-D}\}^T$ in the basic form of Eqn. 4.24, the specific equations and derivation see the controller section of Appendix A. The cartesian components, F_{x-D} and F_{y-D} yield the resultant vector force from the earlier theoretical derivation of $f_{dynamic}$ as defined by Eqn. 4.23 where $\vec{i}$ and $\vec{j}$ represent the cartesian unit vectors.

$$\vec{f}_{dynamic} = F_{x-D}\,\vec{i} + F_{y-D}\,\vec{j} \tag{4.23}$$

$$F_{x-D} = f(\theta_A, \dot{\theta}_A, \theta_B, \dot{\theta}_B) \tag{4.24}$$

After having found the dynamic forces $\{F_{x-D}, F_{y-D}\}$, the steps to calculating $\vec{f}_h$ follow the same steps as before. Equation 4.25 shows the calculation of $|f_h|$ and Eqn. 4.26 shows the calculation of $\vec{e}_h$.

$$|f_h| = \sqrt{(F_{x-D} + |f_{coupling}| cos(\vec{e}_{coupling}))^2 + (F_{y-D} + |f_{coupling}| sin(\vec{e}_{coupling}))^2} \tag{4.25}$$

$$\vec{e}_h = \arctan\left(\frac{F_{y-D} + |f_{coupling}| sin(\vec{e}_{coupling})}{F_{x-D} + |f_{coupling}| cos(\vec{e}_{coupling})}\right) \tag{4.26}$$

Implementation of the dynamic compensator should allow the control system to utilize the dynamics of the system to its advantage. Doing so will also increase the transparency of the MR PTER even though the passive device cannot entirely compensate for its own dynamics.

To gain a better understanding of the magnitude of the dynamic force in relationship to the coupling force, representative data has been pulled from the final test experiment to calculate $\vec{f}_{coupling}$ and $\vec{f}_{dynamic}$. The assumption will be made that the device is operating in the middle portion of the workspace such that the position can be described by Eqn. 4.27.

$$\begin{aligned} \theta_A &= \tfrac{3\pi}{4} \\ \theta_B &= \tfrac{\pi}{4} \end{aligned} \tag{4.27}$$

Data collected from the tests shows that an x and y endpoint velocity shown in Eqn. 4.28 would not be unreasonable.

$$\begin{aligned} \dot{x} &= 100(cm/s) \\ \dot{y} &= 50(cm/s) \end{aligned} \tag{4.28}$$

Also the difference in master and slave position found in Eqn. 4.29 would not be unreasonable in the testbed.

$$\begin{aligned} x_m - \hat{x}_s &= -0.346(cm) \\ y_m - \hat{y}_s &= 0.08(cm) \end{aligned} \tag{4.29}$$

Given those values, the following values in Eqn. 4.30 would be $\vec{f}_{coupling}$ and $\vec{f}_{dynamic}$ with the physical parameters of MR PTER shown in Table A.1 as well as a virtual coupling value of $K = 2.5$.

$$
\begin{aligned}
|f_{coupling}| &= 0.887N \\
\vec{e}_{coupling} &= -.227(rad) \\
|f_{dynamic}| &= 0.283N \\
\vec{e}_{dynamic} &= 0.796(rad)
\end{aligned} \tag{4.30}
$$

The position and velocities in this example may be contrived and might not make complete physical sense; however they do represent real possibilities with respect to magnitude. Regardless, with those values the calculated dynamic force obviously impacts the force felt by the user and the force displayed by the controller.

4.1.3 PHANTOM

A PHANTOM Premium 1.0 shown in Fig. 4.5 provides an alternate master device to yield a solid comparison between the passive device and its active counterpart. Using the PHANTOM SDK and adapting communication code written by Matt Kontz [47], the PHANTOM can easily interface with the LabVIEW controlled devices using internet based communication. The choice of the Phantom 1.0 was made in an attempt to approximately match the workspace of the active device with the workspace of MR PTER. Even though the PHANTOM is a 3 DOF device, constraining it to a single plane in the middle of its workspace produces usable workspace approximately $2\frac{2}{3}$ the size of the workspace of MR PTER.

The PHANTOM control system consists of a PCI parallel card installed in a WindowsXP computer that communicates with the PHANTOM control box. The programming and control software run under WindowsXP and update the device's set point at 1KHz.

The feedback provided by the PHANTOM takes the same virtual spring coupling form as Eqn. 4.18, however unlike MR PTER the active actuators of the PHANTOM

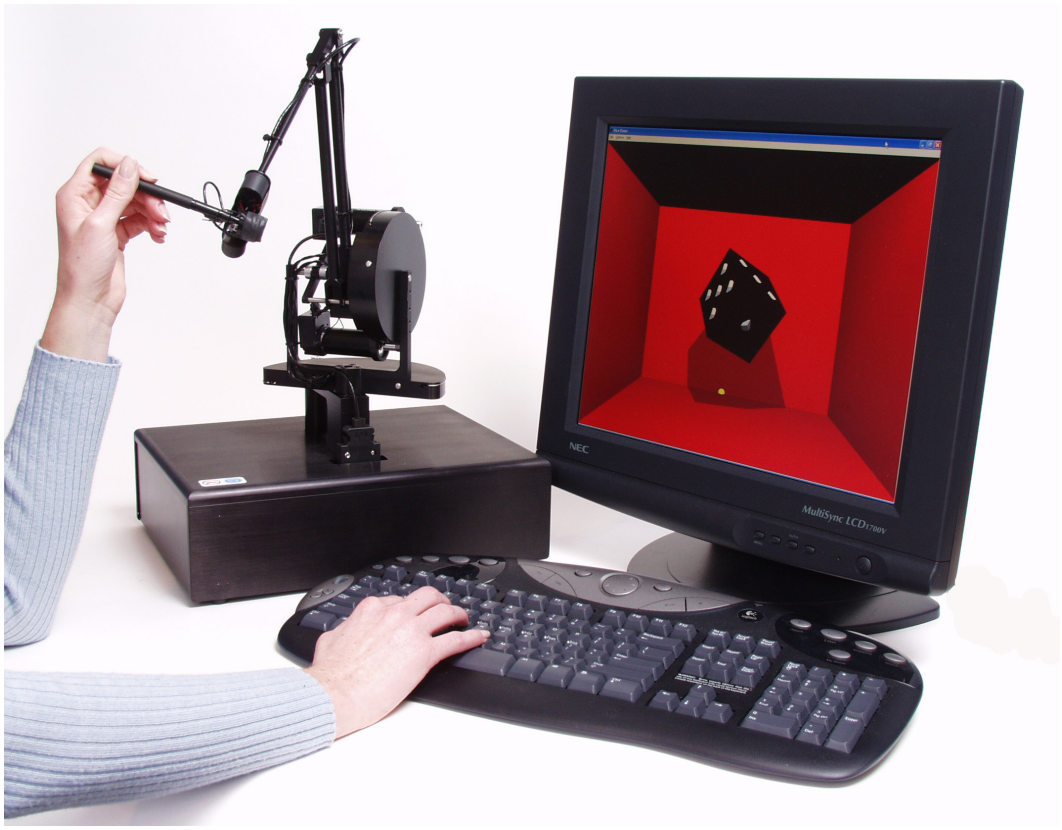

Figure 4.5: Image of PHANTOM haptic interface

restore the user to zero virtual spring displacement, actively driving the difference between the position of the master and slave to zero. Just as with MR PTER, the control system of the PHANTOM shifts and scales the workspace to better match the workspace of the slave device. However to maintain stability of the active human-master-slave system, the virtual spring constant K is significantly lower for the control system of the PHANTOM than for the controller used with MR PTER.

4.2 Slave Device

The research presented here uses two different slave devices. The first device (a linear motor) maps the 2 DOF workspace of the master onto a single DOF slave device. The research then expands to using a 2 DOF slave device whose workspace and kinematics better match those of the master. Both of the devices provide useful

Figure 4.6: Photograph of linear motor testbed

information regarding the teleoperation system, the details of which will be discussed in the next chapter which covers testing. The following section will describe each piece of hardware and its control system.

4.2.1 Linear Motor

The first step of assembling the teleoperation system includes a linear motor as the slave device. The single DOF device was originally intended only to be used briefly as a stepping stone on the way to a more realistic system. However, the use of the single DOF slave produces interesting similarities between the teleoperation scenario and previous research in the IMDL using passive haptic devices. Constraining the master to the 1-D workspace of the slave yields teleoperation similar to previous velocity field controllers applied to the passive system [73][81]. The results generated using the linear motor and their comparison to the velocity field controllers will be discussed in the following chapter on testing.

4.2.1.1 Hardware

The linear motor being used as a slave device is an Anorad linear motor and amplifier and can be seen in the background of Fig. 4.6. A Reinshaw micron-resolution encoder provides position feedback from the device, and is pre-processed using a US Digital LS7084 chip exactly like the one used in MR PTER. This high resolution encoder at 1x processing produces approximately 375,000 counts through the workspace of the device.

4.2.1.2 Control System

The linear motor slave device is controlled by a "headless" NI PXI-8145 RT with a 266MHz Pentium Processor. The feedback and analog output to control the motor go through a PXI-6070E data acquisition board. Using feedback from the linear motor's encoders, the controller runs a PD loop under LabVIEW Real Time. The set point for the PD control is received from the master via an ethernet connection (designed to use either TCP/IP or UDP/IP). Similarly, the ethernet connection is used to send the slave position information back to the master controller to calculate the feedback to be displayed to the user.

4.2.2 HuRBiRT

Developed by Book and Love [58] and used most recently by Tognetti [83], the Human Robot Bilateral Research Tool (HuRBiRT) makes a suitable slave device to be used for the research presented here. Figure 4.7 shows a line drawing of the device.

4.2.2.1 Hardware

Originally designed with the concept of being an "athletic trainer," HuRBiRT has had many lives as a research device in the IMDL. The current iteration of the device was constructed by Love and has most recently been used by Tognetti to explore two-port network theory [58] [83].

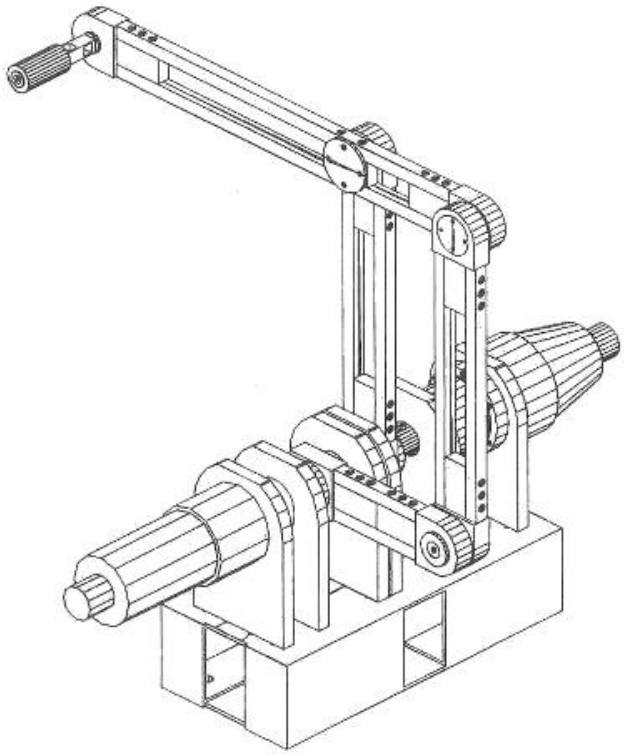

Figure 4.7: Line drawing of HuRBiRT

Table 4.1: Settings for using HuRBiRT with NI PXI-7344 hardware

Subject		Axis 1	Axis 2
Trajectory Settings	velocity $\left(\frac{counts}{sec}\right)$	$2 * 10^7$	$2 * 10^6$
	acceleration $\left(\frac{counts}{sec_2}\right)$	$5 * 10^7$	$8 * 10^6$
	following error (counts)	$3.2 * 10^4$	$3.2 * 10^4$
Control Settings	K_P	18	10
	K_D	1000	1050
	K_I	2	3

4.2.2.2 Control System

In the research presented here, the same basic control system used for the linear motor is used to control HuRBiRT. The control hardware consists of a "headless" NI PXI-8145 RT with a 266MHz Pentium Processor. However unlike the control of the linear motor, the decision was made to control HuRBiRT using a National Instruments dedicated 4-axis motion control card, PXI-7344, connected through an NI UMI-7764 interface box. The card uses dedicated motion control hardware to achieve low-level control. With HuRBiRT's motors connected to Axis 1 & Axis 2, and the encoders connected to the corresponding axes, Table 4.1 shows the controller gains and other pertinent information.

For more information on the specifics of the hardware setup (including the specifications for the motors, power supplies, gear ratios, encoders, and limit switch system) see the theses of Love or Tognetti [58] [83].

4.3 Communication Protocols

One of the primary reasons that LabVIEW was chosen as a platform for this research centered around the fact that as a programming language, it contains built in blocks for handling internet-based communication. The first versions of LabVIEW used for the research (LabVIEW 7.0 and 7.1) included simple blocks to handle TCP/IP and

UDP/IP communication. However with the upgrades to LabVIEW 8.0 and 8.2, a new communication protocol was available, NI's Shared Variable data type.

4.3.1 TCP and UDP Communication

Early testing presented in the next chapter will compare the TCP/IP and UDP/IP communications protocols as implemented within LabVIEW and on the Georgian Institute of Technology local network (specifically that of the Love Building). Typically control applications utilize UDP/IP communication over TCP/IP communication. The handshaking and error correcting built into the TCP/IP protocol mean that it takes longer to transfer data between two computers than if UDP/IP were used. However, without the handshaking and error checking, UDP/IP risks loss of packets or corruption of packets. Regardless, the benefits of increasing speed typically outweigh the possible difficulties caused by lost packets.

With respect to implementation, it is important to note that the NI blocks have built in buffers for TCP/IP and UDP/IP communication. For most applications this might be very appropriate; however for a control application such as the ones presented here, the buffers can cause a noticeable delay if not handled properly. An effective way for decreasing the buffer or even removing the buffer could not be found, so to overcome the problem, the control code listens to the TCP/IP or UDP/IP port at a higher rate than the other computer writes to it.

If the receiving computer pulls data off the TCP/IP or UDP/IP buffer stack at a slower rate than the sending computer adds information to the stack, then the stack will build up and the delay between the two computers will constantly grow. If instead the receiving computer pulls data off the stack more quickly than the sending computer adds to the stack, there will never be any build up of information. Even if there were some delay at the system startup, this difference in reading from and writing to the stack quickly re-synchronizes the two systems. Appendix B shows

multiple examples of the communication code used to interface the computers used in the experimentation.

The introduction of the PHANTOM device as a secondary master for testing purposes means that the LabVIEW control code used with the slave device as well as the code running the graphical user interface has to communicate with the PHANTOM control code built in VisualBASIC. For this purpose, UDP/IP provides a perfect solution. In a very basic sense, network-based communication should be able to be blind to the operating systems of the devices on each end of the communication channel. As long as the bits of information are being encoded and decoded properly on each end, the transfer of data flows smoothly. That said, after defining a data structure to communicate position between the master and the slave devices, the implementation of UDP/IP communication performed almost flawlessly.

4.3.2 Shared Variable Data Type

Used for the perception experimentation, National Instrument's Shared Variable data type creates a dedicated TCP/IP or UDP/IP (selectable by the user) channel between two or more computers running LabVIEW code. With respect to implementation, using a shared variable yields by far the simplest code and overall implementation of any of the internet-based communication options. However, due to the fact that much of the specifics of the communication protocol is effectively hidden within a LabVIEW block, using it in a research application makes little sense.

In addition, using a Shared Variable to pass information between master, slave and GUI would be much more difficult (perhaps even impossible) to implement with the PHANTOM controller running under WindowsXP. Even though the Shared Variable would work well to communicate between the multiple computers used in the various experiments (up to three different computers communicating at once), ultimately the need to use the PHANTOM dictated that use of Shared Variables be dropped.

CHAPTER V

EXPERIMENTATION

Due to the complexities of the human-machine interface, true understanding and testing of a haptic system must involve human-factors testing. The research and testing culminates with a Georgia Tech Internal Review Board (IRB) approved 23 person study testing the passive device in teleoperation and comparing it to an active device in three tasks. However, before administering the final test procedure, three smaller tests are completed to better understand the hardware, software and the human's interaction with it.

The first of the tests explores the network-based communication protocols and their performance under LabVIEW. The experiment covers TCP/IP and UDP/IP protocols used on the local network as well as over longer distances. The second section of experiments focuses on simulating the input of a human using a quasi-constant force and subsequently an industrial robotic arm. The final section of the tests before the culminating experiment attempts to define a resolution of human perception of the direction of an arbitrary force. Results and conclusions from the first three portions of testing tie together and impact the generation of the control algorithms for the final test as well as the software used to administer it.

In the final experiment, subjects use both a passive and an active device to teleoperate a remote slave device. The subjects are tested on their ability to feel shapes within the workspace of the slave device as well as their speed in completing two point-to-point motion tasks. While the tests actually compare two specific devices, some of the results can be abstracted to gain a better general understanding of passive devices as compared to active devices.

5.1 Communications Testing

In an attempt to better understand the communications algorithms under LabVIEW, a brief tangential project explores the performance of TCP/IP versus UDP/IP network communications protocols. More specifically, the study focuses on the two protocols operating under LabVIEW operating systems and on NI hardware so that the results can apply directly to the research presented here.

Due to the buffer built into the NI blocks, if the slave loop runs slower than the master loop the behavior of the slave scales with respect to time (a constantly growing time delay). Information from NI's R&D department confirmed that the buffer cannot be programmatically controlled or set. If the master were sending information at 100Hz and the slave were only picking it up off the stack at 80Hz, there would be a constantly growing lag, piling up 20 control inputs per second

Also, the blocking nature of the communication block depends on the structure of the VI (program). By nature, the UDP/IP receive command is non-blocking. Practically that means that if the communication block resides in a loop with something else, then the rest of the code will execute while the UDP/IP waits to timeout or receive information. This can be taken advantage of in the research by structuring the code such that the UDP/IP read initiates at the beginning of the control loop and then everything else in the loop can execute while it waits. Therefore the loop does not wait on the read command. Later iterations of the control code will make take even more advantage of this property by putting the read and write commands in their own threads.

There are however, interesting points about making the TCP communication work properly. Since TCP/IP involves a bi-directional handshaking protocol, the packet size must be known if the receive command is to work properly. The default state of the "read size" variable of the TCP/IP read function block is "0" which causes the program to read constantly and communication breaks. Furthermore, with the

variable being passed ranging from 0-10,000 (loop iteration number) its size did not remain constant. To send, LabVIEW automatically casts the integer as a string, and in doing so stores the variable in a form that ranged between 3 & 5 bits. In later versions of the programming solution, all numbers are cast into a specific structure designed to minimize excess overhead.

To test the speed of communication, a LabVIEW host program sends its iteration number to a target over the network connection and waits for a response from the target. The target receives the number and immediately bounces it back to the host then waits for the next packet to come from the host. In this way, both programs constantly sit and wait then send information as quickly as possible. LabVIEW code for the testing program can be found in Figs. B.5 & B.5 in Appendix B. The programs represent the code for the TCP/IP and UDP/IP portions of the test respectively.

5.1.1 Results - Local Tests

Using the procedure mentioned above and averaging over 70,000 trials, Fig. 5.1 shows the results for data transfer within the Love Building subnet on the Georgia Tech campus. Surprisingly the typical loop rates (communication and whatever processing is required for the send / receive) for the TCP/IP were slightly faster (a statistically significant difference) than those for UDP/IP. Note also that the error bars for standard deviation have been removed from the graph due to the fact that they were small enough to be negligible (on the order of 0.003ms).

Another method for judging the quality of a communication protocol focuses on the worst case execution time (WCET). In a controls sense, implementation of loop rates faster than the WCET value can lead to loops not finishing in time. Figure 5.2 shows the WCET values for the 70,000 on the Love Building subnet.

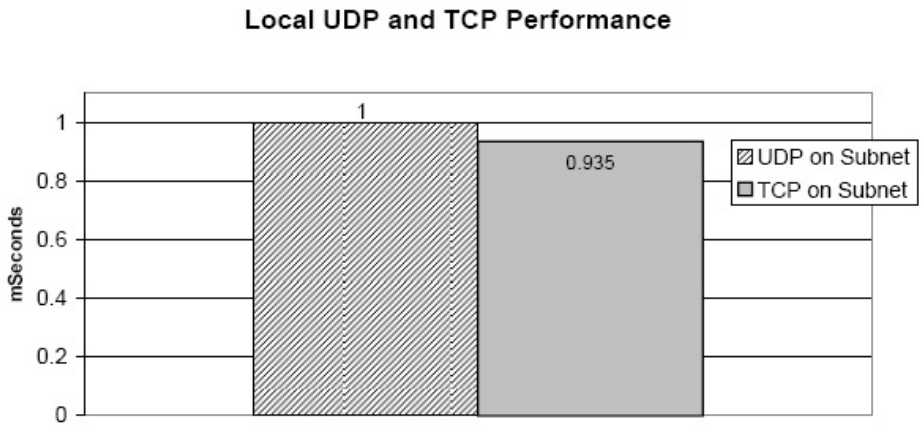

Figure 5.1: Local network communication results

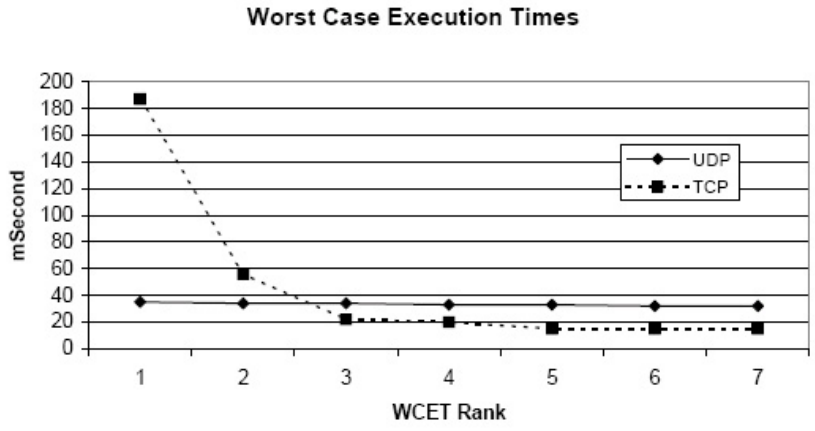

Figure 5.2: Worst case execution time for local test

5.1.2 Results - Off-Campus Tests

Even though the research presented here focuses on teleoperation within a specific subnet so that the effects of time delay and packet loss can be ignored, the testing of network communication protocols was extended to include off-campus sites. The experiment was changed slightly to send a larger more realistic control packet between the two computers; however other than that nothing changed from the local experiment.

Using contacts at Rice University in the Mechatronics and Haptic Interfaces (MAHI) Lab, a computer on Rice's research network acted as a host machine. Also, a contact at National Instruments provided a second computer located in Austin, Texas as another data point. The computer at NI resided on their corporate network that prohibits testing of the UDP/IP protocol. Figure 5.3 shows the results from the off-campus tests. The third column labeled "UDP w/o Missed" represents the data from Rice with dropped packets eliminated. When using the UDP protocol it might be beneficial to set a timeout for the communication block that forced the thread from hanging up, effectively creating this third column. The error bars show the standard deviation from the values listed over the 10,000 iterations.

Again with the off-campus trials, Fig. 5.4 shows the worst case execution times for the communication loops. Due to the longer communication delays and the larger deviation, Fig. 5.4 shows 50 of the WCET times ranked from the slowest in descending order.

5.1.3 Conclusions

Contrary to expectation, the TCP/IP and UDP/IP network-based communications protocols display very little difference as implemented on LabVIEW hardware in the way in which the first portion of experiment was run. Operating on the local network, the two protocols show very little difference in performance with respect to loop rates

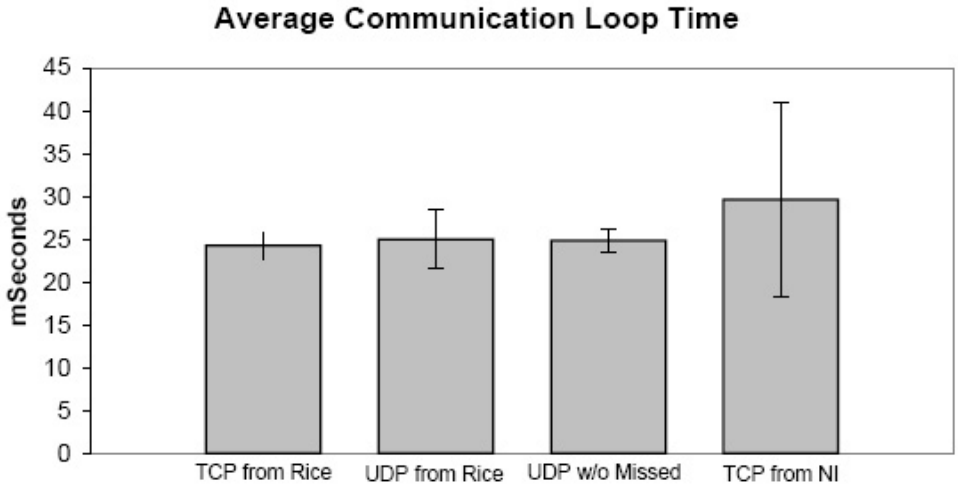

Figure 5.3: Internet communication results for off-campus test

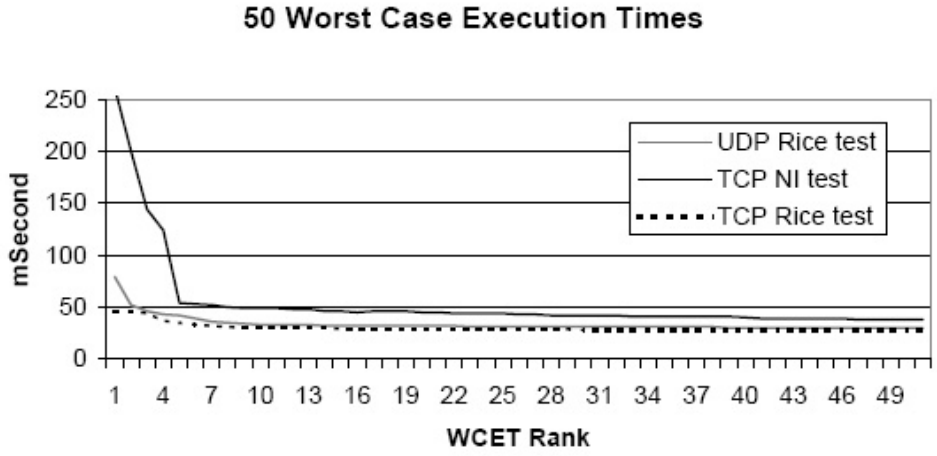

Figure 5.4: Worst case execution time for off-campus test

and fastest average execution times seen in Fig. 5.1. The only surprising fact centers on the slightly faster performance of the TCP/IP communication as compared to the UDP/IP communication, a small yet statistically significant difference of 0.065ms.

The reporting of the worst case execution time (WCET) illustrates the major difference between the TCP/IP and UDP/IP communication blocks. Looking at Fig. 5.1 in conjunction with Fig. 5.2 demonstrates that while the average loop rates and their standard deviation might be similar between the two protocols, the TCP/IP communication protocol suffers from large occasional delays.

Operating on a relatively low-traffic local network creates the best possible conditions for network-based communication. Realistically, many of the problems that typically plague TCP/IP or UDP/IP communication such as packet loss or network delay increase with the distance between the two communicating computers, as well as the routing of the packets between the two computers.

Looking at the results reported in Figs. 5.3 and 5.4, in the test between Georgia Institute of Technology and Rice University, very little difference appears between the two protocols. The results can be partially explained by the high speed connection that the two research institutions benefit by using. The high quality connection means that many of the assumptions that can be made on a local network are again valid. It is interesting to note that by removing lost packets from the UDP/IP test results, both the average values of the communication delay and the standard deviation improve significantly. WCET values show the same trend of being very similar between the TCP/IP and UDP/IP in the tests between Georgia Tech and Rice.

The results of the test between Georgia Tech and National Instruments show the most interesting results as compared to the other tests. Not only does the test show a higher mean value for the communication delay, but the standard deviation and WCET times show a significant difference compared to the other tests. The quality, type and traffic on the NI network provide the best explanations for these large

differences. It would have been very interesting to complete a UDP/IP test between Georgia Tech and NI to see how the communication protocols compared in the less than ideal situation.

Using a t-test shows that the communication delay values for each of the cases are statistically significant. The p-values for the comparison of each of the two communication protocols between Georgia Tech and Rice and the data for the TCP/IP data between Georgia Tech and NI are on the order of magnitude of $1 * 10^{-33}$ and $1 * 10^{-44}$ respectively. The difference between UDP/IP and TCP/IP between Georgia Tech and Rice showed slightly less statistical significance, but with a p-value on the order of $1 * 10^{-5}$, the two sets of data still show significant differences.

Based on the results and despite statistical differences, very little appreciable difference can be found between the two communications protocols as implemented in the LabVIEW programming language and on the NI control hardware. The final experimentation uses the same hardware and communication blocks, so again based on the results no real advantage can be gained by using one protocol over the other. The only difference is that the PHANTOM software and communications protocols use UDP/IP threads, dictating the use of UDP/IP in the final experiment. Also for the final experiment more time will be spent investigating the packing and unpacking of various variables, generating little or no overhead in the information being sent back and forth between the two control computers.

5.2 Simulated Human Testing

Before a full human-factors test can be undertaken the decision was made to simulate human input to validate the early actuation schemes control algorithms. Recent research in the IMDL has explored modeling of the human operator. Table 5.1 shows a brief report of some second order models found in literature and cataloged by Tognetti who added his own model [83]. Looking at the table, it quickly becomes

Table 5.1: Human dynamic models

Parameter	Hogan [37]	Kosuge [48]	Kosuge [49]	Hannaford [78]	Tognetti [83]
m (Kg)	0.8	1.95	11.6		6
b (N*sec/m)	5.5	2.46	17.26	300	110
k (N/m)	568	55	243	1000	10000
ω_n (Hz)	4.24	0.85	0.73	0.53	6.5
ζ	0.13	0.12	0.16		0.225

obvious that the behavior of the human can cover a broad range; however in the early testing of MR PTER the decision was made to follow some of these models.

5.2.1 Quasi-Static Test

The slave device being used for this test is the Anorad linear motor and amplifier. A constant force input is created using a mass attached to the handle of the master via a string and assuming a quasi-static situation. The on-off actuation, the multi-brake actuation with virtual coupling feedback using three K values, as well as an uncontrolled case are tested. For each of the five controls, the test is run starting in 2 different positions. Each starting position test is run for three directions of input force. All of the tests are run three times so that averages can be taken. Figure 5.7 illustrates the workspaces of the master and the slave as well as the starting positions and applied force directions. The test is ended either when the master stops moving (the brake forces balance the input force) or when the master reaches the virtual constraint at 60% of the slave's workspace.

Previous work has shown that UDP/IP communication provides the best method for internet based control communication [66]. Following that research, the communication between the master and PXI controllers of the master and slave devices takes place via the UDP/IP protocol using LabVIEW's built-in communication blocks. Due to the internal workings of the NI UDP block, the communication on the master side

Figure 5.5: Quasi-static experimental setup

of the loop is blocking, meaning that the control loop will only iterate when it receives a data point from the UDP/IP stack. This forces event-based control similar to the work of Elhajj [22] [23].

The programs for the master and slave are written in LabVIEW 7.1 graphical programming language, a portion of which can be seen in Fig. 5.6. Pre-built LabVIEW blocks, and formula nodes are used whenever possible to simplify coding. The master control program utilizes a prioritized multi-loop structure that allows the user-interface and the control to run in separate threads at different priorities. The master GUI updates at 10Hz to alleviate strain from the system.

The communication loop between the master and the slave operates at 40Hz, and the design of the NI UDP/IP blocks forces synchronization. A non-rigorously tuned PD control runs locally on the linear motor and updates the set point at

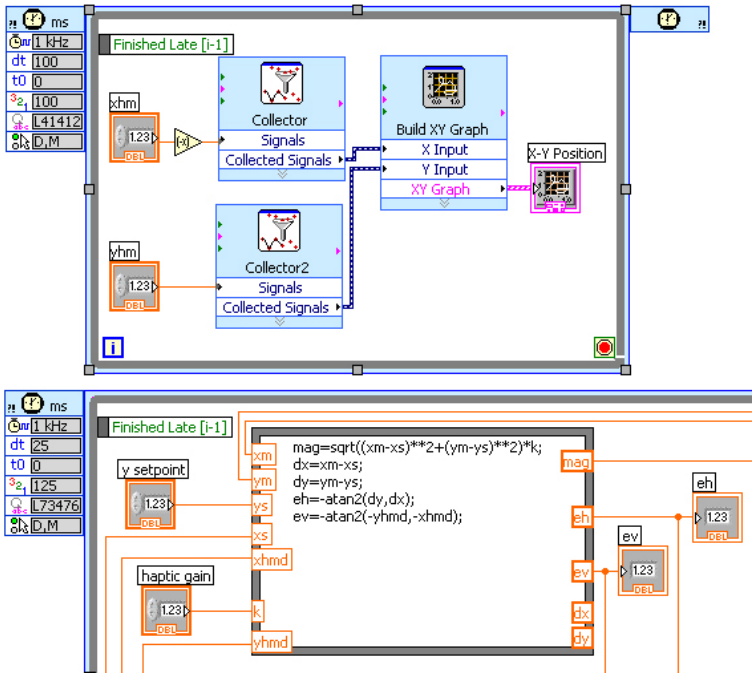

Figure 5.6: Quasi-static experiment screen shot

500Hz which guarantees stability. This multi-loop prioritized architecture (similar to multi-threading in other programming languages) is possible due to the "timed loop" structure within LabVEIW and LabVIEW Real-Time. In the slave, the local control occurs at a much faster rate than the communications loop. In the master the communication loop happens within the local control control loop and constrains the master control to operate at 40Hz. In the following implementations, the master control in RT will allow faster loop rates.

5.2.1.1 Results & Analysis

The analysis of results follows similar methods to those used in previous passive haptic research by Swanson [81]; however the standards used to judge the control have been reduced to three: position tracking, force replication, and time to task completion. To judge the ability of the master to track the slave and vice versa, the difference between their positions is calculated at each time step. The ability of the control

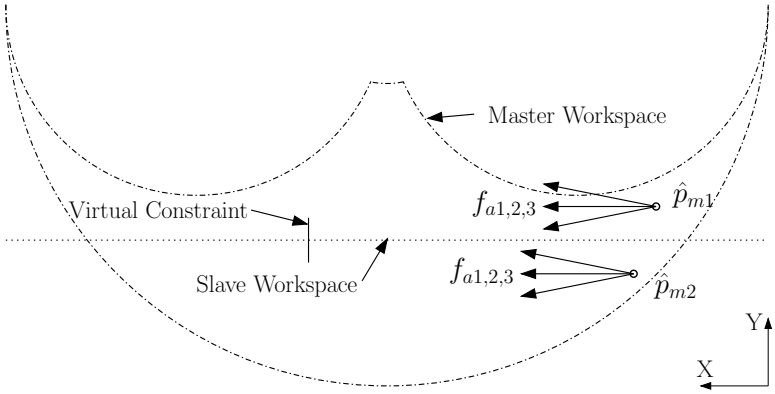

Figure 5.7: Workspace for simulated human testing

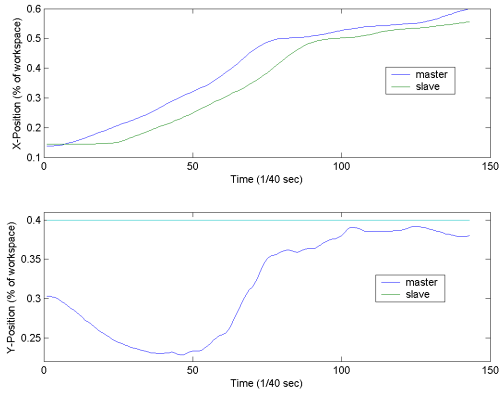

Figure 5.8: Raw data for quasi-static test

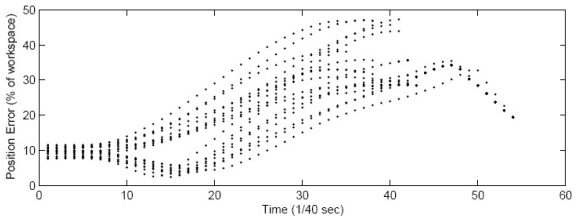

Figure 5.9: Quasi-static test with no control

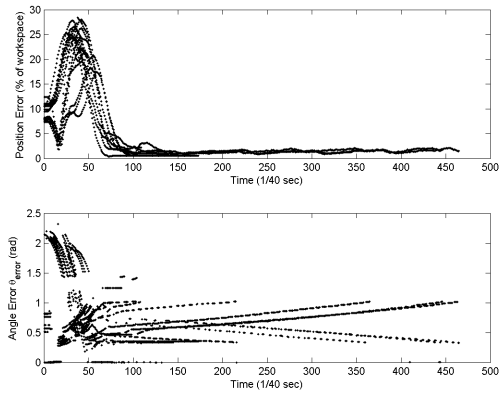

Figure 5.10: Quasi-static results with on-off actuation

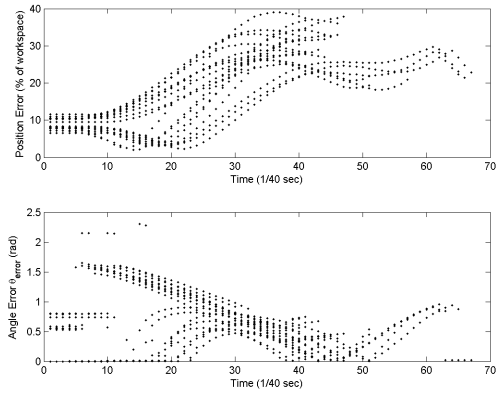

Figure 5.11: Quasi-static results with multi-brake and a gain of $K = 10$

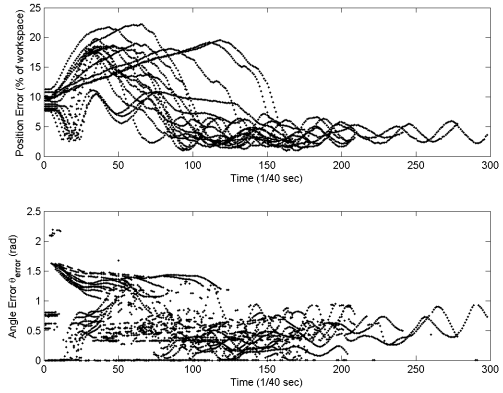

Figure 5.12: Quasi-static results with multi-brake and a gain of $K = 100$

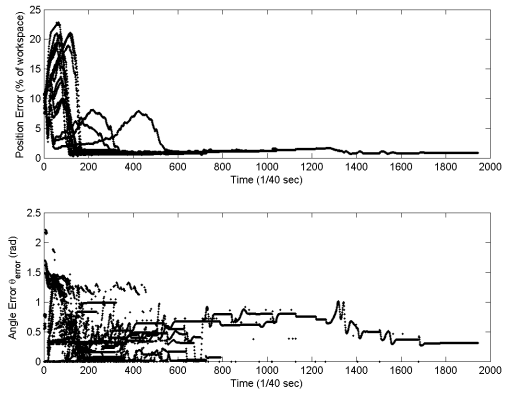

Figure 5.13: Quasi-static results with multi-brake and a gain of $K = 500$

Table 5.2: Results from quasi-static test

Control	Position Difference	Angle Error	Time to Finish	Trials Unfinished
no control	21.54%	N/A	1.53 sec	0
on-off actuation	3.32%	0.68 rad	11.46 sec	0
multi-brake K=10	19.67%	0.53 rad	1.67 sec	0
multi-brake K=100	6.84%	0.54 rad	7.34 sec	0
multi-brake K=500	1.80%	0.48 rad	N/A sec	18

to replicate a force is judged against the control's ability to match the haptic force $\vec{f_h}$. Since the brake actuation is on-off and also since a constant force drives the test, only the angle between the direction of force generated the actuated brake and the direction of $\vec{f_h}$ is used to judge force replication. The angular difference is shown as θ_{error} and originally discussed in conjunction with in Fig. 3.4. Finally, reaching the virtual constraint at 60% of the slave device's workspace marks task completion. If the control completely stops the motion of the system before reaching task completion, that is noted as well. The data collected from the 36 trials is averaged and displayed in Table 5.2.

Figures 5.9-5.13 show the data for the position and angle errors for all tests. Note that the time axes for each graph are different, corresponding to the length of the

trials and the maximum magnitude of the values.

While on-off actuation provides low position error, it increases task completion time and therefore increases user workload. The multi-brake actuation with virtual spring force feedback improves the task completion time while only slightly increasing the position error. Furthermore, multi-brake actuation allows better replication of $\vec{f_h}$, as it provides a better ability to generate force in an arbitrary direction (demonstrated by the lower values of θ_{error}). The multi-brake actuation with K=100 provides a balance between position tracking, angle error and speed.

5.2.2 CRS Robotic Test - flexible rod coupling

As a step between the quasi-static experiments and actual human experiments, a side project attempted to create an interface between MR PTER and a CRS 6 DOF industrial robotic arm. Undergraduate Research Assistant Carwyn Jones provided design and construction assistance bringing the project from concept to reality.

In an earlier side project, Matt Litman created a rigid coupling between MR PTER and the CRS robot. The concept was to extend his rigid coupling into some form of flexible coupling with the ability to vary its dynamic properties (the spring constant and damping ratio of the physical coupling). In theory, the flexibility would allow the input from the CRS robot to better approximate the input of a human. Table 5.1 shows a short list of the values in a second order dynamic model of human behavior that will be approximated by the CRS system.

The first design iteration can be seen in Fig. 5.14. The coupling utilizes a flexible rod of varying thickness, length and material to connect the two devices. The flexible rod is fixed to MR PTER and a metal rod is inserted in the top of it. The CRS robot is fixed with a manipulator that consists of an I-bolt that the metal rod can freely move up and down in. Assuming relatively smooth sliding between the metal rod and the I-bolt, the only forces transmitted between the CRS robot and MR PTER

Figure 5.14: Testing setup using CRS robot

are due to the bending of the flexible member. Figure 5.14 as well as Fig. 5.15 shows an image of the coupling setup and a table of the physical parameters of the flexible rods respectively and are taken from the final report of Carwyn Jones.

With the hardware set up basically the same as the quasi-static testing, MR PTER is used to control the linear motor, and the CRS robot moves from right to left in the workspace of MR PTER. The CRS robot is programmed to move with a sinusoidal motion centered about the workspace of the linear motor as it moves from right to left. Figure 5.16 shows the sinusoidal motion of the CRS robot and its path back to the starting point as well as the path of the linear motor. While a sinusoidal input makes little sense compared to the true motion of a human user, it does provide a constantly changing difference between the position of the master and the slave, p_m and p_s. It therefore forces the control algorithm to provide a constantly changing $\vec{f}_h$ as calculated by Eqn. 3.14.

Each of the couplings is tested using an on-off actuation scheme as well as the multi-brake actuation scheme with the simple virtual coupling at three different K values. Data is also collected with one relatively inexperienced human (obviously not

Picture	Rod number	Material	Stiffness (Durometer)	Length	Outside diameter	Inside diameter
	Flex 1	Polyurethane	40A	6”	1-1/4”	1/2”
	Flex 2	Silicon rubber	50A*	6”	1-1/4”	1/2”
	Flex3	Neoprene Spring Rubber	75A	6”	1-1/4”	1/2”
	Flex 4	Neoprene Spring Rubber	75A	6”	1-7/8”	1/2”

*This is as assumed value contact Mcmaster.com for a more reliable value (code, 5546T16)

Figure 5.15: Flexible couplings used for CRS experiment

enough to make a solid comparison, but enough to allow ball-park validation).

5.2.2.1 Results & Analysis

Figure 5.17 shows a representative plot of the coupling that most closely matched the human results from the preliminary experiment. The results shown in Table 5.3 judge the couplings with each of the control algorithms based on the percent deviation between the endpoint of MR PTER and the position of the linear motor.

Testing with the flexible coupling showed a few fundamental flaws in its design.

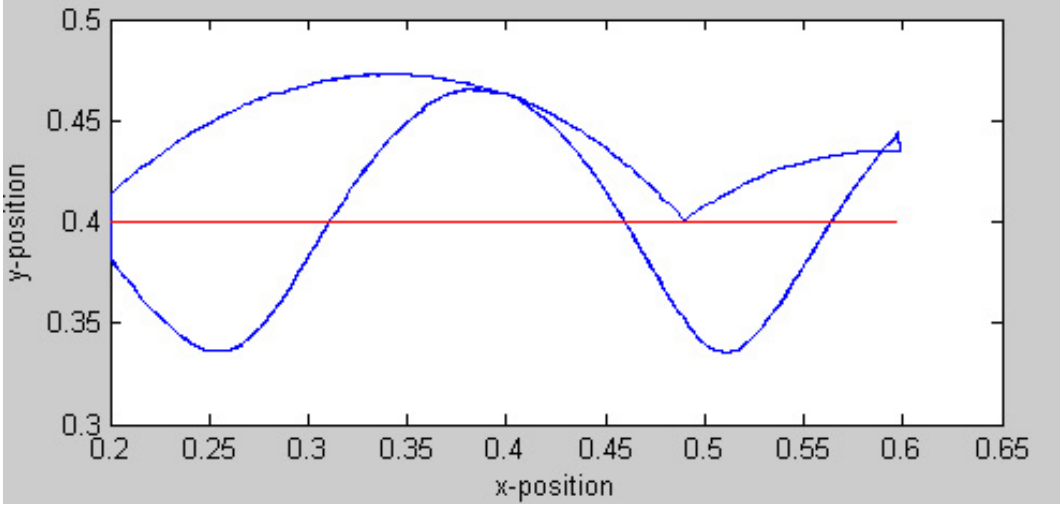

Figure 5.16: CRS input for testing

Table 5.3: Results from CRS testing

	no control	on-off	multi K=10	multi K=100	multi K=500	average
CRS-flex 1	5.00	2.93	4.05	3.09	3.05	3.62
CRS-flex 2	5.15	3.43	2.68	3.59	3.16	3.59
CRS-flex 3	5.19	3.47	4.84	4.15	3.25	4.18
CRS-flex 4	5.00	4.14	4.67	4.54	4.66	4.62
CRS-rigid	5.03	4.80	4.28	4.98	4.67	4.77
human input	4.76	4.15	3.40	3.12	3.16	3.72

If the difference between p_m and p_s were great enough and the force generated by MR PTER as feedback were large enough, the large resulting angle of the flexible rod with respect to MR PTER would cause the connection to bind. Also, changing the coupling to match a human model involves finding another material with a size or with physical properties that match some form of a dynamic equation. To answer those two questions, the next version of the coupling device features a tunable dynamic system.

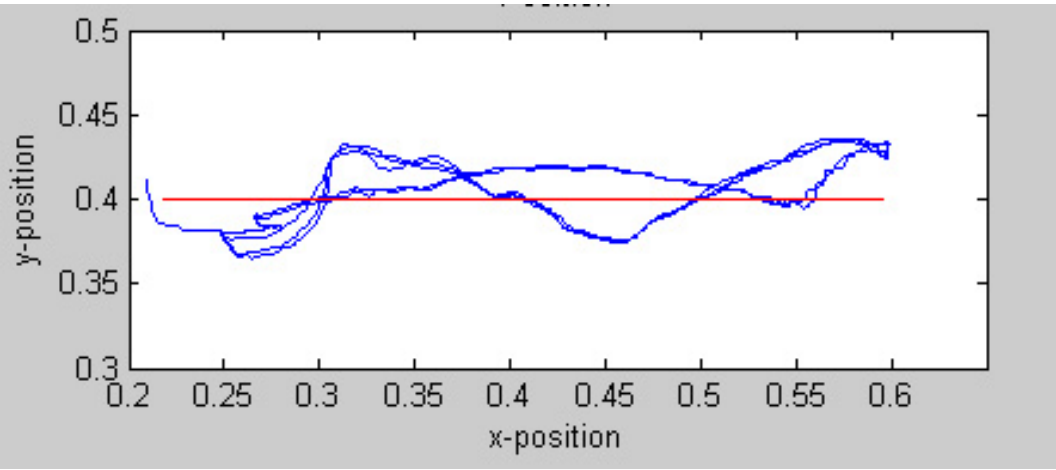

Figure 5.17: Results with flexible coupling no. 2

5.2.3 CRS Robot Test - tunable "mitt"

For the second iteration of the coupling design, Carwyn Jones again assisted in designing and constructing a more robust and more tunable flexible coupling between the CRS robot and MR PTER. A balanced 3-member design shown in Fig. 5.18 is chosen for its simplicity and ease of construction. Each of the three members contains both a spring that can be replaced to create various spring constants and an adjustable damper.

Figure 5.19 shows the attachment of the tunable mitt to the handle of MR PTER. However, due to various complications, testing and results similar to that done with the flexible rod coupling were not completed with the dynamic mitt. While very effective in theory, the adjustable dashpot dampers used in the construction of the mitt are very fragile and prone to failure when used in the teleoperation system. Also due to the fact that there exists very little agreement on modeling of a human user, the idea of rigorously producing a surrogate for testing purposes is inherently flawed. The human acts like a passive system in some cases and like an active system at other times, not just responding as a physical second order system but responding as a complex system with many modes that change depending on the stimuli. Therefore

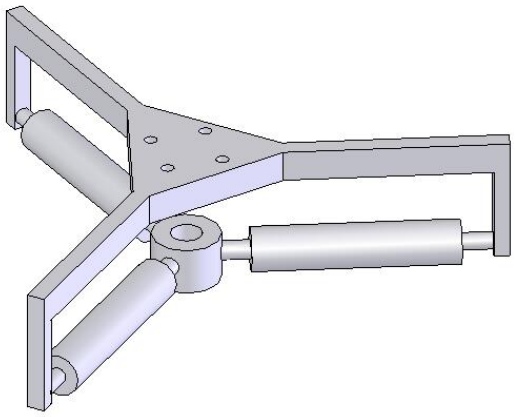

Figure 5.18: CRS tunable "mitt"

further development of a robust dynamic system to interface the CRS robot with MR PTER was abandoned and the focus turns to human perception and the interaction of the human user with the haptic device.

5.2.4 Conclusions

While the desire to match a specific human model seemed at first to be a valid one, in reality, the most important results of the simulated human testing came from the quasi-static test. Specifically the results shown in Figs. 5.10 and 5.12, the on-off actuation scheme and the multi-brake actuation with a moderate gain constant respectively, illustrate the proper functioning of the basic principles of the actuation schemes and basic control.

The results summarized in Table 5.2 show that position tracking is achieved at the expense of task completion time, yielding a higher workload to the user and more dissipated energy. The results show expected trends; the multi-brake control with a low gain behaves like the uncontrolled case, and the multi-break control with a

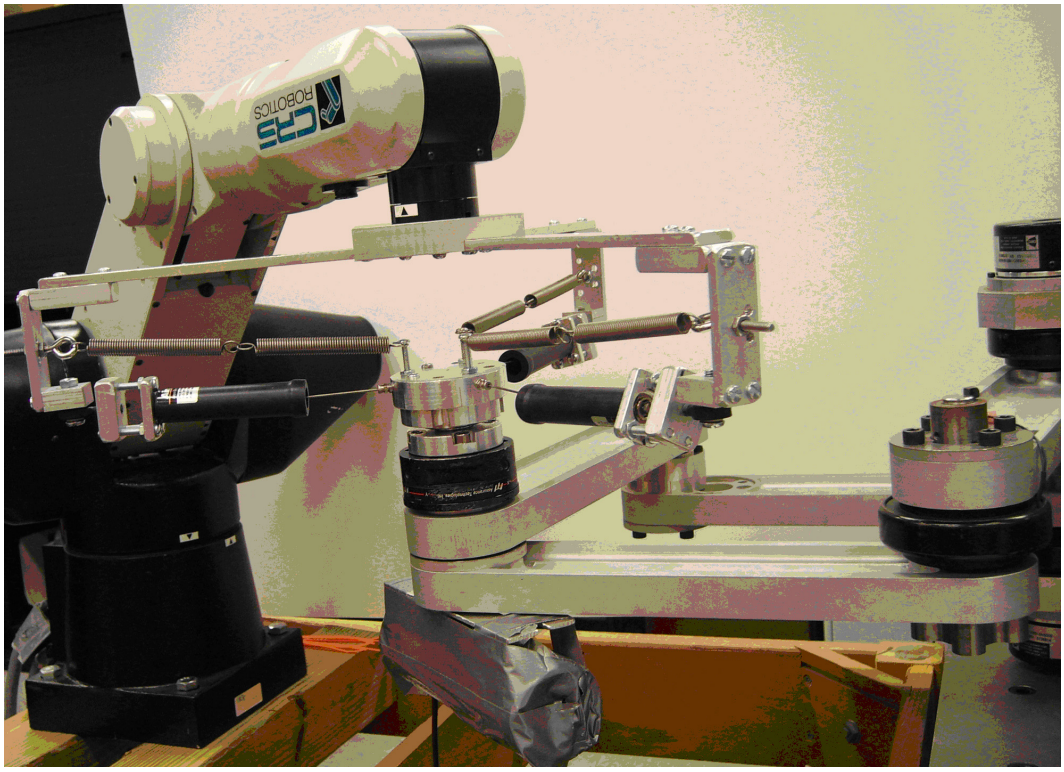

Figure 5.19: CRS "mitt" coupled to MR PTER

high gain behaves like On-Off control due to the saturation of the brakes. The best possible controller would be able to produce results to match the completion time of an un-controlled case while producing very little position error.

Most importantly, the results shown in Fig. 5.10 show the expected behavior of the on-off actuation scheme. An increase in the position difference between the linear motor and MR PTER immediately follows the starting the test and release MR PTER. At that point in time, the direction of the haptic force lies in the direction of the velocity; however, as MR PTER crosses the line representing the workspace of the linear motor, the control algorithm can again apply a force. The on-off actuation then creates an oscillation around the workspace of the linear motor. Figure 5.12 shows similar behavior with the multi-brake actuation scheme combined with the virtual coupling controller.

These results follow the expected trends and at the very least partially validate the

functionality of the controllers. Even more, the test follows the velocity field research of previous IMDL students [73] [81]. The oscillating behavior of the device as it repeatedly crosses the workspace of the linear motor produces feedback forces similar to those that would be generated by a velocity field controller. If the predetermined path in the velocity field matched the workspace of the linear motor, the results would be very similar to the ones collected with this experiment. The results and conclusions from these tests have been published by Black and Book [5][6].

5.3 Perception Experiment

In an attempt to better understand human perception, especially with respect to the passive MR PTER, two experiments looked at the ability of a human to resolve the direction of a force being applied to them through the handle of the haptic master.

The term "just noticeable difference" refers to the minimum required difference in two stimuli that a human is able to perceive. While force has both magnitude and direction, previous research exploring the JND threshold has focused mainly on the magnitude component. Using active haptic devices, this line of reasoning makes perfect sense since an endpoint force can be produced in nearly any direction. However with a passive device, arbitrary force production is obviously not possible and therefore it becomes important to understand how close of a replicated force is "close enough."

Both of the following perception tests use the same hardware, controller and basic software. MR PTER functions as the haptic master and is controlled using a National Instruments PXI-8175 operating in real-time under the National Instruments Real-Time operating system running on a PentiumIII 866MHz processor with 512MB of RAM. A PXI-6070E DAQ card along with a PXI-6711 analog output card provides the digital and analog I/O. The three MR brakes require external Advanced Motion Controls 12A8 PWM amplifiers and an Advanced Motion Controls PS4X300W Power

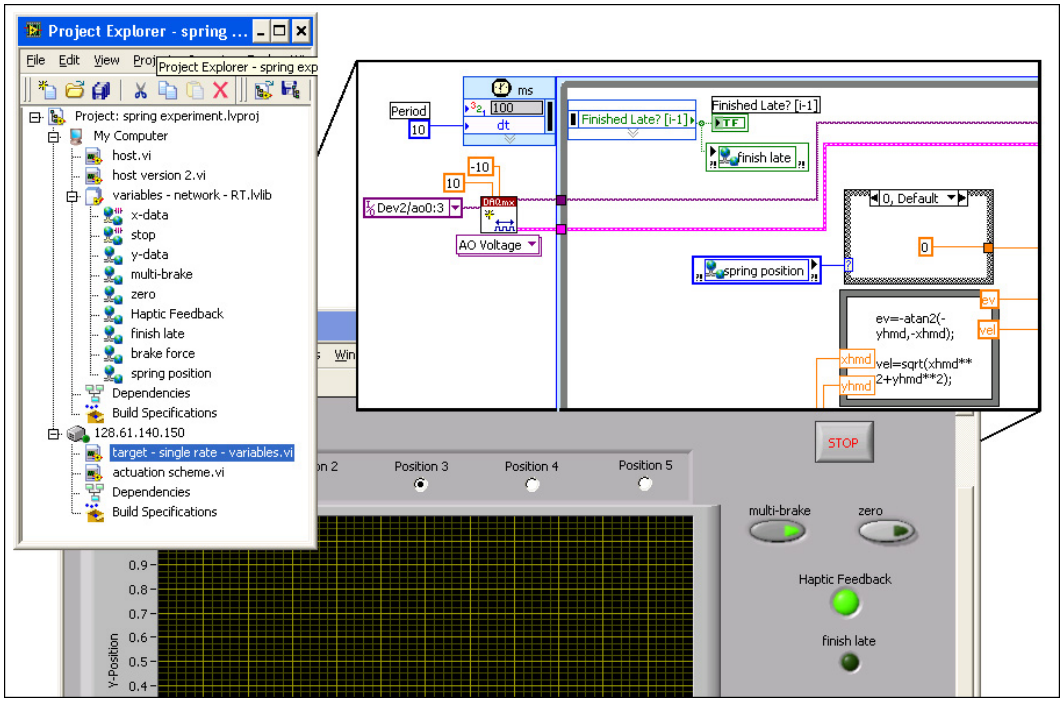

Figure 5.20: Screenshot of software used in perception experiment

Supply.

A multi-computer system controls the haptic device and runs a graphical user interface (GUI). A host desktop computer running Windows 2000 and LabVIEW 8.0 provides the GUI that the test administrator sees during the testing routine and allows high-level system control. A target PXI running LabVIEW Real-Time provides the low-level control for the haptic system. The two computers communicate over a public LAN via TCP/IP and LabVIEW's shared variable data type. Further, the project-based file structure allows observation of the real-time program running on the target PXI without interrupting its operation. The program that provides the GUI runs at a 10hz loop rate while the control algorithm on the target runs at 100Hz. Figure 5.20 shows a portion of the timed loop being used to run the real-time control of the haptic master, a portion of the GUI used to administer the experiment, and the project explorer that allows access to the entire project.

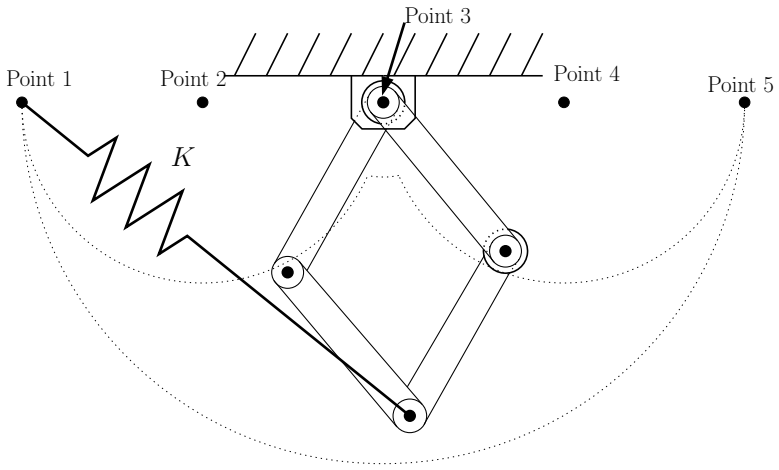

Figure 5.21: Analysis of discrete force experiment

5.3.1 Discrete Spring Experiment

Five subjects were recruited from members of the IMDL research group, each having a working knowledge of the haptic hardware and a limited amount of experience operating it. The haptic device was programmed to produce a haptic force to simulate a virtual spring attached between the endpoint of the device and one of five locations along the device's backplane, a line drawing of which was shown to the subjects and is reproduced here in Fig. 5.21.

To draw conclusions about perception resolution in force direction, it must be assumed in this experimental design that the subject operates within the center of the workspace of the device. Only under that assumption will it be possible to make a judgment about the angular difference between a force that replicates a spring attached at point 1 and a force that replicates a spring attached at point 2. Making that assumption, the angular distance between any two forces is roughly 15 deg as illustrated in Fig. 5.22.

Each subject was first given five minutes to familiarize himself with the device, during which time he was allowed to feel the haptic force intended to represent the virtual spring at each of the five attachment points. After the familiarization time,

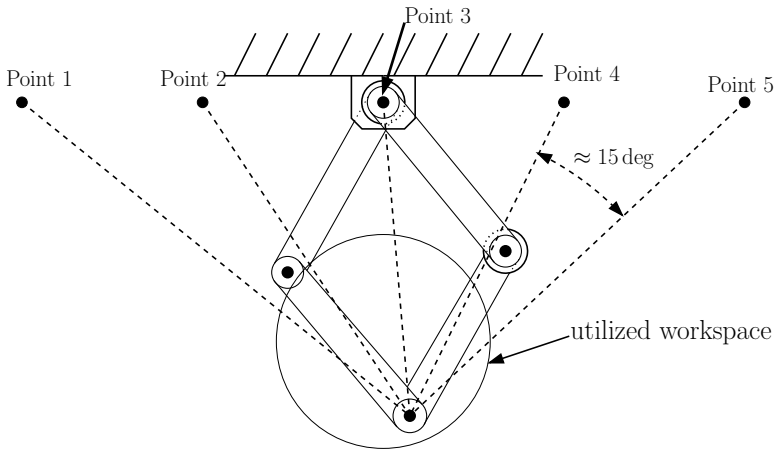

Figure 5.22: Design of first perception experiment

Table 5.4: Results from first perception experiment

Subject	±0	±1	±2
1	50%	90%	100%
2	70%	100%	100%
3	67%	100%	100%
4	53%	100%	100%
5	73%	100%	100%
Total	63%	98%	100%

the subject completed fifteen trials in which he was asked to pick the point on the backplane to which the other end of the virtual spring was attached.

5.3.1.1 Results & Analysis

The responses from each subject were collected and judged against the correct response for each trial. To draw conclusions from the results, notation is made when the subject records the perceived location of the endpoint of the virtual spring correctly, off by one location or off by two locations. Table 5.4 shows the tally of these responses by each of the subjects as well as a total average over all of the trials.

After analyzing the results from this perception experiment, it became obvious that the testing procedure being used contained some inherent flaws. First, the test

pool was not only incredibly small, but it also represented a very limited cross section of a population, too small and too homogeneous to provide usable results. Because of their knowledge of the device and their advanced understanding of robotics and kinematics, the subjects were able to relatively quickly create a functional heuristic for determining the location of the virtual spring attachment without focusing on the direction of haptic feedback. Effectively, the subjects very quickly figured out how to "cheat" the system. The subjects also violated the key assumption of the experimental design discussed above and illustrated in Fig. 5.22. Finally, the experiment does not provide enough resolution to make a numerical estimation of human perceptive resolution with respect to force direction. The use of five discrete connection points for the virtual springs leads to a very low resolution. To address some of these concerns, a second perception experiment was designed.

5.3.2 Constant Force Experiment

Again, five subjects were recruited from members of the research group, each again having a working knowledge of the haptic hardware but with a limited amount of experience operating it. Even though it produced undesirable results before, this recruitment method was used again to avoid the need of undertaking a full human-factors test that includes approval of the Institutional Review Board (IRB). Also for this experiment, the haptic device was programmed to produce a haptic force in a constant direction with a constant level of actuation. Due to the kinematics of the device, the actual force magnitude varied slightly throughout the active portion of the workspace. Figure 5.23 shows the sixteen possible evenly spaced directions that the user might experience.

The subjects were each given five minutes to familiarize themselves with the device during which they were allowed to feel a force in a known direction, force 1. After familiarization, the user completed twenty trials in which he was asked to move in

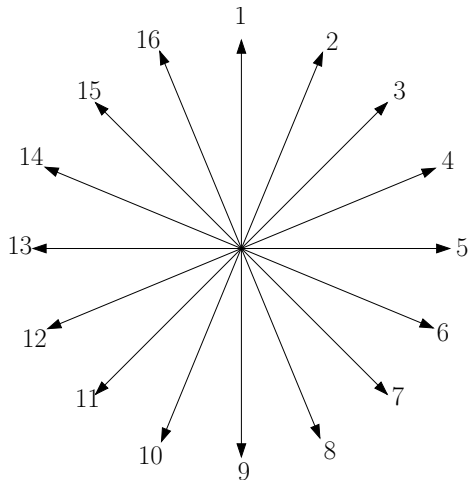

Figure 5.23: Force directions for second perception experiment

the direction of greatest resistance and then make a judgment as to which direction that motion corresponded, referencing a figure matching Fig. 5.23. In addition to the responses from the subject, data was collected measuring the forces at the endpoint of the device as well as the brake actuation and position of the device for the duration of each test.

5.3.2.1 Results & Analysis

The responses from each subject were collected and judged against the correct response for each trial. To judge the results, notation was made when the subject records the perceived direction of greatest resistance correctly (off by 0), off by one location (± 1) or off by two locations (± 2) as shown in Fig. 5.24. Table 5.5 shows the tally of these responses by each of the subjects as well as an average over all of the trials.

5.3.3 Conclusions

Neither of the tests actually determine a JND quantity by the strict definition of "just noticeable difference" due to the fact that the tests were not administered such that a subject felt a stimulus, the stimulus changed and the person was asked if they had

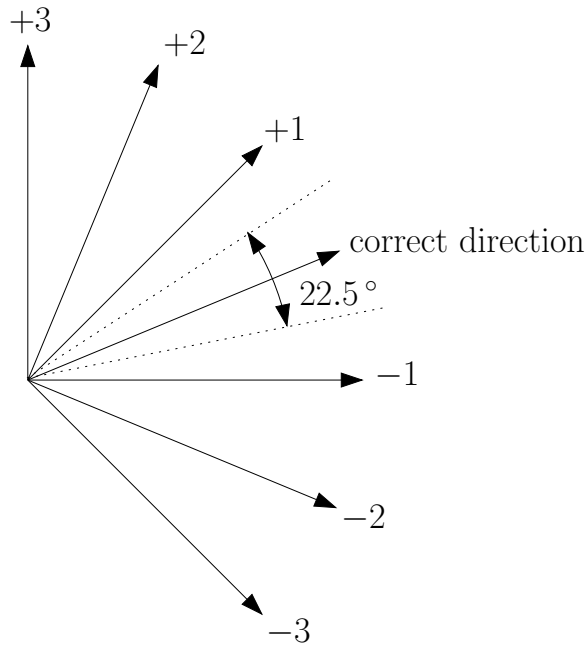

Figure 5.24: Definition of the resolution of the test

Table 5.5: Results from second perception experiment

Subject	±0	±1	±2
1	40%	90%	100%
2	30%	85%	100%
3	45%	100%	100%
4	40%	75%	90%
5	70%	95%	100%
Total	45%	89%	98%

felt the change; however the results provide information that possibly provides even more insight into the teleoperation task than a JND value would. As an operator uses the haptic master to move a slave the following results apply to the way in which the operator perceives the contact force that he feels as the slave interacts with something in its environment.

Possibly the most important results with respect to understanding the passive haptic controller come from these perception tests. While electronic force sensors have resolution on the order of magnitude of hundredths or thousandths of a degree, humans have a much coarser resolution according to these results. Even more specifically, these results apply directly to the passive hardware used in the final experiment.

To draw conclusions about about perceptive resolution in force direction from the first experiment, it must first be assumed that the subject operates roughly in the center of the workspace. Under that assumption, the angle difference between each of the positions of the virtual spring is approximately 15°. Under those assumptions, the data and analysis indicated that the human perception of force has a resolution better than 15° or roughly 4% of a 360° workspace, a result not out of the range of the threshold of JND for force magnitude reported in the literature; however the results as well as observations of the subject behavior indicate that the assumptions are not valid. In this test, subjects tended to not operate within the center of the workspace, and therefore the angle between the virtual springs varied greatly.

The second test had a maximum resolution of 22.5 ° due to the even spacing of the 16 options through out the 360 ° range of perception. Figure 5.24 shows that if a subject chooses the correct direction, that region has a maximum size of 22.5 °. Similarly, if a subject guesses incorrectly by one position, his error lies in a 67.5 ° region, and if off by two positions, the region increases to 112.5 °.

The the subjects producing the results reported above were able to judge with 89% certainty that the direction of force lay somewhere within a region of 67.5 °. From

that, the results provide a rough estimate of the human perceptive resolution with respect to force magnitude of aproximately 18.75% over the 360° range of perception. With respect to the literature, the results produced here agree relatively well with the 5-10% results for JND with respect to other types of stimuli and on the order of results presented by other researchers [39] [82].

Defining a perceptive resolution of roughly 67.5° works in the favor of passive haptic hardware. Such low resolution means that the hardware can produce usable feedback without being able to exactly replicate an arbitrary force. All of these tests assume that the device properly replicates the desired force, and it is obvious that cannot be 100% accurate with the passive device.

5.4 Final Human Factors Experiment

The culminating experiment for this research includes a full human-factors test that compares the control algorithms implemented on MR PTER to each other and to a PHANTOM for three tasks: shape identification, point-to-point move with obstacle avoidance, and a point-to-point move with a guiding fixture (akin to a peg-in-hole task). Before implementation, the study was thoroughly described and subsequently approved by the Georgia Institute of Technology Internal Review Board (IRB) as Protocol Number H07033, the relevant portions of which are included in Appendix C.

5.4.1 Experiment Hardware and Software

For this portion of the experiment the system takes the form shown in Fig. 5.25. One host is used to control the experiment while the master and slave communicate separately. The system is configured so that changing the master from the PHANTOM to MR PTER and back again changes nothing that the operator sees nor does it change the loop rates or communication protocols used.

The hardware used is very similar to that described in the preceding testbed

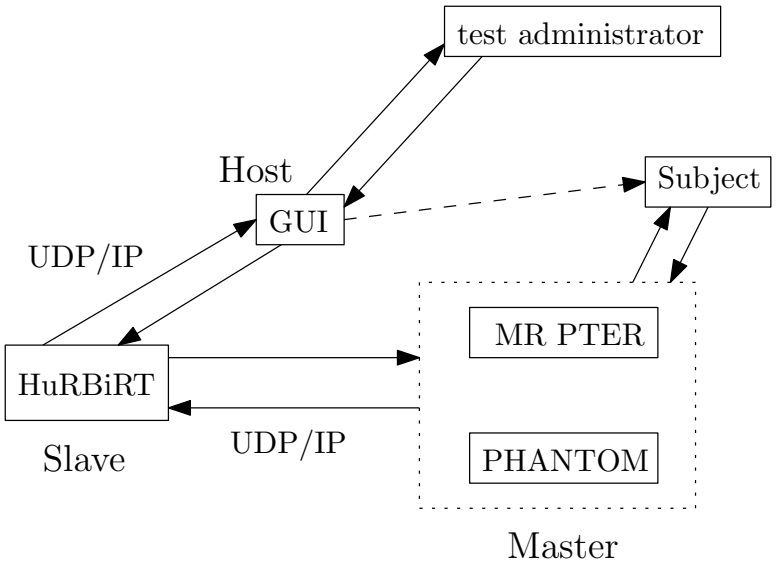

Figure 5.25: Block diagram of final experiment

chapter. The control system of HuRBiRT is exactly as described and communicates with the master controller via two UDP/IP threads (one for sending and one for receiving) at 200Hz. As described in depth earlier, a NI dedicated controller card takes care of the low-level control of HuRBiRT at a high loop rate.

The host computer running WindowsXP shows the GUI to the test administrator and to the test subject at the same time via a video splitter. For portions of the testing, turning off the monitor in front of the subject hides the GUI from the subject while allowing the administrator to continue to monitor the system. The GUI and host application communicate with the slave controller at 6.7Hz, just enough to provide a visual interface of the system state and to produce data for analysis without interfering with the control systems.

As before, the software to run the experiment takes the architectural form of a multi-threaded asynchronous priority based program. Each of the communication threads as well as the control threads for each system run separately with the control thread having highest priority, the master-slave communication thread having second priority and the slave-host communication thread having the lowest priority.

Figures 5.26 and 5.27 show the system setup. The slave device is located in the same room but behind the user as is seen in Fig. 5.26. The two master devices are located next to each other and the PHANTOM is raised so that its workspace height matches that of MR PTER. The test administrator sits around the edge of the table from the subject in the orange chair visible in Fig. 5.27. A low resolution video camera provided the user with a small window showing the position of HuRBiRT so that the subject could better understand the correlation between the motion of the master and the motion of the slave without turning around. The subjects tended to pay attention to this visual feedback only for the initial training period, but the window stayed visible during all tests that the subjects could use the monitor.

5.4.2 Experimental Design

After signing the appropriate consent form, each of the final pool of 23 subjects first completed a simple questionnaire regarding their handedness, their use of computers and video game systems as well as their participation in other haptic research projects. The subject was given an opportunity to ask questions about the lab and their surroundings and a brief explanation of the research was given.

For the first task, the subject was asked to identify a shape being displayed in the workspace of the slave device using one of the haptic master devices. The subject either began with MR PTER or with the PHANTOM in a random distribution to help minimize the influence created by starting with one or the other. The subject was given a sheet shown Fig. 5.28 of Appendix C that illustrates the 7 possible shapes: convex circle, concave circle, convex triangle, concave triangle, convex square, concave square or a flat surface. These shapes are programmed into the workspace of HuRBiRT so that the robot interacts with a virtual shape instead of a physical surface. Done to increase safety because of the strength of HuRBiRT, use of a virtual shape versus a physical shape is assumed to make no difference with respect to the

Figure 5.26: Overall view of final human-factors test

Figure 5.27: Testing station for final human-factors experiment

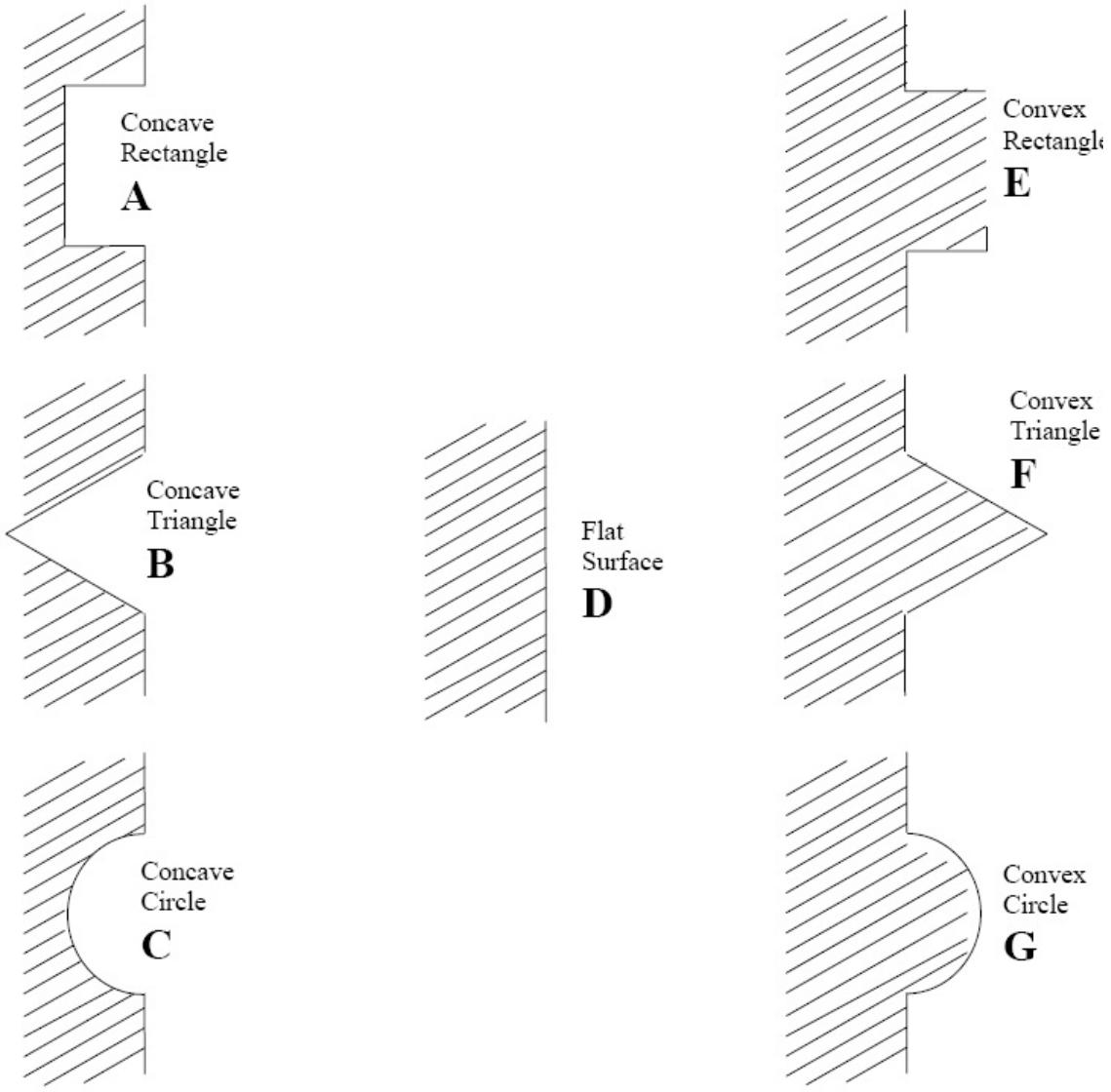

Figure 5.28: Shapes displayed to subject during testing

feedback felt by the user other than simplifying the dynamic interaction of the slave device and the surface. Since the dynamics of this interaction likely cannot be felt by the user of a passive haptic device, the simplification seems appropriate.

The subject interacted with a shape that remained the same size in the workspace of the slave device regardless of the master device being used. However, the workspace of the master devices were scaled so that they matched well with the workspace of the slave, meaning that a motion of 10cm in the workspace of MR PTER lead to a motion of 33.75cm in the workspace of HuRBiRT. Similarly, a motion of 10cm by the PHANTOM would lead to a motion of 90cm in HuRBiRT's workspace. The scaling allows full use of the workspace of the master, but forces the subject to scale the shapes in their head. However, humans have a very good ability to perform this scaling transformation. Take for example the use of a microscope. A scientist can change the magnification yet very easily continue to manipulate even very tiny objects under the magnified lens. The workspace of the two master devices was scaled such that shapes appeared to be $2\frac{2}{3}$ times larger when using MR PTER as compared to when using the PHANTOM.

The subject was given up to 5 minutes to practice with the monitor turned on while feeling the flat wall and the convex circular shape. After turning off the monitor, the subject then identified a number of shapes; 10 shapes with the PHANTOM or 8-10 with each of the 3 controllers when using MR PTER. The order of shapes displayed was determined beforehand using a random number generator. After finishing with the first device, the subject completed a NASA-TLX workload index survey to rate the workload of their experience. The subject then switched haptic master devices, practiced just as before and then completed the rest of the shape identification tasks with the second device. After another response to the NASA-TLX survey to gain feedback on the second device, the subject was completed with the first and longest of the tasks in the experiment.

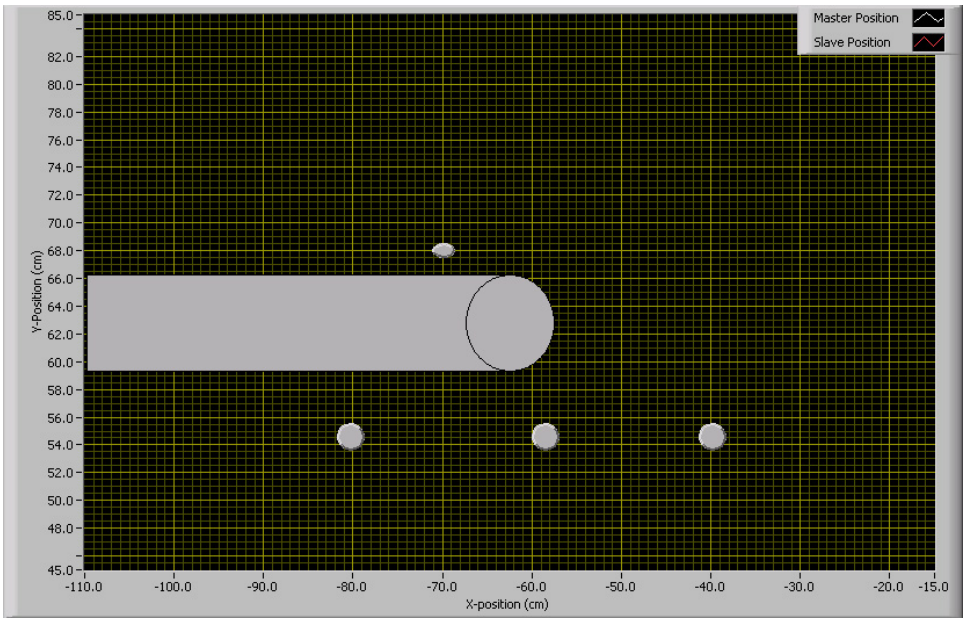

Figure 5.29: Screen shot from the obstacle avoidance task

The second and third tasks were chosen at random and either asked the user to complete the obstacle avoidance task or the guided movement task. While the user will now have experience with the device, the randomization will insure that experience should be statistically the same for each task.

For the obstacle avoidance task, the subject was asked to start at one of the three starting positions, below the obstacle in Fig. 5.29 and told to move as quickly as possible to the oval above the obstacle. After giving the subject up to five minutes to practice, the test was run either twice from each starting point with the PHANTOM or once from each starting point if using each of MR PTER's controllers. The order of the tasks and the order of the controllers was randomized for each subject. For all of this portion of the experiment, the subject could see visual feedback from the GUI of their position as well as the position of the slave device.

For the final task, the subject moved either from starting point A or starting point B to the finishing point as shown in Fig. 5.30. Guiding surfaces programmed into the workspace of the slave took a triangular shape that funneled the user to the finishing

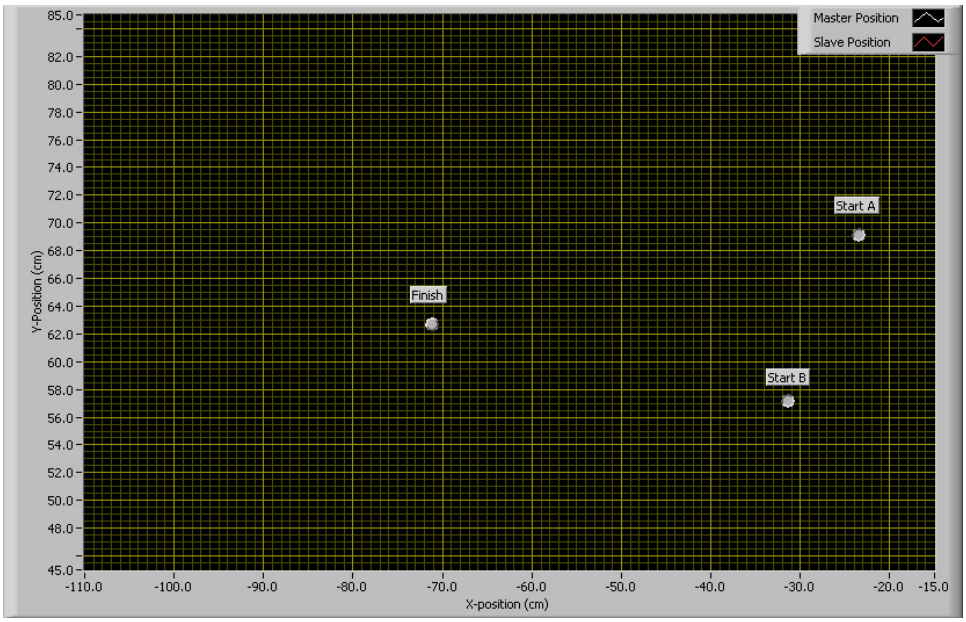

Figure 5.30: Screen shot from the guidance task

point, but the user could see the surfaces. As with the obstacle avoidance task, the user practiced for up to 5 minutes before the test began. The subject then was timed as he completed the motion starting at each point twice in a random order.

A full explanation of the experiment can be found in Appendix C along with the documentation seen by the subjects in each test.

5.4.3 Experimental Results & Analysis

The following reporting of results and their subsequent analysis illustrate examples and summaries of the full results. More complete results can be found in Appendix C.

5.4.3.1 Shape Identification

The concept of identifying a shape placed in the workspace of a slave robot corresponds very well with any typical teleoperation exploration task. The goal of the subject is to be able to identify when the device moves from operation in free space

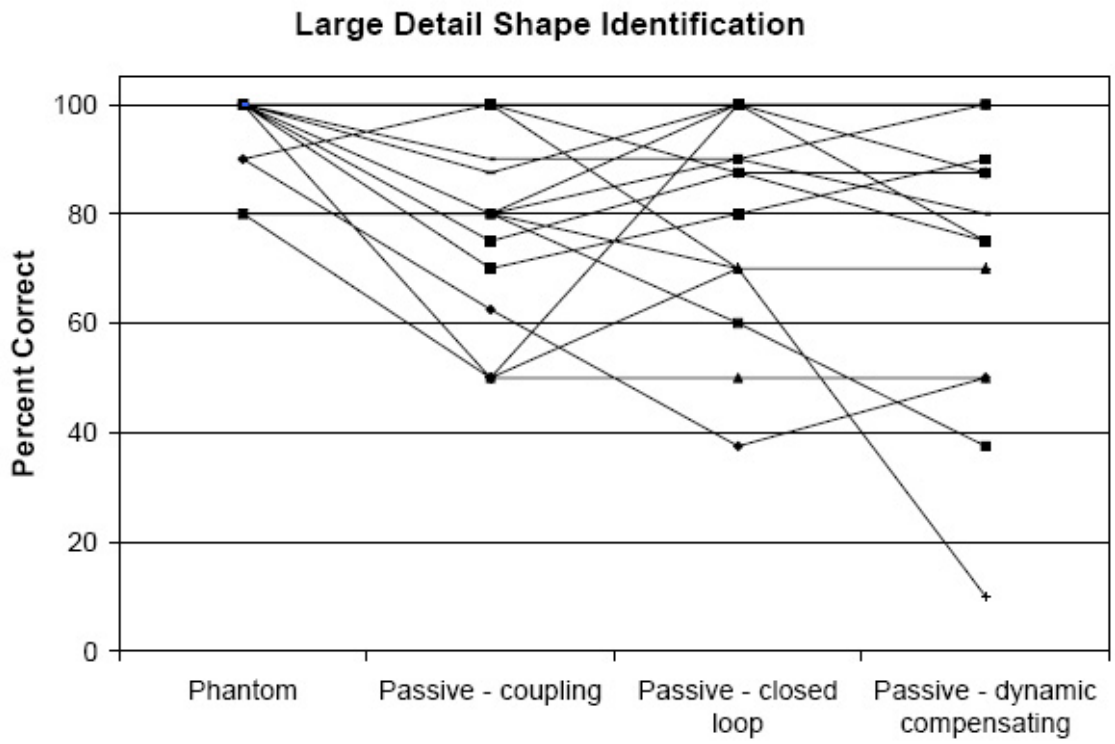

Figure 5.31: Complete results from large detail shape identification

to operation in some sort of contact condition. Depending on the user's spacial reasoning skills, they can translate the contact that they feel into the outline of one of the seven shapes with which the remote robot interacts. The possible shapes, shown in Fig. 5.28.

The complete results from the shape identification tasks are shown in Figs. 5.31 and 5.32. The figures show the percent correct with each master for each subject connected by a line. Following the analysis techniques used by Hurmuzulu, Fig. 5.33 summarizes all responses of all subjects [39]. Numerical values for these results are summarized in Appendix C in Table C.2

Breaking the results down further, Fig. 5.34 illustrates the wrong answers given for the convex circle in a pie chart form. Note that subjects picked other convex shapes for the majority of wrong answers. Figure 5.35 shows a summary of each of the wrong answers given by the subjects for all of the shapes. A numeric tabular

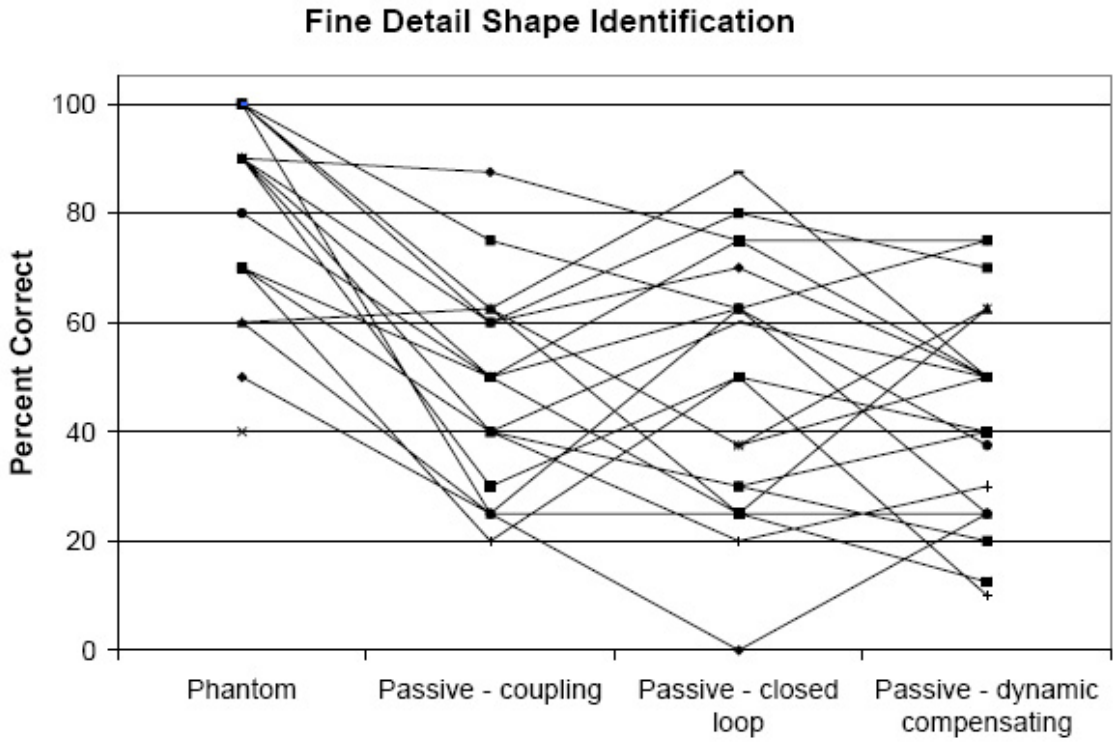

Figure 5.32: Complete results from fine detail shape identification

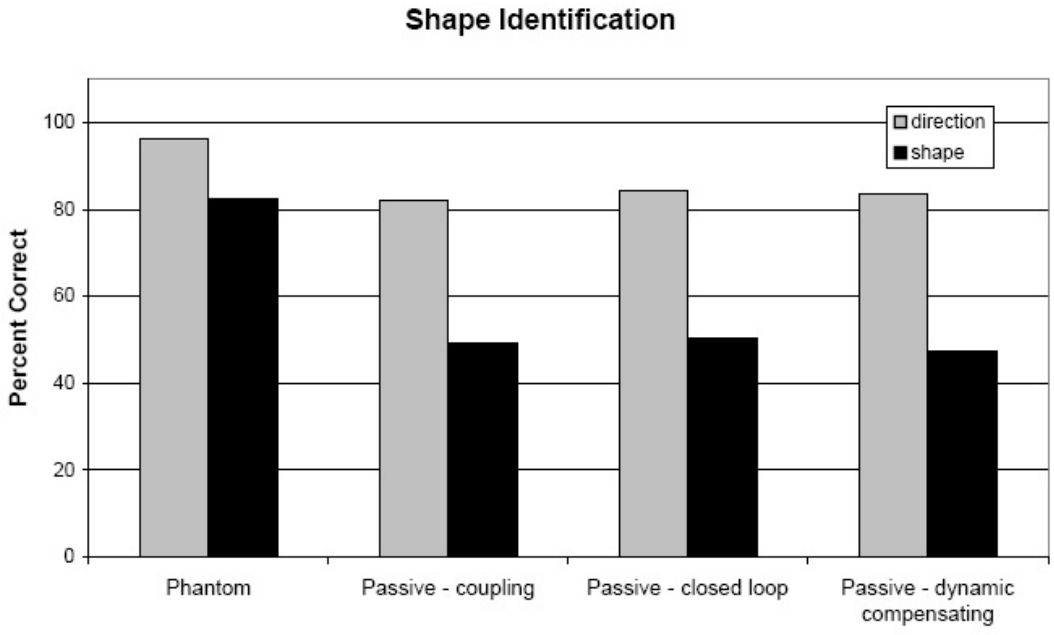

Figure 5.33: Summary of results from the shape identification experiment

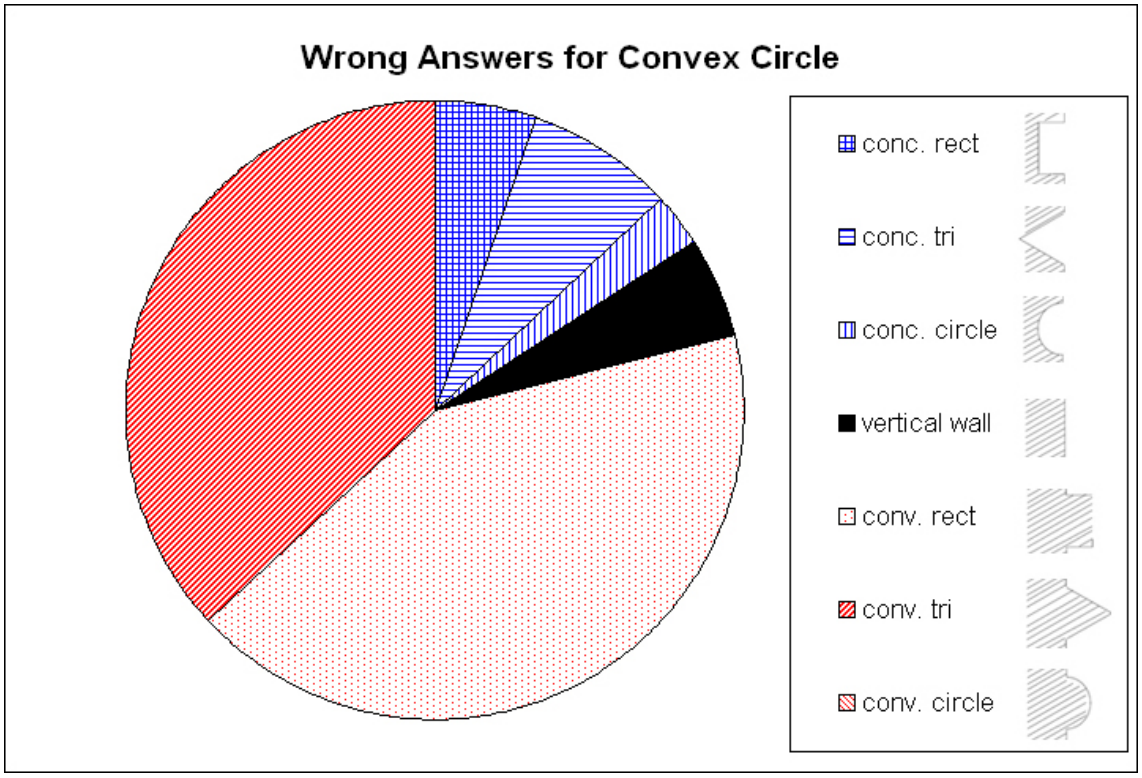

Figure 5.34: Wrong shape identification answers given for the convex circle

version of the same results can be found in Table C.3 in Appendix C.

The wrong answer results as a whole show that the wrong answers chosen by the subject most likely matched the correct answer in direction. Meaning that if the shape being displayed were concave, the subject most likely chose another concave shape as their incorrect answer. Figure 5.35 shows this trend for all of the shapes. In light of the overall results from the shape identification task from Fig. 5.33, this trend should not be surprising.

5.4.3.2 Obstacle Avoidance

Designed to simulate a realistic teleoperation task where an operator uses a tool to move from point to point without encroaching into a protected region, the obstacle avoidance task could easily simulate many tool manipulation, construction or medical robotics tasks. Originally the plan for the judging performance of a subject in this

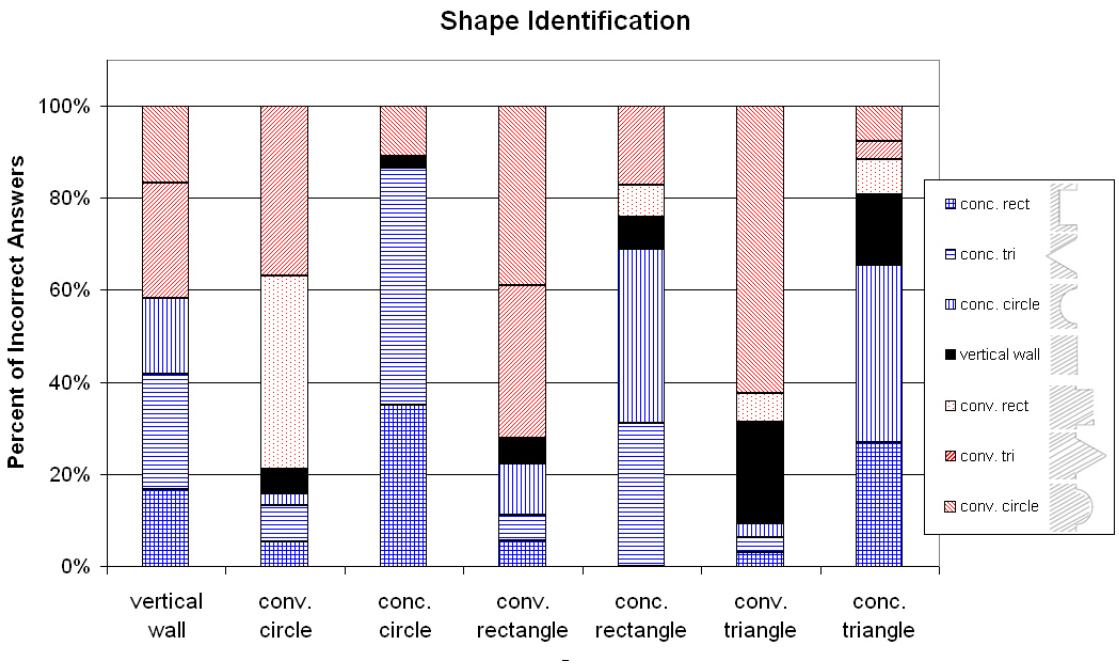

Figure 5.35: Summary of wrong answers from shape identification experiment

task included the analysis of incursion into the protected area; however, it turns out that the experimental design did not create enough difficulty to lead to the users penetrating into the protected area. Only a very small few of the subjects experienced any incursion into the protected area; therefore, this portion of the data yields no interesting results.

The results from the experiment then take the form of times required for completion. For each subject and each controller or master device, the data is recorded in as the sum of the time for each portion of the trial. For instance, subject 7 completed a motion from all three starting points (left, middle and right) to the finish point around the obstacle. His time for each of those motions with the dynamic compensating controller are 5.85 seconds, 5.04 seconds and 4.78 seconds respectively. The total time for that trial is 15.67 seconds. In attempt to compensate for the difference between subjects, all data has been normalized with respect to the time for the subject to compete the trial with the PHANTOM. Figure 5.36 shows a summary of

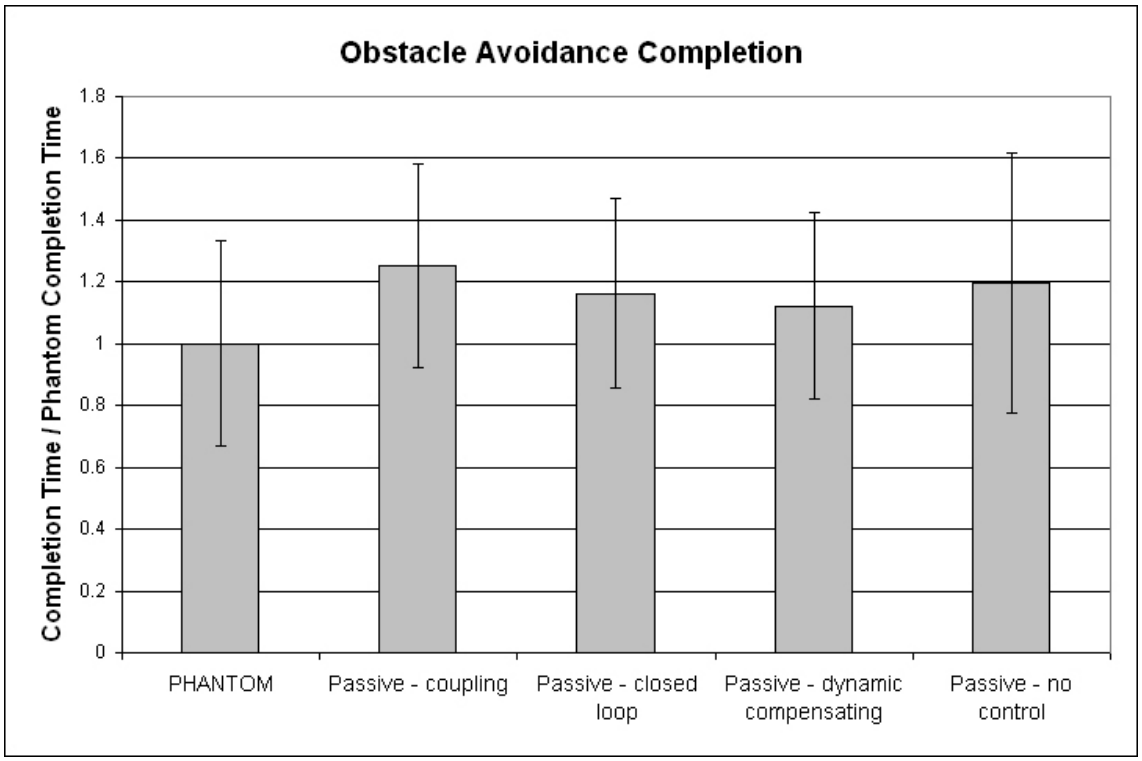

Figure 5.36: Summary of results for obstacle avoidance task

the results for this portion of the experiment, and the error bars show the standard deviation of the individual results.

Note that due to the normalization of the time data with respect to the PHANTOM results, each subject has a unit value for the completion time of the task. However, this would yield a standard deviation of zero, which would erroneously lead to the conclusion that each subject took the same amount of time. To remedy that, the error bars shown in Fig. 5.36 for the PHANTOM represent the standard deviation between all of the subjects divided by the mean time. This effectively normalizes the standard deviation as well. Table C.4 in Appendix C shows the actual values represented by Fig. 5.36.

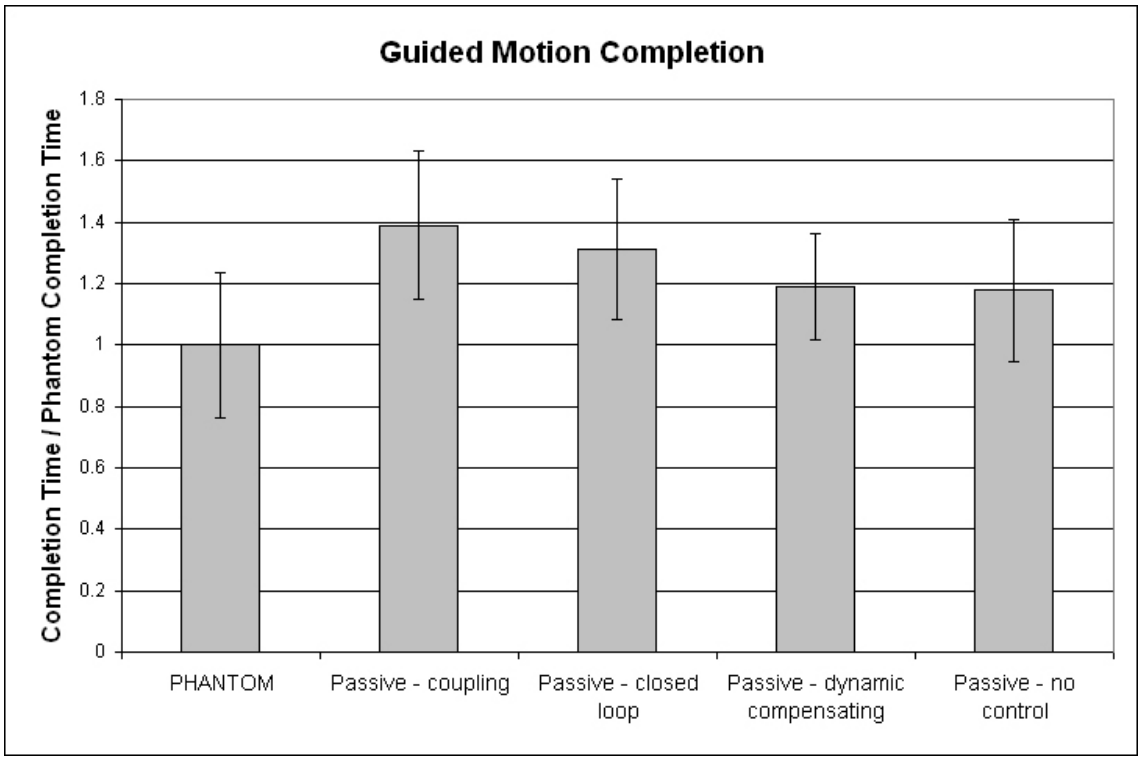

Figure 5.37: Results from the guided motion experiment

5.4.3.3 Guided Motion

As with the analysis of the obstacle avoidance experiment, normalization of the data for the guided motion portion of the experiment with respect to the values for the PHANTOM trials compensates for individual variation. For this task, each subject repeats each motion (such as point A to finish) twice with each control using MR PTER and again with the PHANTOM. Figure 5.37 shows a summary of the results of the trials the numeric values of which can be found in Table C.5 in Appendix C

5.4.3.4 NASA-TLX Data

The final portion of summarizable and reportable results from this experiment involve a qualitative analysis of the workload experienced by each subject. After using the PHANTOM and again after using MR PTER each subject answered the questions involved in the NASA-TLX workload index survey, and Fig. 5.38 summarizes the

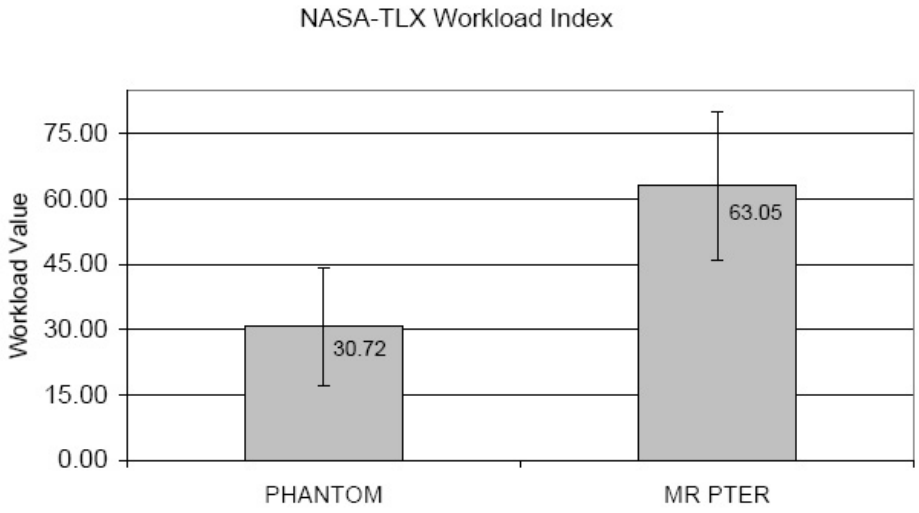

Figure 5.38: Average NASA-TLX workload for each master device

results. The survey breaks down the workload into six categories including, mental demand, physical demand, temporal demand, performance, effort and frustration. An average and analysis of these seven categories for MR PTER can be seen in Fig. 5.39, the exact values of which can be found in Table C.6 in Appendix C. Similar subresults are shown for the PHANTOM in Fig. 5.40 and Table C.7.

5.4.4 Conclusions

The full human factors testing represents the culmination of the research presented here. The results of the previous tests have been used to shape the controller and experimental design of the final testing.

5.4.4.1 Shape Identification

The results of the shape identification task seen in Fig. 5.33 have been divided into correct guesses of shape and correct guesses of direction (either into, flat with or out of the surface of the wall). Guessing the correct shape shows a subject's ability to judge fine detail while while judging the direction correctly shows a user's ability to judge larger surface features. None of the three passive controllers shows significant

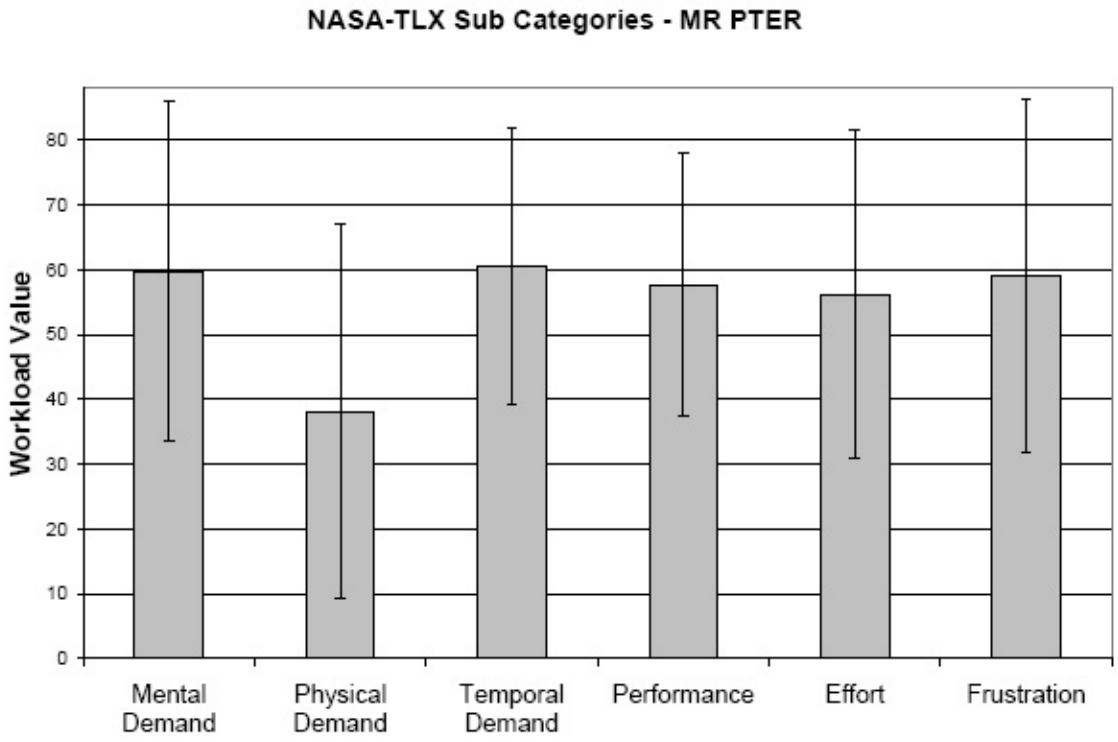

Figure 5.39: Breakdown of workload categories for MR PTER

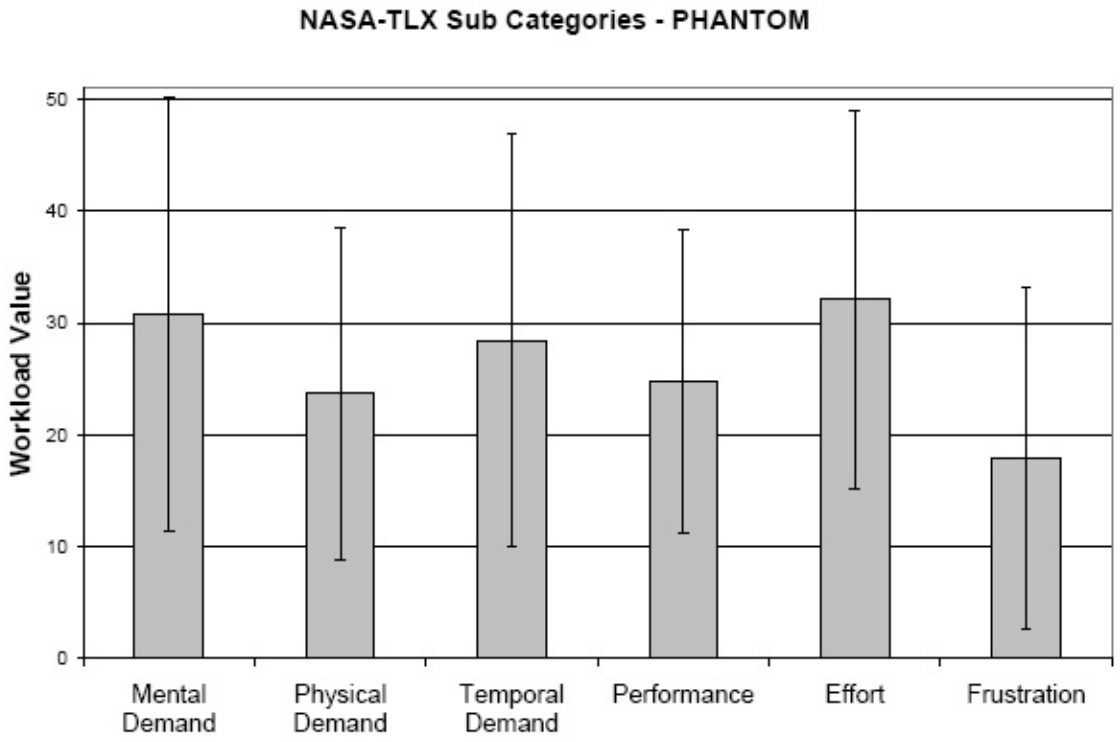

Figure 5.40: Breakdown of workload categories for the PHANTOM

difference from the others with respect to judging either fine or large detail. Furthermore, in comparison to the PHANTOM, MR PTER showed only a small decrease in the subject's ability to judge and discern large detail. However, the ability of the subjects to discern fine detail showed a significant difference between the use of the PHANTOM and of MR PTER.

Looking at the wrong answers from the shape identification test presented in Fig. 5.35 shows clearly that for the convex shapes, the typical wrong answers involve other convex shapes. The same results hold true for the concave shapes.

5.4.4.2 Obstacle Avoidance & Guided Motion

Both the obstacle avoidance and guided motion tasks produced similar results with the given hardware, software and experimental design. For both tasks, on average the user completed the required motions most quickly with the PHANTOM hardware. Similarly in both tasks, performance increases as the passive control algorithm changes from basic coupling to closed loop to dynamic compensating control. The only appreciable difference between the results of the two tasks comes from the results of the uncontrolled task with the passive device. The results for these segments can be see in Figs. 5.36 and 5.37.

Encouragingly, the results show that the additional components added to the force feedback felt by the user (error feedback and dynamic terms) increase performance. Furthermore results show the expected trend that the dynamic compensating controller performs the best in the tasks involving dynamic behavior.

Interestingly, the uncontrolled results for the obstacle avoidance and guided motion tasks do not match. In the obstacle avoidance task, the average results showed poorer performance than either the closed loop controller or the dynamic compensating controller; however, the results show a very large the standard deviation. In

the guided motion task, the uncontrolled results have a much lower standard deviation and the best average time of any of the trials. This unexpected trend can be attributed in part to the tasks selected for the experiment. The guided motion task involved a short straight motion while the obstacle avoidance task required a longer, curved motion. This difference in the tasks can possibly explain the large difference in the results.

5.4.4.3 NASA-TLX Data

Not surprisingly, NASA-TLX data in Fig. 5.38 showed that the user experienced a larger workload with the passive device than with the active device. The passive device has more mass than the active device, the workspace is larger and possibly most importantly the device dissipates energy.

The subcategories from Fig 5.39 show the average scores of the specific subcategories of the NASA-TLX test. While intuition might lead one to think that the physical demand would be the highest category, on the contrary it represents the lowest, and the only significantly different value of the five categories.

CHAPTER VI

CONCLUSIONS

Looking back to the questions presented in the introduction, the research presented here attempts to answer three central questions:

- Can a passive haptic device produce usable feedback when used in teleoperation?
- Does the passive haptic device provide as effective feedback as an active device in teleoperation?
- In what tasks do the differences between the feedback provided by the passive and active devices become negligible?

A brief look at the results relatively easily answer the first question with a "yes" and the second with a "not across the board." However answering the third question proves to be significantly more difficult.

Unfortunately results from the final experiment do not include an exit survey to provide the subjects with the ability to voice opinions about the devices. However, many of the subjects commented that they enjoyed using MR PTER in the dynamic experiments (point to point motion) more than using the PHANTOM. The comments included the fact that MR PTER seemed to move more smoothly and that it felt more natural than PHANTOM. While the subjects' opinions do not represent hard results, they do provide good feedback about the quality of the user experience.

For the experiments completed here, the passive device with the dynamic compensator shows very similar results to the active device for the point-to-point motion tasks. The results obviously illustrate the improved performance of the passive device

with dynamic compensation. Moreover the passive device with any controller shows similar results to the active device in determination of large surface details.

Taking a step back and looking at the combination of the results from all of the tests, some conclusions can be drawn about producing haptic feedback with a passive device. The perception tests illustrate clearly that re-producing remote forces with 100% accuracy need not be the primary concern of the haptic control algorithm. That leads in turn to the question of what type of feedback should instead be the main concern of the haptic controller. Research by Niemeyer and Kuchenbecker highlights the importance of vibrational feedback [51], and applying that theory to the passive device means that the control scheme needs to be updating the force felt by the user as quickly as possible so as to minimize delay and to minimize the amplitude of possible oscillations. The reserach presented here made every attempt possible to increase the speed of the control scheme by decreasing the information passed between master and slave and by running all portions of the resarch under real-time control. However an update rate of 200Hz falls short of other haptic systems including the PHANTOM.

To draw general conclusions about passive haptic hardware versus active haptic hardware used in teleoperation, the tests should have used two haptic devices with the same workspace, mass, construction, friction, etc, only made different by their actuators. The tests in this research use two quite different master devices, and thus the results only directly compare the PHANTOM with MR PTER. However, more general conclusions can be abstracted from the results presented here.

The displaying of fine surface detail will always be more difficult with a passive device as compared to using an active device. In an exploration task, once the user has penetrated into a surface the passive device has no way to push the user back to the boundary of the object. To improve surface detection with a passive device, the virtual coupling can be strengthened by increasing the spring constant; however that leads to larger forces felt by the user in free space due to the lag of the slave

behind the master. That in turn leads to more difficulty in distinguishing between free space and contact. The active device can push the user back to the surface of the object, and the user can apply very small forces to explore fine detail, explaining the differences in the results. On the other hand, in determining large detail it does not matter if the master penetrates into the surface of the shape slightly. Therefore the passive and active devices should perform similarly as the results suggest.

In dynamic tasks such as point to point motion or following of a line, a passive device has the ability to perform as well as an active device. The passive device with a dynamic compensating controller can approach the transparency of an active device. Even if the passive device does not compensate for all of its dynamic forces, the non-intuitive centripetal or coriolis forces can often be canceled making the device feel like a simple mass accelerating and decelerating. For a well designed passive device (fully steerable or low $Avg(\theta_{error})$), the performance of the passive device in dynamic tasks will approach that of an active device without any of the stability concerns of the active device.

6.1 Contributions

The following points represent the key contributions to come out of the research presented here (the list represents an expanded version of the list from the introduction).

1. Evaluation of a passive haptic device in teleoperation. Until this research, passive haptic devices have only been used to interact with a virtual environment. While the feedback generated when teleoperating or controlling a virtual device can be similar to the feedback generated when controlling a real device, typically the control systems operate differently. Interactions with a virtual device or environment typically assumed some known model of that system. Conversely, the teleoperation research presented here requires no such knowledge (only requiring the knowledge of the position of the two devices) and therefore

applies broadly to different slave devices and situations.

2. Quantification of the effectiveness of a passive haptic device in arbitrary force generation. Previous ways of looking at passive haptic devices such as steerability or the force manipulability ellipsoid focus on controlling the velocity of the device. This research focuses on position control of the haptic master and therefore, a different method of judging a haptic device needed to be developed. The idea of average angle error over the workspace of a device provides a method of judging and comparing the effectiveness of a device, and when combined with the force generating capabilities of the device provides a full view of its capabilities. Integrating this with the results from the perception testing yields a threshold for quantitatively judging a passive haptic device by looking at the portions of its workspace in which $Avg(\theta_{error})$ is greater than the perceptive threshold.

3. Creation and evaluation of a dynamic compensating controller for passive haptic devices. The controller developed for teleoperation takes principles used in active devices to increase transparency then adapts and extends them to the passive hardware. Due to the limitations of the device, the controller focuses on compensating for coriolis and centripetal forces, the less intuitive dynamic forces felt by the operator. This same controller can easily be applied to a passive device interacting with a virtual environment and could be extended to include more dynamic forces with the addition of accelerometer feedback to the system.

4. Quantification of human perceptive resolution with respect to force direction specifically on a passive haptic device. Very little research has been done to date on JND with respect to force direction. While not providing the resolution of some other current research presented in literature, the research here defines a

rough resolution of human perception of force direction with respect specifically to passive hardware, and more importantly to the passive hardware used for the subsequent tests.

5. Comparison of performance enhancement gained by the use of a passive and an active haptic device. An extensive literature review failed to yield any full human-factors testing using a dissipative passive haptic device, much less any research comparing the use of a passive device to the use of an active device in a head-to-head experiment. This research represents the first implementation of this. The tasks were chosen to replicate common teleoperation tests; shape identification, obstacle avoidance and guided motion. These types of tasks can be found widely in research using active devices either in teleoperation or in interfacing with a virtual environment. Therefore the tests performed in the research presented here can be easily compared with other accepted research.

6. Identification of tasks in which the passive haptic device provides task performance similar to that of an active device. This point represents possibly the most interesting as well as the most difficult to define of the contributions drawn from the research presented here. While the results represent a test between two very different devices (in workspace size, mass and magnitude of force generation), some general conclusions can abstracted from the collected data. The results show that while there are distinct disadvantages to using the passive device in teleoperation, the subjects were able to perform nearly as well in some tasks. While the users were not able to discern fine detail as well with the passive device, the results showed little difference between the passive and active devices with respect to discerning large detail. Furthermore, the results show that in the point to point motion tasks, the passive device with the dynamic

compensating controller performs nearly as well as the active device. Distilling these results slightly leads to the conclusion that the passive device and active device perform similarly in dynamic tasks and in tasks where the loss of fine detail is acceptable. In applications where safety is of utmost concern, the slight losses in performance might be well outweighed by the guarantees of safety provided by using a passive haptic master.

6.2 Future Work

Simple next steps in this research might include improving the perception test. Creating an addendum to the IRB proposal to extend the human-factors test to include a perception experiment would quickly cut through much of the paperwork and lead to an easy step in furthering this research. Refining the test to have a finer resolution and increasing the subject population would produce better publishable results. An extra step could also extend the dynamic compensating controller to include terms where $\ddot{x}$ and $\ddot{y}$ are not zero, drawing feedback from an accelerometer implemented in the hardware system.

In a theoretical sense, the research should be extended to apply to longer serial chains. While the groundwork from this research can be relatively easily extended, a rigorous exploration of of longer chains could be useful in generating more control options.

As a "life's work" type of extension, the most important direction of future work should focus on integrating human perception theory better into haptic research. The combination becomes especially important in a passive device that cannot produce arbitrary forces. Whether that combination takes the complex form of simulating and using the knowledge of the human response in real time or whether the simulation is only used in testing and honing of the control algorithm, a better understanding of the human response to a given haptic force will greatly improve the ability of a device

to effect human behavior and performance. This process would be incredibly long and difficult to explore fully; however even the inclusion of simple stimulus-response models into control algorithms could greatly improve their functionality.

Specifically with respect to the passive devices, control testing will benefit from an improved hardware testbed. Knowing that speed of response (actuators, control calculations and communication rates) and system dynamics greatly affect the quality of feedback felt by the user, a redesigned system could produce better feedback results. By keeping these factors as well as the judging criteria developed here in mind as design parameters, a far improved device could be constructed. Building hardware with faster actuators and less massive links will likely produce better results for the passive device. Similarly, moving the "elbow" joint brakes to the base of the system would move their mass so that the user would not feel their dynamics. Finally gearing or belting would allow the device to produce larger forces with similarly low-torque brakes.

The most interesting and most likely next steps of research involve combining passive and active actuators into one device. If the passive actuators maintain a significant power margin over the active actuators, the device will retain the benefits of the passive device while gaining the ability to produce small amounts of active feedback. A passive device such as MR PTER with a low-power active end effector will remain safe yet will be able to provide small amounts of restoring force.

APPENDIX A

DERIVATIONS - KINEMATICS & EQNS. OF MOTION

This section will show the rigorous development of the kinematic and dynamic equations of MR PTER in the rhomboid configuration, a state in which the length of the base linkage of the five-bar mechanism is equal to zero. The previous research of Matt Reed developed similar equations for the more complex configuration without coaxial base joints [73], meaning that the base linkage was given an arbitrary length. The second section will focus on the derivation of the equations of motion using a constrained Lagrange method using 5 generalized coordinates to describe the 2-dimensional system.

A.1 Kinematics

Figure A.1 shows a line drawing of the device used in this research. The base angles are measured as θ_A and θ_B. Links 1, 2, 3 & 4 have lengths L_1, L_2, L_3 & L_4 respectively. The position of the endpoint, the center of Joint D, will be used as generalized coordinate (x, y). Therefore, (x, y) can be a function of θ_B & θ_C or θ_A & θ_E

$$x = L_1 cos(\theta_B) + L_2 cos(\theta_C) \tag{A.1}$$

$$y = L_1 sin(\theta_B) + L_2 sin(\theta_C) \tag{A.2}$$

or

$$x = L_4 cos(\theta_A) + L_3 cos(\theta_E) \tag{A.3}$$

$$y = L_4 sin(\theta_A) + L_3 sin(\theta_E) \tag{A.4}$$

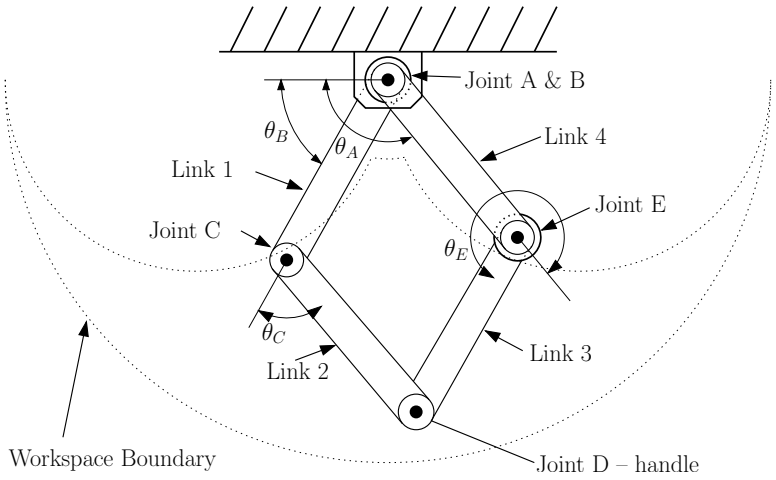

Figure A.1: Reference for derivation of kinematic equations

However due to the fact that the base joints are coaxial and that the link lengths are equal:

$$L_1 = L_2 = L_3 = L_4 = L \tag{A.5}$$

$$\theta_C = \theta_A - \theta_B \tag{A.6}$$

$$\theta_E = \theta_B - \theta_A \tag{A.7}$$

Therefore:

$$x = L(cos(\theta_A) + cos(\theta_B)) \tag{A.8}$$

$$y = L(sin(\theta_A) + sin(\theta_B)) \tag{A.9}$$

For the inverse kinematics, Fig. A.2 shows the variables used in the development of th equations. The angle β defines the angle of a line connecting the base joints to the endpoint, and the angle α defines the angle between that line and Link 1.

$$\beta = tan^{-1}(\frac{y}{x}) \tag{A.10}$$

$$\beta = \theta_B + \frac{1}{2}(\theta_A - \theta_B) \tag{A.11}$$

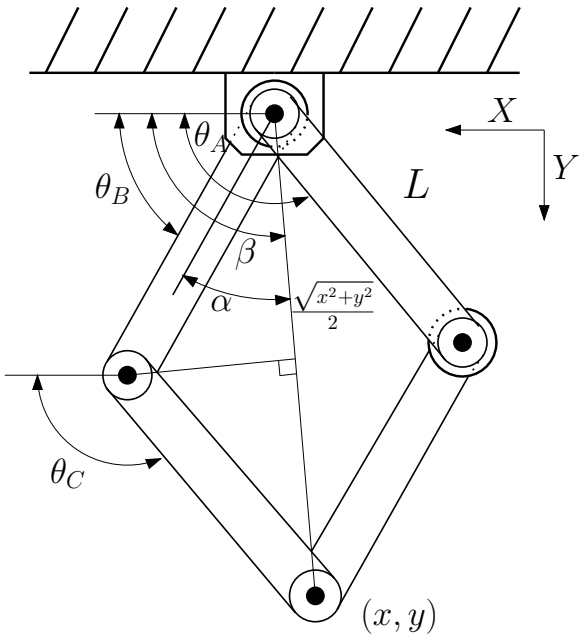

Figure A.2: Reference for derivation of inverse kinematics

$$\beta = \frac{1}{2}(\theta_B + \theta_A) = tan^{-1}(\frac{y}{x}) \tag{A.12}$$

$$\theta_B + \theta_A = 2tan^{-1}(\frac{y}{x}) \tag{A.13}$$

Looking at half of the distance from the base point to the endpoint yields another relationship:

$$\frac{1}{2}\sqrt{x^2 + y^2} = Lcos(\alpha) = Lcos(\frac{\theta_A - \theta_B}{2}) \tag{A.14}$$

$$\theta_A - \theta_B = 2cos^{-1}(\frac{\sqrt{x^2 + y^2}}{2L}) \tag{A.15}$$

Combining Eqn. A.15 and A.13 yields:

$$\theta_A = tan^{-1}(\frac{y}{x}) + cos^{-1}(\frac{\sqrt{x^2 + y^2}}{2L}) \tag{A.16}$$

$$\theta_B = tan^{-1}(\frac{y}{x}) - cos^{-1}(\frac{\sqrt{x^2 + y^2}}{2L}) \tag{A.17}$$

Differentiating the kinematic equations yields:

$$\dot{x} = -L(sin(\theta_A)\dot{\theta}_A + sin(\theta_B)\dot{\theta}_B) \tag{A.18}$$

$$\dot{y} = L(cos(\theta_A)\dot{\theta}_A + cos(\theta_B)\dot{\theta}_B) \tag{A.19}$$

For reference:

$$\frac{d}{dt}\left(tan^{-1}(\alpha)\right) = \frac{1}{1+\alpha^2} \tag{A.20}$$

$$\frac{d}{dt}\left(cos^{-1}(\alpha)\right) = \frac{-1}{\sqrt{1-\alpha^2}} \tag{A.21}$$

Differentiation of the inverse kinematics yields:

$$\dot{\theta}_A = \frac{\dot{y}x - \dot{x}y}{x^2+y^2} - \frac{L(\dot{x}x + \dot{y}y)}{\sqrt{-(x^2+y^2)(x^2+y^2-4L^2)}} \tag{A.22}$$

$$\dot{\theta}_B = \frac{\dot{y}x - \dot{x}y}{x^2+y^2} + \frac{L(\dot{x}x + \dot{y}y)}{\sqrt{-(x^2+y^2)(x^2+y^2-4L^2)}} \tag{A.23}$$

A.2 Jacobian

The Jacobian matrix describes the relation ship between cartesian endpoint velocity and joint velocity as well the relationship between endpoint force and joint torques. In the derivations presented here, the Jacobian matrix takes the form of Eqn. A.24.

$$\dot{x} = J\dot{\theta} \tag{A.24}$$

Looking back at Eqns. A.18 and A.19 and putting them in matrix form, the following Jacobian matrix J_{AB} represents the relationship between endpoint velocity and joint velocities. Where the capital subscripts represent the two joints being used in the calculation, the first subscript corresponds to the column of the Jacobian matrix, and the lower case subscript corresponds to the row.

$$J_{AB} = \begin{bmatrix} J_{ABx} & J_{BAx} \\ J_{ABy} & J_{BAy} \end{bmatrix} = \begin{bmatrix} -Lsin(\theta_A) & -Lsin(\theta_B) \\ Lcos(\theta_A) & Lcos(\theta_B) \end{bmatrix} \tag{A.25}$$

Equation A.26 represents the relationship between θ_A, θ_B, and θ_E differentiating and rearranging yields Eqn. A.27. Substituting that into Eqns. A.18 and A.19 and

putting those into matrix form yields similar Jacobian matricies relating joint E to the endpoint velocity.

$$2\pi = \theta_A - \theta_B + \theta_E \tag{A.26}$$

$$\dot{\theta}_A = \dot{\theta}_B - \dot{\theta}_E \tag{A.27}$$

$$J_{AE} = \begin{bmatrix} J_{AEx} & J_{EAx} \\ J_{AEy} & J_{EAy} \end{bmatrix} = \begin{bmatrix} -Lsin(\theta_A) - Lsin(\theta_B) & -Lsin(\theta_B) \\ Lcos(\theta_A) + Lcos(\theta_B) & Lcos(\theta_B) \end{bmatrix} \tag{A.28}$$

A.3 Dynamics

Derivation of the equations of motion takes the following form with M defined as the generalized mass matrix, V contains the non-linear coriolis terms, G contains the gravity terms and Q represents the generalized forces. The state vector of generalized coordinates q and its derivatives define the states of the system

$$M(q)\ddot{q} + V(q, \dot{q}) + G(q) = Q \tag{A.29}$$

However, the system will be derived using the five generalized coordinates in Eqn. A.30, meaning that the two-dimensional system is overdefined.

$$q = \{x, y, \theta_A, \theta_B, \theta_E\} \tag{A.30}$$

$$Q = \{F_x, F_y, \tau_A, \tau_B, \tau_E\} \tag{A.31}$$

To solve for this problem, the system of equations is derived using the Lagrange method with constraint equations, the form of which can be found in Eqn. A.32 where the λ variables represent the Lagrange multipliers.

$$\begin{bmatrix} M(q) & -A^T(q,\dot{q}) \\ -A(q,\dot{q}) & [0] \end{bmatrix} \begin{bmatrix} \ddot{q} \\ \lambda \end{bmatrix} = \begin{bmatrix} Q - V(q,\dot{q}) - G(q) \\ \dot{A}(q,\dot{q})\,\dot{q} \end{bmatrix} \tag{A.32}$$

For the system, there are no values of the G matrix, and the A matrix can be derived using the constraint equations in Eqns. A.33, A.34 & A.35.

$$C_1 \Rightarrow Lcos(\theta_A) + Lcos(\theta_B) - x = 0 \tag{A.33}$$

$$C_2 \Rightarrow Lsin(\theta_A) + Lsin(\theta_B) - x = 0 \tag{A.34}$$

$$C_3 \Rightarrow 2\pi - \theta_A + \theta_B - \theta_E = 0 \tag{A.35}$$

The relationship between the A matrix and the constraint equations comes from Eqn. A.36.

$$A_{ij} = \frac{\partial C_i}{\partial q_j} \tag{A.36}$$

Evaluation of A yields the matrix in Eqn. A.37, and its derivative can be seen in Eqn. A.38.

$$A = \begin{bmatrix} -1 & 0 & -Lsin(\theta_A) & -Lsin(\theta_B) & 0 \\ 0 & -1 & Lcos(\theta_A) & Lcos(\theta_B) & 0 \\ 0 & 0 & -1 & 1 & -1 \end{bmatrix} \tag{A.37}$$

$$\dot{A} = \begin{bmatrix} 0 & 0 & -Lcos(\theta_A)\dot{\theta}_A & -Lcos(\theta_B)\dot{\theta}_A & 0 \\ 0 & 0 & -Lsin(\theta_A)\dot{\theta}_A & -Lsin(\theta_B)\dot{\theta}_A & 0 \\ 0 & 0 & 0 & 0 & 0 \end{bmatrix} \tag{A.38}$$

The generalized mass matrix and the coriolis matrix are derived using the normal Lagrange approach (the typical form of which is shown in Eqn. A.39), starting with

the kinetic and potential energy equations for the system; however since MR PTER is planar perpendicular to gravity and has no springs, the potential energy disappears from the derivation.

$$\frac{d}{dt}\left(\frac{\partial T}{\partial \dot{q}_j}\right) - \frac{\partial T}{\partial q_j} + -\frac{\partial V}{\partial q_j} = Q_j \tag{A.39}$$

Also to simplify the differentiation, the typical form of Lagrange's equations has been put into a form more suited for symbolic differentiation in Maple. This form can be found in Eqns. A.40 and A.41 where $i = 1, 2, 3, 4, 5$, $j = 1, 2, 3, 4, 5$ and the summation goes from $k = 1$ to $k = 5$.

$$M_{ij} = \frac{\partial}{\partial \dot{q}_j}\frac{\partial T}{\partial \dot{q}_i} \tag{A.40}$$

$$V_j = \frac{\partial T}{\partial \dot{q}_j} + \sum \frac{\partial}{\partial q_k}\frac{\partial T}{\partial \dot{q}_j}\dot{q}_k \tag{A.41}$$

For MR PTER, the kinetic energy T can be broken down into the parts in Eqns. A.42-A.49 that represent the kinetic energies of each link (the subscripts denote the joints that create the endpoints of the link) and the kinetic energies of the other components (brake and handle). The moments of inertia I and the masses m are also labeled with subscripts to correspond to their links.

$$T_{AE} = \frac{1}{2} I_{AE} \dot{\theta}_A^2 \tag{A.42}$$

$$T_{BC} = \frac{1}{2} I_{BC} \dot{\theta}_B^2 \tag{A.43}$$

$$T_{CD} = \frac{1}{2} I_{CD} \left(\dot{\theta}_A + \dot{\theta}_B\right)^2 + \frac{1}{2} m_{CD} v_{CD}^2 \tag{A.44}$$

with

$$v_{CD} = \sqrt{\left(-Lsin(\theta_B\dot{\theta}_B - \frac{L}{2}sin(\theta_A)\dot{\theta}_A)\right)^2 + \left(Lcos(\theta_B\dot{\theta}_B + \frac{L}{2}cos(\theta_A)\dot{\theta}_A)\right)^2} \quad \text{(A.45)}$$

$$T_{ED} = \frac{1}{2}I_{ED}\left(\dot{\theta}_A + \dot{\theta}_B\right)^2 + \frac{1}{2}m_{ED}v_{ED}^2 \quad \text{(A.46)}$$

with

$$v_{ED} = \sqrt{\left(-Lsin(\theta_A\dot{\theta}_A - \frac{L}{2}sin(\theta_B)\dot{\theta}_B)\right)^2 + \left(Lcos(\theta_A\dot{\theta}_A + \frac{L}{2}cos(\theta_B)\dot{\theta}_B)\right)^2} \quad \text{(A.47)}$$

$$T_{brake} = \frac{1}{2}m_{brake}\left(\dot{\theta}_A L\right)^2 \quad \text{(A.48)}$$

$$T_{handle} = \frac{1}{2}m_{handle}\left(\dot{x} + \dot{y}\right)^2 \quad \text{(A.49)}$$

The overall kinetic of the energy of the system T is the sum of the kinetic energies of the four links and the other components, represented in Eqn. A.50

$$T = T_{AE} + T_{BC} + T_{CD} + T_{ED} + T_{brake} + T_{handle} \quad \text{(A.50)}$$

Applying Eqn. A.40 yields the following values for the equivalent mass matrix, M. Note that by definition $M_{ab} = M_{ba}$.

$$M_{11} = m_{handle} \quad \text{(A.51)}$$

$$M_{12} = M_{13} = M_{14} = M_{15} = 0 \quad \text{(A.52)}$$

$$M_{22} = m_{handle} \quad \text{(A.53)}$$

$$M_{23} = M_{24} = M_{25} = 0 \tag{A.54}$$

$$M_{33} = 2I_{CD} + \frac{1}{4}m_{CD}L^2 + m_{ED}L^2 + I_{AE} + m_{brake}L^2 \tag{A.55}$$

$$\begin{aligned} M_{34} \quad &= 2I_{CD} + \tfrac{1}{2}m_{CD}L^2 sin(\theta_A)sin(\theta_B) + \tfrac{1}{2}m_{CD}L^2 cos(\theta_A)cos(\theta_B) \\ &+ \tfrac{1}{2}m_{ED}L^2 sin(\theta_A)sin(\theta_B) + \tfrac{1}{2}m_{ED}L^2 cos(\theta_A)cos(\theta_B) \end{aligned} \tag{A.56}$$

$$M_{35} = 0 \tag{A.57}$$

$$M_{44} = I_{BC} + 2I_{CD} + m_{CD}L^2 + \frac{1}{4}m_{ED}L^2 \tag{A.58}$$

$$M_{45} = 0 \tag{A.59}$$

$$M_{55} = 0 \tag{A.60}$$

Using Eqn. A.41 to evaluate the column vector V yields the following values:

$$V_1 = 0 \tag{A.61}$$

$$V_2 = 0 \tag{A.62}$$

$$\begin{aligned} V_3 \quad &= \tfrac{1}{2}L^2\dot{\theta}_B^2 \left(m_{CD}sin(\theta_A)cos(\theta_B) - m_{CD}cos(\theta_A)sin(\theta_B)\right) \\ &+ \tfrac{1}{2}L^2\dot{\theta}_B^2 \left(m_{ED}sin(\theta_A)cos(\theta_B) - m_{ED}cos(\theta_A)sin(\theta_B)\right) \end{aligned} \tag{A.63}$$

$$
\begin{aligned}
V_4 \;&= -\tfrac{1}{2}L^2\dot{\theta}_A\dot{\theta}_B\left(m_{CD}sin(\theta_A)cos(\theta_B) - m_{CD}cos(\theta_A)sin(\theta_B)\right) \\
&\quad -\tfrac{1}{2}L^2\dot{\theta}_B^2\left(m_{ED}sin(\theta_A)cos(\theta_B) - m_{ED}cos(\theta_A)sin(\theta_B)\right)
\end{aligned} \tag{A.64}
$$

$$
V_5 = 0 \tag{A.65}
$$

Specifically for the dynamic compensating controller, the system dynamics were rearranged to facilitate solving for dynamic forces. Again with the assumptions of constant velocity and no friction, Eqn. A.66 becomes valid.

$$
\ddot{x} = \ddot{y} = \tau_A = \tau_B = \tau_E = 0 \tag{A.66}
$$

Since $\ddot{x}$ and $\ddot{y}$ equal zero, the system of dynamic equations can be easily rearranged to solve for F_x and F_y. The new mass matrix M' is the same as M with the components M_{11} and M_{22} set to -1. For a similar reason, A' will be th same as A except the first two columns will be all zeros. The rearrangement yields Eqn. A.67.

$$
\begin{bmatrix} M'(q) & -A^T(q,\dot{q}) \\ -A'(q,\dot{q}) & [0] \end{bmatrix}
\begin{bmatrix} F_x \\ F_y \\ \ddot{\theta}_A \\ \ddot{\theta}_B \\ \ddot{\theta}_E \\ \lambda_1 \\ \lambda_2 \\ \lambda_3 \end{bmatrix}
=
\begin{bmatrix} -V_1(q,\dot{q}) \\ -V_2(q,\dot{q}) \\ -V_3(q,\dot{q}) \\ -V_4(q,\dot{q}) \\ -V_5(q,\dot{q}) \\ \dot{A}\dot{q}_1 \\ \dot{A}\dot{q}_2 \\ \dot{A}\dot{q}_3 \end{bmatrix} \tag{A.67}
$$

Again rearranging yields Eqn. A.68.

Table A.1: MR PTER physical properties used in controller

variable	value	units
m_{handle}	1.3	kg
m_{brake}	0.8	kg
m_2	0.87	kg
m_3	0.96	kg
I_1	327	$kg * cm^2$
I_2	347	$kg * cm^2$
I_3	358	$kg * cm^2$
I_4	358	$kg * cm^2$
L	30.5	cm

$$\begin{bmatrix} F_x \\ F_y \\ \ddot{\theta}_A \\ \ddot{\theta}_B \\ \ddot{\theta}_E \\ \lambda_1 \\ \lambda_2 \\ \lambda_3 \end{bmatrix} = \begin{bmatrix} M'(q) & -A^T(q,\dot{q}) \\ -A'(q,\dot{q}) & [0] \end{bmatrix}^{-1} \begin{bmatrix} -V_1(q,\dot{q}) \\ -V_2(q,\dot{q}) \\ -V_3(q,\dot{q}) \\ -V_4(q,\dot{q}) \\ -V_5(q,\dot{q}) \\ \dot{A}\dot{q}_1 \\ \dot{A}\dot{q}_2 \\ \dot{A}\dot{q}_3 \end{bmatrix} \tag{A.68}$$

Knowing the state of the system gives q and estimating the velocities yields $\dot{q}$. Therefore, this yields known equations for F_x and F_y.

The following list of properties is used in the equations previously derived to calculate the dynamic forces in the dynamic compensating controller. The values are approximations that include the mass of the various components including lock-plates and fasteners.

APPENDIX B

SAMPLE CODE

B.1 Simulation Code

The LabVIEW code in Fig. B.1 and B.1 is used to test the dynamic equations. Figure B.1 appears as the block with a "D" in the upper left section of Fig. B.1. Note that the initial conditions supplied to the solver for the dependent variables x, y & θ_E are calculated based on the independent variables θ_A & θ_B.

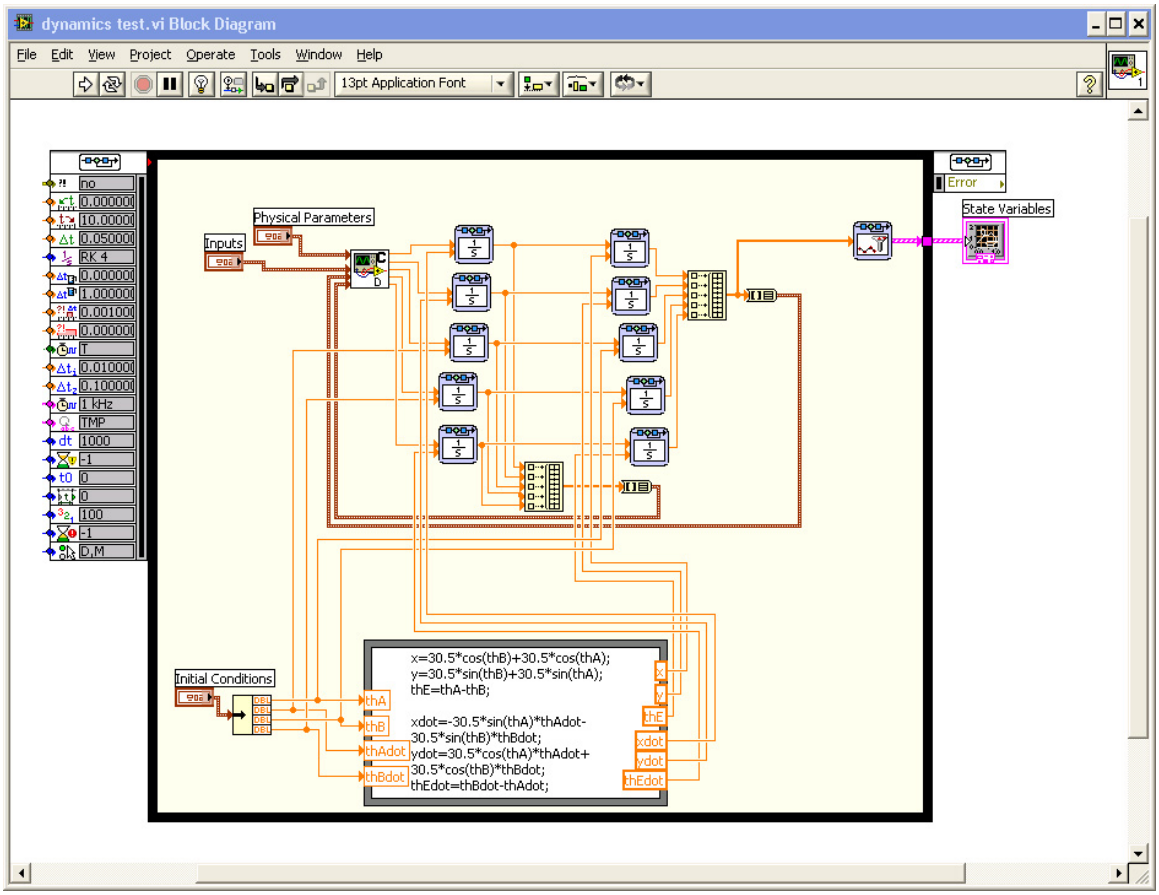

Figure B.3: Dynamic solver code

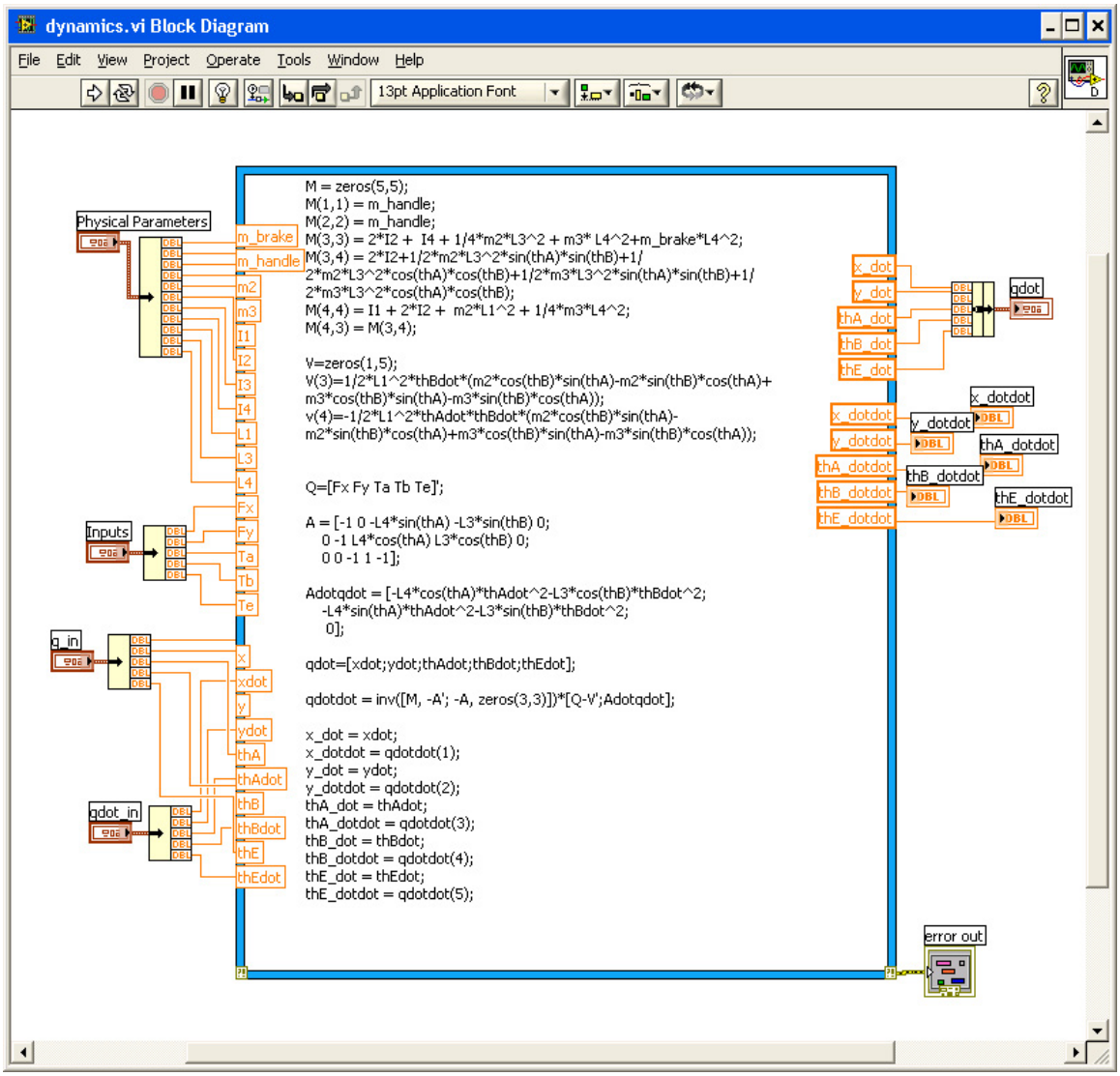

Figure B.4: Dynamic equations - DAE form

B.2 Final Master Control Code

The entire group of code used to control the master, slave and host devices is managed using the LabVIEW 8.2 project explorer depicted in Fig. B.2. This construct allows the operator to manage multiple real-time computers as well as the entire library of code easily and efficiently. The rest code used to control the master device can be found in the front panel shown in Fig. B.2 and the block diagram shown in Fig B.2.

In each set of code shown in this section, it is important to note the multi-threaded architecture. Each of the programs has a main control thread and multiple communications threads. The communication thread between the master and slave devices operates at 250Hz for the receive portion and 200Hz for the send thread (as discussed in the section on communication protocols and software). The state of the system is passed to the host from the slave system due to the fact that when using the PHANTOM the master controller changes to a WindowsXP based program. Sending the information to the host from the slave keeps the communication the same between the two masters. This communication thread iterates at a much slower rate, $6\frac{2}{3}$Hz send rate and 10Hz receive rate. The slow rate provides sufficient GUI information while not straining the system.

B.3 Final Slave Control Code

Similar to the code shown in the master section, the control code can be found in Fig. B.3 that shows the front panel used to control the slave and Fig. B.3 that represents the block diagram used to control the device.

B.4 Final Host Code

The final section of code shows the programs used to implement the host program and the GUI. The block diagram in Fig. B.4 provides the interface for the subject as well as the test administrator to monitor the states of the system. Figure B.4 shows

the control code behind the GUI.

B.5 Communication Testing Code

The following section includes the code used for the testing of the communication protocols. The first section displays the code used to test the TCP/IP protocol, and the second group of three tested UDP/IP.

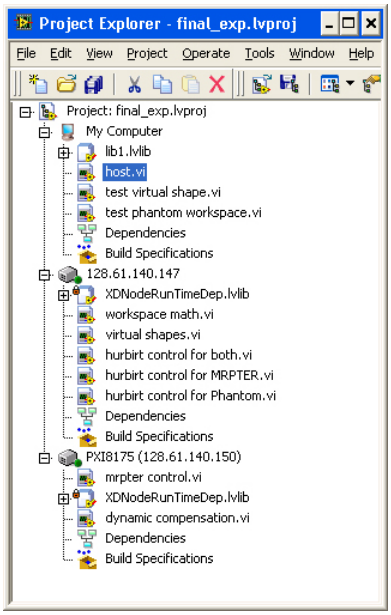

Figure B.5: Project explorer from final human-testing experiment

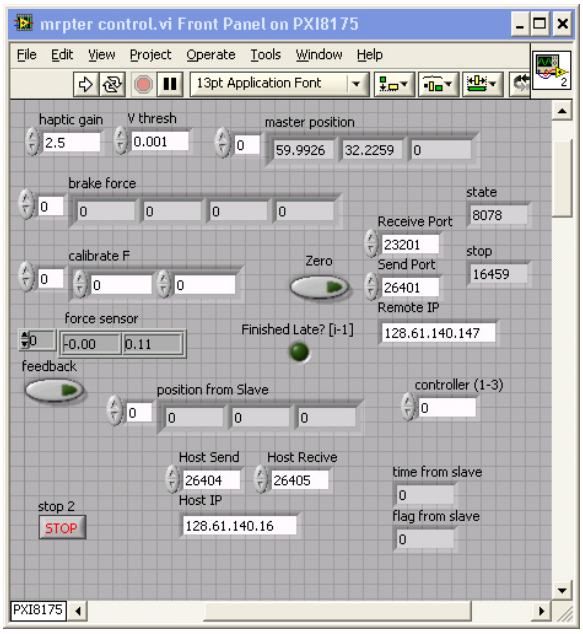

Figure B.6: Front panel of control code for MR PTER in the final experiment

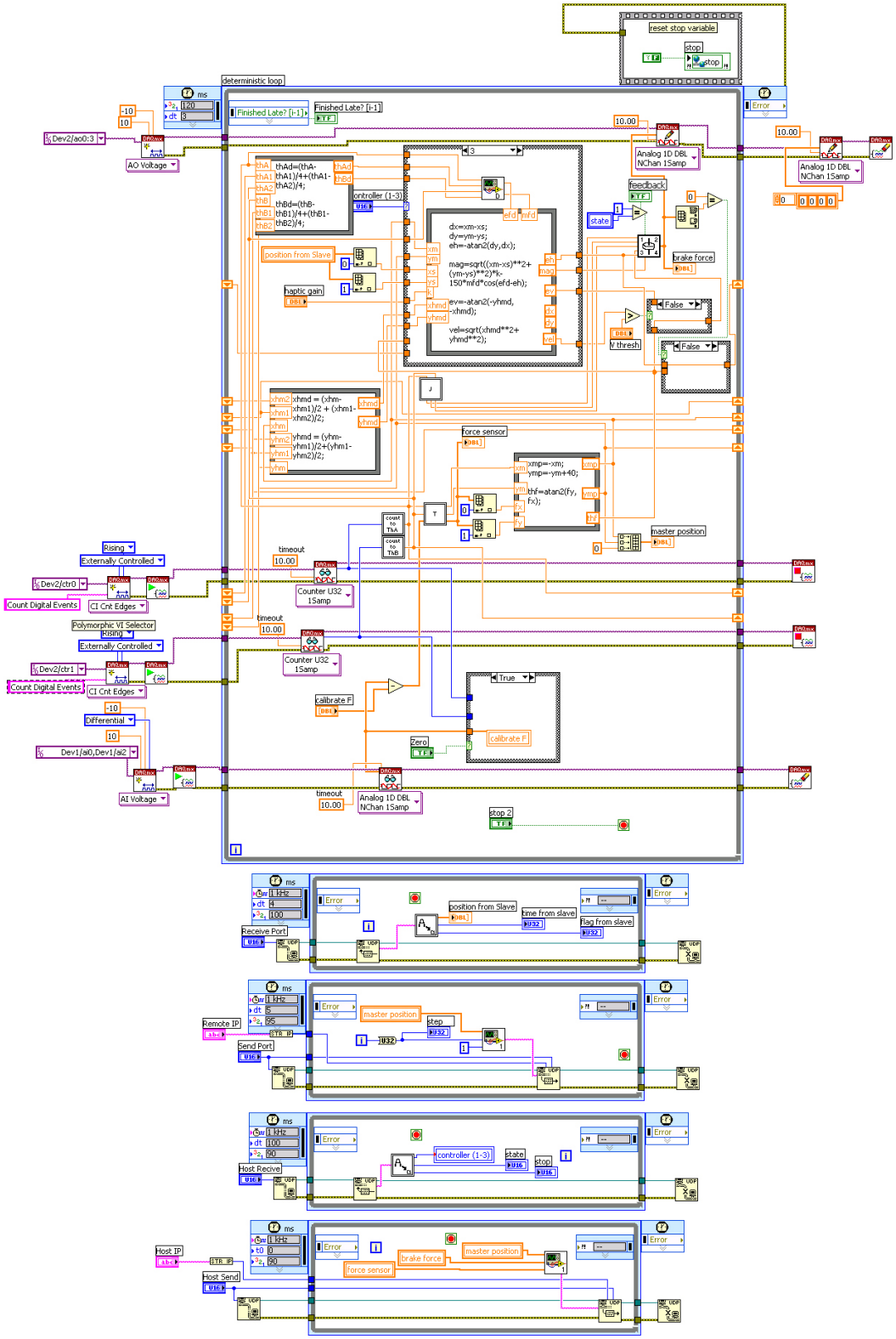

Figure B.7: Block diagram used to control MR PTER in the final experiment

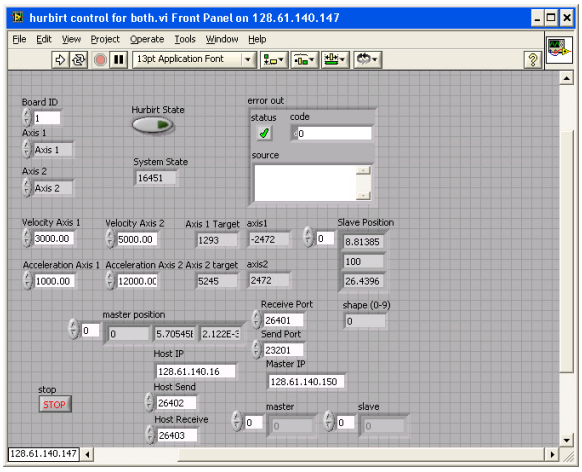

Figure B.8: Front panel of HuRBiRT control code from the final experiment

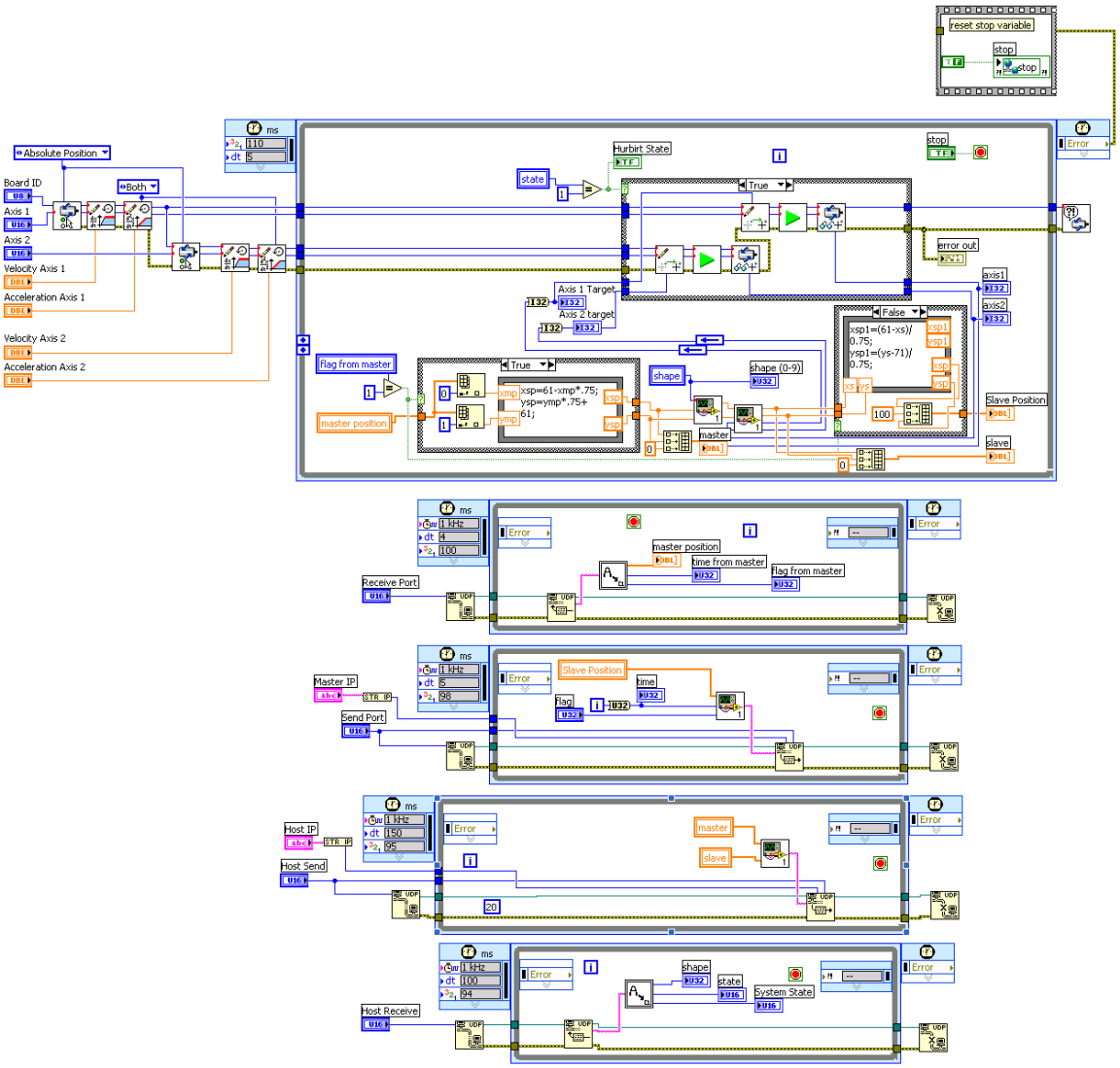

Figure B.9: Block diagram used to control HuRBiRT in the final experiment

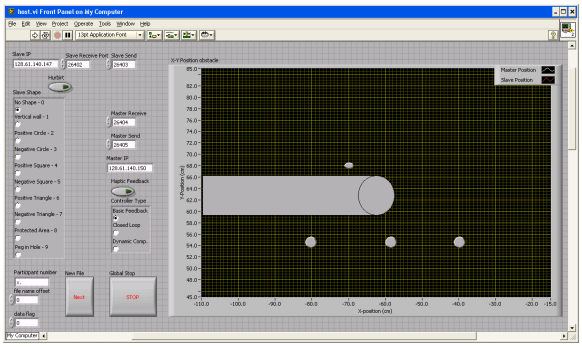

Figure B.10: Front panel of host code from the final experiment

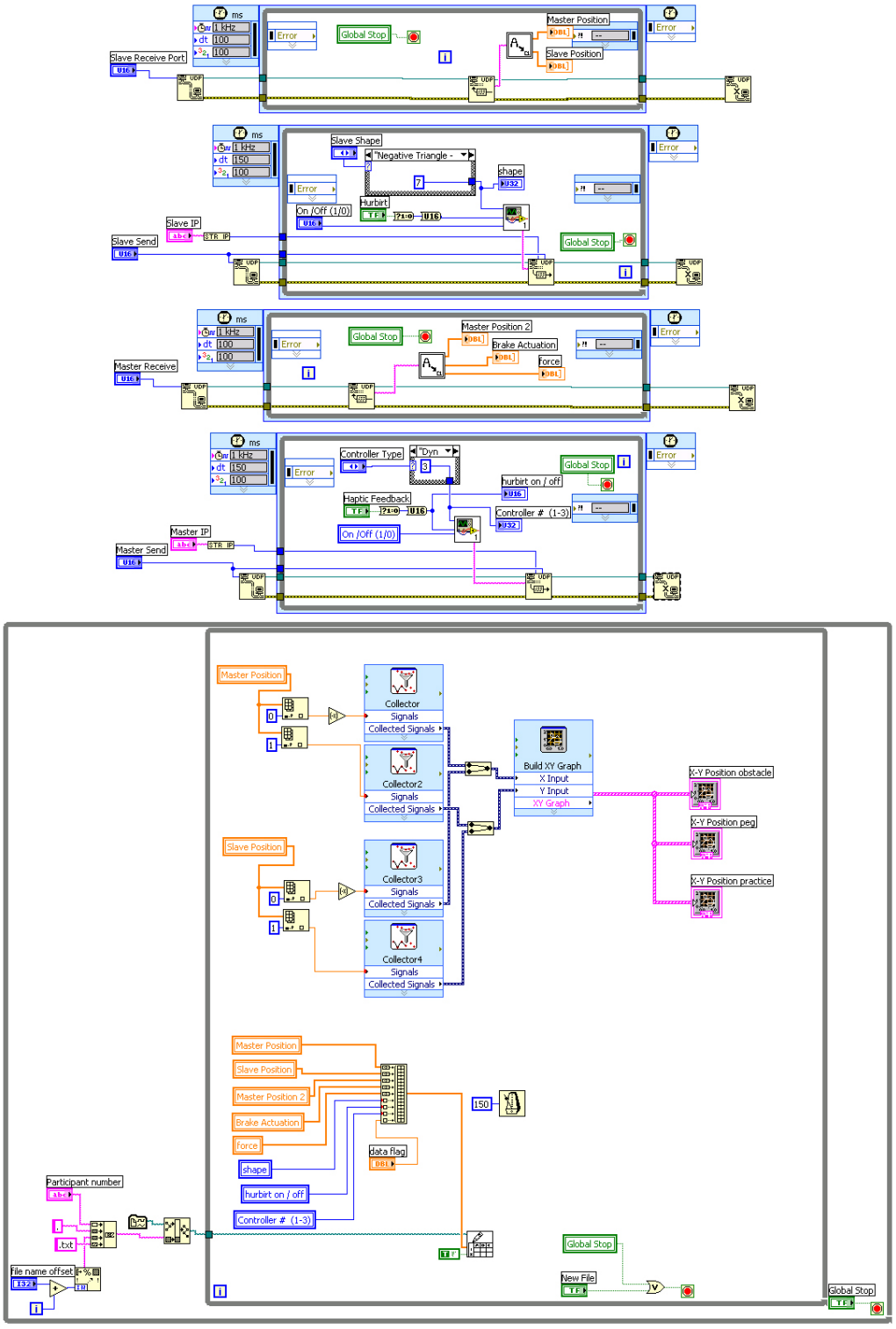

Figure B.11: Block diagram from host code in the final experiment

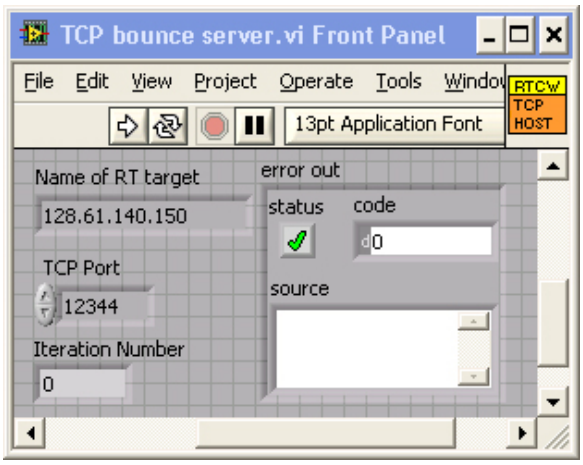

Figure B.12: Front panel of the TCP/IP communication test code

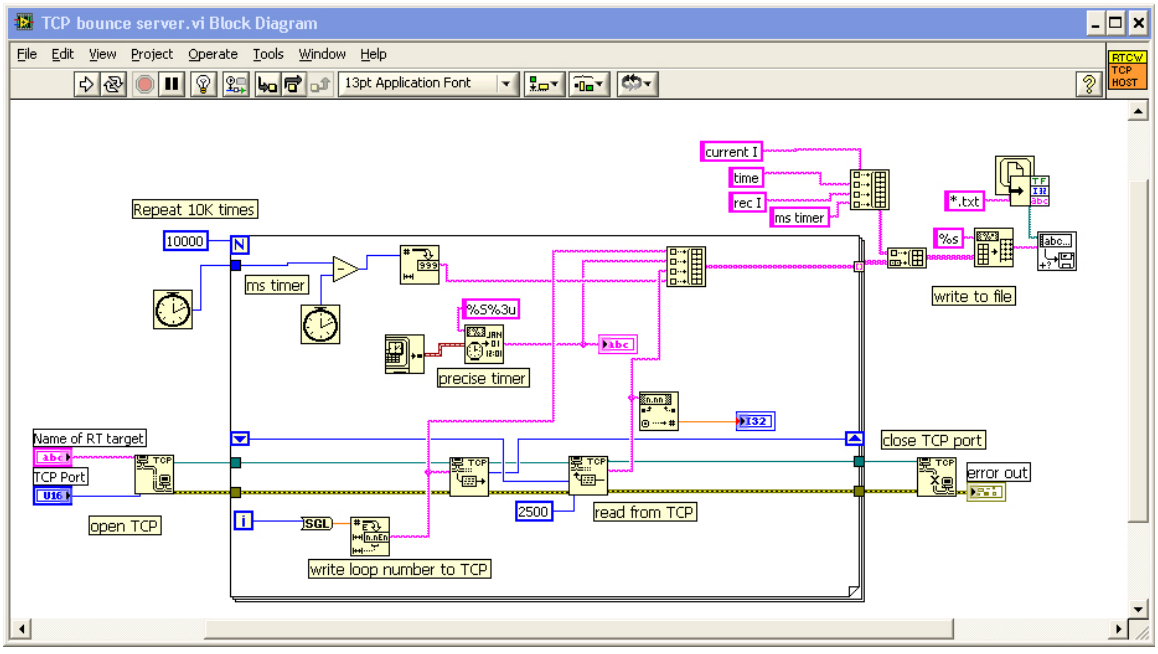

Figure B.13: Block diagram for TCP/IP communication test - "server"

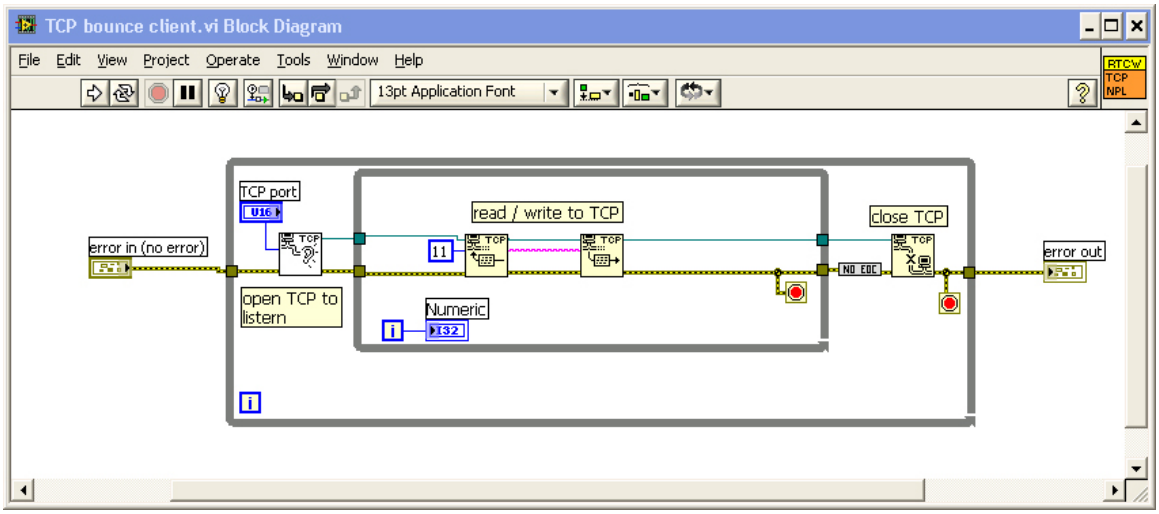

Figure B.14: Block diagram for TCP/IP communication test - "client"

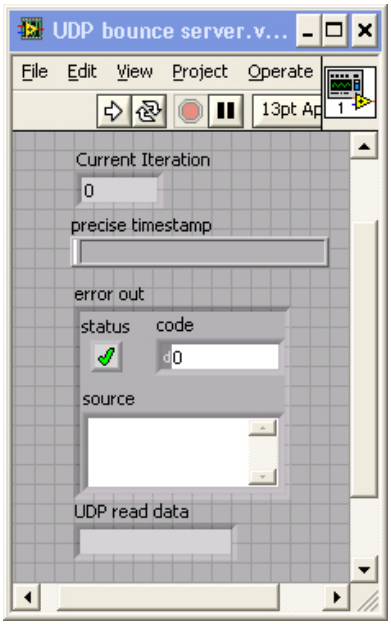

Figure B.15: Front panel of the UDP/IP communication test code

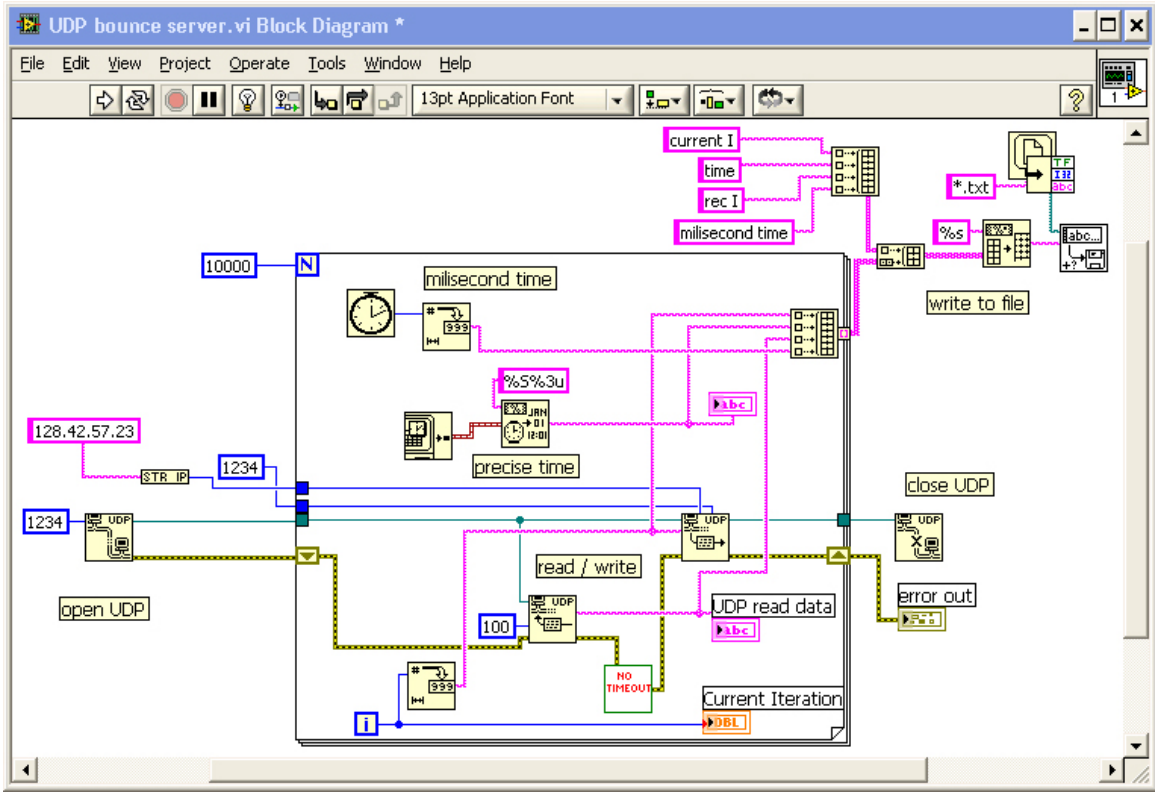

Figure B.16: Block diagram for UDP/IP communication test - "server"

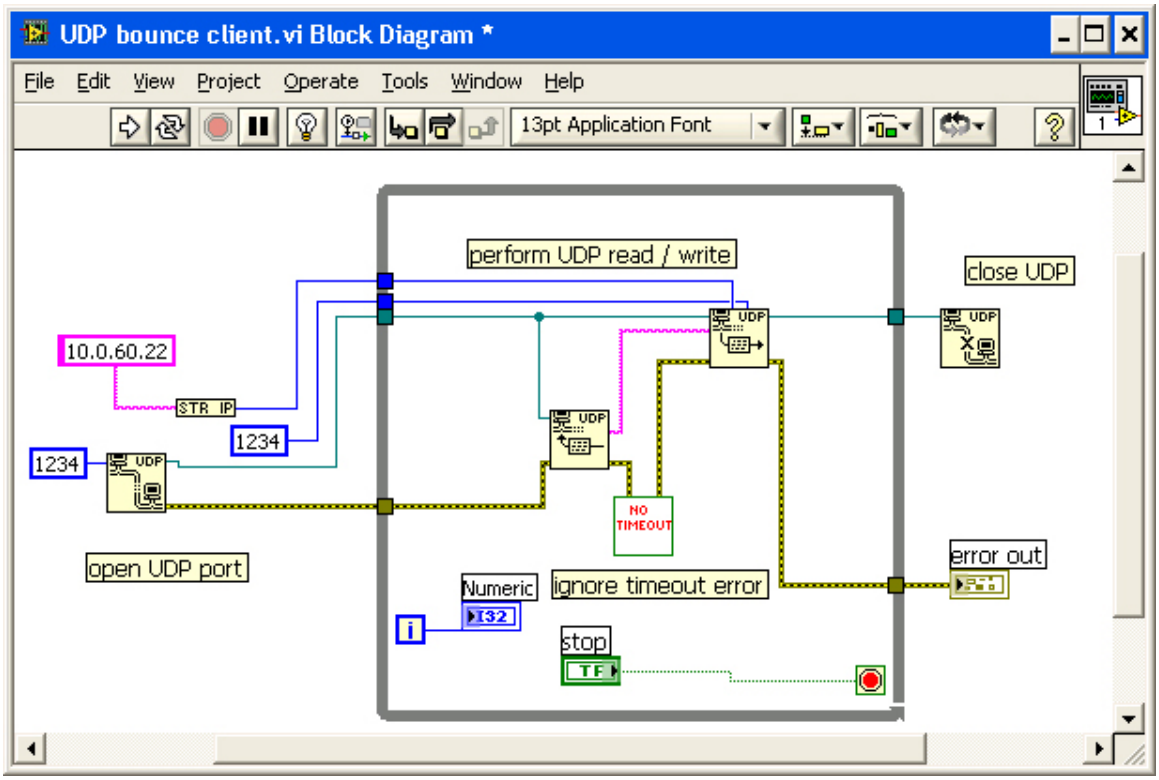

Figure B.17: Block diagram for UDP/IP communication test - "client"

APPENDIX C

HUMAN FACTORS MATERIALS

C.1 IRB Material

Georgia Institute of Technology

Office of Research Compliance
Atlanta, Georgia 30332-0420 U.S.A.
PHONE 404•894•6944
FAX 404•385•2081
irb@gatech.edu
iacuc@gatech.edu

Protocol Number: H07033
Funding Agency: N/A
Review Type: Expedited, Category 7
Title: Human Evaluation of Internet-Based Passive Bilateral Teleoperation
Number of Subjects: 25
Number Enrolled: N/A

March 20, 2007

Wayne Booke
School of Mechanical Engineering
0405

Dear Dr. Booke:

The Institutional Review Board (IRB) has carefully considered your proposal referenced above. The proposed procedures afford reasonable protection to the human subjects involved and therefore you are granted approval.

Research qualified for expedited review in accordance with federal expedited category # 7.

Inclusion of minors in this study is acceptable in accordance with 45 CFR 46.404.

Per 45 CFR 46.116 (d) this study qualifies for a waiver of parental permission.

Your approval and stamped consent form are effective **March 19, 2007** with an expiration date of **March 18, 2008.** Thereafter, continued approval is contingent upon submission of a continuation form/progress report that must be reviewed and approved prior to the expiration date.

Approval is contingent upon your agreement to obtain informed consent from your subjects, to abide by the Georgia Institute of Technology Assurance of Compliance for the Protection of Human Subjects, and to keep appropriate records concerning your subjects.

You are required to submit to the IRB for review any changes in procedures involving human subjects prior to the implementation. Any serious reactions or unanticipated problems must be reported immediately to the IRB.

Please note that all correspondence or e-mail you send to the IRB regarding this topic must include the full title and Protocol Number (shown in the upper right corner of this letter).

If you have any questions concerning this approval or regulations governing human subject activities, please feel free to contact me at 404/894-6942.

Sincerely,

Melanie Clark, CIP
IRB Administrator

Enclosure
cc: Dr. Phil Sparling, IRB Chair

Georgia Institute of Technology
Project Title: Human Evaluation of Internet-Based Passive Bilateral Teleoperation
Investigators: Professor Wayne J. Book, Ben Black
Consent title: Adult Consent Form for Experiments Pertaining to the Sense of Touch v1.0 (2/1/07)

Research Consent Form

You are being asked to be a volunteer in a research study in remote-control with a user interface pertaining to the sense of touch.

Purpose:

This research intends to help engineers develop joystick devices to be used as remote control a robot from a distance. In particular, the devices will provide force sensation from the remote robot, allowing a user to feel what the robot feels. The joystick sends an instruction for the robot to move, and the robot returns force information to the joystick, effectively informing the user what the robot feels in the environment. This setup provides the user with enhanced awareness of the robot environment.

The purpose of this specific experiment is to evaluate two types of joystick-like controllers and to understand the differences between the feedback that they provide. A sample size of 25 individuals will be used in this experiment. Eligible individuals consist of right-handed college students with a healthy sense of touch not affected by disease and/or physical handicap or any known hand, wrist or shoulder injuries that would impede motion.

Procedures:

First you will be asked to fill out a short questionnaire. Then you will be introduced to the machines, a Phantom brand force generating device and a similar device named MR PTER, built for research purposes. These devices are essentially joysticks, but with motors or brakes to provide force sensation to the user. Throughout the experiment, the subject will use the Phantom or MR PTER as the joystick to control a robot in an unseen location. You will be asked to complete up to four tasks using the joystick to control the remote robot.

The first task is shape identification. You will be asked to use each of the computer input devices (the Phantom and MR PTER) as a remote control for a second robot in a different, unseen location. There will be no visual display of the position of the remote robot or joystick-like device. A two-dimensional shape will be placed in front of the remote

robot, and you will be asked to identify the shape based only on the force information provided by the joystick.

The second task is maze navigation. A maze will be place in contact with the remote robot. You will attempt to navigate the maze to the destination based on force information provided by the joystick. You will not be able to see the remote robot, but you will be able to see the robot position on a computer display.

The third task is a simple point to point motion. A computer monitor will show the position of the joystick as well as the position of the remote robot. You will be asked to move the remote robot from point A to point B while avoiding an obstacle.

The fourth task is designed to represent a more practical task. You will be asked to move the remote robot in a way that mimics use of a tool.

The amount of time expected for this study per subject is 90 to 120 minutes with built-in breaks after each of the tasks.

Risks/Discomforts

The risks involved are no greater than those involved in daily activities such as pushing a book with a hand. Safety is insured in this experiment. The Phantom is a commercially available off the shelf computer input device used extensively in industry and can only exert about 2 lbs of force as stated by the Phantom manufacturer Sensable. An average user can easily overpower it. Additionally, MR PTER has been designed in a way such that it cannot move the subject on its own due to the passive components used in its construction. Again, it is no more dangerous than sliding a book across a table.

Benefits

There is no direct benefit to you as a participant; however, we hope the results of this study will allow us to improve upon remote control applications as well as computer interface devices in the future.

Compensation to You

A US$10.00 gift card for Barnes and Noble bookstore will be given to the subject immediately after he or she has attempted to complete the tasks assigned.

Confidentiality

The following procedures will be followed to keep your personal information confidential in this study: The data that is collected about you will be kept private to the extent allowed by law. To protect your privacy, your records will be kept under a code number rather than by name. Your records will be kept in locked files and only study staff will be allowed to look at them. Your name and any other fact that might point to you will not appear when results of this study are presented or published.

To make sure that this research is being carried out in the proper way, the Georgia Institute of Technology IRB may review study records. The Office of Human Research Protections may also look at study records.

Costs to You

This study does not incur any financial cost to you the subject.

In Case of Injury/Harm

If you are injured as a result of being in this study, please contact Professor Wayne Book at wayne.book@me.gatech.edu or (404)894.3247. Neither the Principal Investigator nor Georgia Institute of Technology has made provision for payment of costs associated with any injury resulting form participation in this study.

Subject Rights

- Your participation in this study is voluntary. You do not have to be in this study if you don't want to be.
- You have the right to change your mind and leave the study at any time without giving any reason, and without penalty.
- Any new information that may make you change your mind about being in this study will be given to you.
- You will be given a copy of this consent form to keep.
- You do not waive any of your legal rights by signing this consent form.

Questions about the Study or Your Rights as a Research Subject

- If you have any questions about the study, you may contact Professor Wayne Book at wayne.book@me.gatech.edu or (404)894.3247.
- If you have any questions about your rights as a research subject, you may contact Ms. Melanie Clark, Georgia Institute of Technology at (404)894-6942.

If you sign below, it means that you have read (or have had read to you) the information given in this consent form, and you would like to be a volunteer in this study.

_____

Subject Name

Subject Signature	Date
Signature of Person Obtaining Consent	Date

Georgia Institute of Technology
Project Title: Human Evaluation of Internet-Based Passive Bilateral Teleoperation
Investigators: Ben Black, Professor Wayne J. Book

Questionnaire

Research Subject Number: _____

MALE or FEMALE ? (circle one)

Do you write RIGHT or LEFT handed? (circle one)

If asked to kick a soccer ball, do you use your RIGHT or LEFT foot? (circle one)

If asked to play softball or baseball, do you bat RIGHT or LEFT handed? (circle one)

Over the past month, approximately how many hours per week do you spend using a computer for work or entertainment? _____

Over the past month, approximately how many hours per week do you spend playing video games (PC, PS2, XBOX, etc.)? _____

Have you previously participated in remote-control or haptic research experiments?
YES / NO (circle one)

Have you ever been involved in conducting your own haptic research?
YES / NO (circle one)

Georgia Institute of Technology
Project Title: Evaluation of Internet-Based Bilateral Teleoperation
Investigators: Ben Black, Professor Wayne J. Book (PI)

Question Sheet for Contour Surface Identification

For each trial, please pick the contour or shape that you feel from the list below. Please put the corresponding letter next to each trial number.

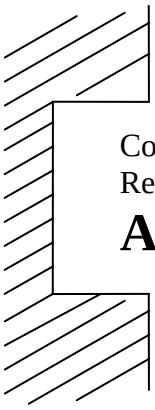

Concave
Rectangle
A

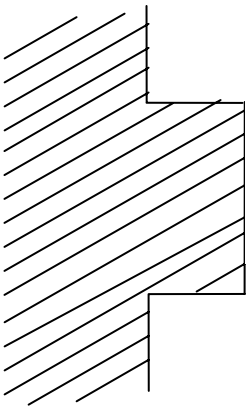

Convex
Rectangle
E

Concave
Triangle
B

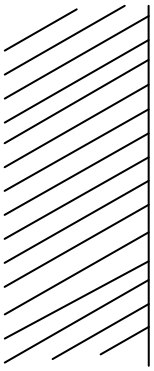

Flat
Surface
D

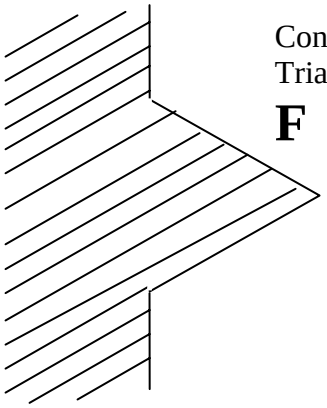

Convex
Triangle
F

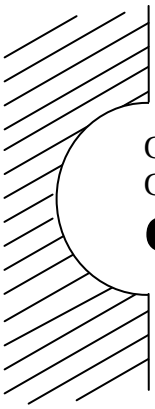

Concave
Circle
C

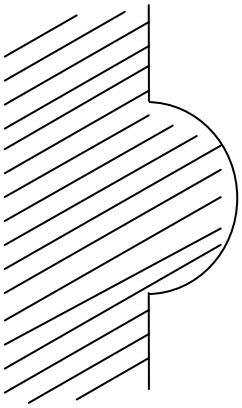

Convex
Circle
G

Please pick the contour / shape from the above chart that you feel. Write the corresponding letter in the blank next to the trial number.

1. _____
2. _____
3. _____
4. _____
5. _____
6. _____
7. _____
8. _____
9. _____
10. _____
11. _____
12. _____
13. _____
14. _____
15. _____
16. _____
17. _____
18. _____
19. _____
20. _____
21. _____
22. _____
23. _____
24. _____
25. _____
26. _____
27. _____
28. _____
29. _____
30. _____
31. _____
32. _____
33. _____
34. _____
35. _____
36. _____
37. _____
38. _____
39. _____
40. _____

Rating Sheet

Subject ID: _____ Task ID: _____

Rate the task you just performed on the following scales.

EXAMPLE:

Deliciousness of Donut

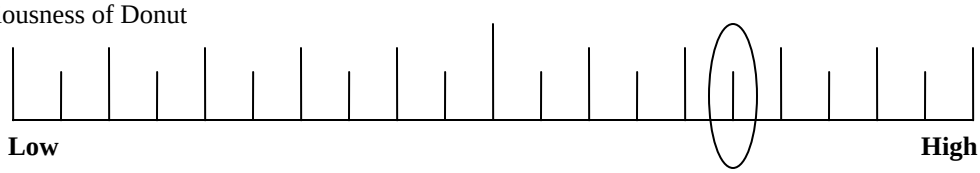

Low **High**

Mental Demand

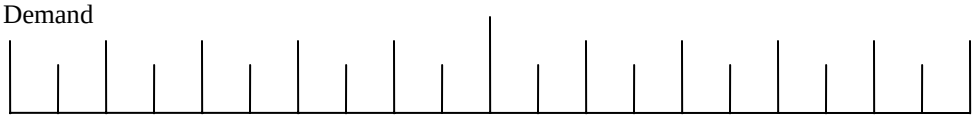

Low **High**

Physical Demand

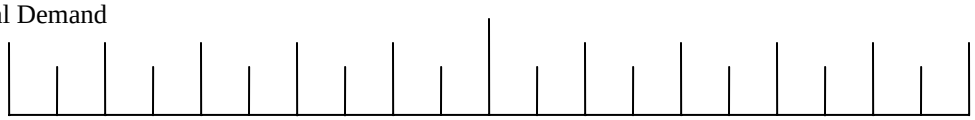

Low **High**

Temporal Demand

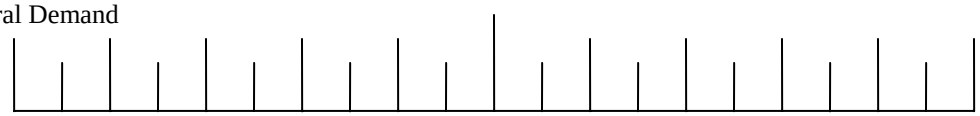

Low **High**

Effort

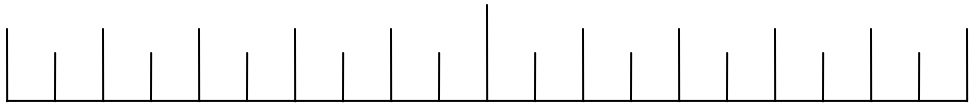

Low **High**

Performance

Good **Poor**

Frustration

Low **High**

Smoothness

Low **High**

Rating Scale Definitions

Title	Endpoints	Descriptions
MENTAL DEMAND	*Low/High*	How much mental and perceptual activity was required (e.g., thinking, deciding, calculating, remembering, looking, searching, etc.)? Was the task easy or demanding, simple or complex, exacting or forgiving?
PHYSICAL DEMAND	*Low/High*	How much physical activity was required (e.g., pushing, pulling, turning, controlling, activating, etc.)? Was the task easy or demanding, slow or brisk, slack or strenuous, restful or laborious?
TEMPORAL DEMAND	*Low/High*	How much time pressure did you feel due to the rate or pace at which the task or task elements occurred? Was the pace slow and leisurely or rapid and frantic?
EFFORT	*Low/High*	How hard did you have to work (mentally and physically) to accomplish your level of performance?
PERFORMANCE	*Good/Poor*	How successful do you think you were in accomplishing the goals of the task set by the experimenter? How satisfied were you with your performance in accomplishing these goals?
FRUSTRATION LEVEL	*Low/High*	How insecure, discouraged, irritated, stressed and annoyed versus secure, gratified, content, relaxed and complacent did you feel during the task?
SMOOTHNESS	*Low/High*	How smooth was the motion of the device? Did it glide freely or was the motion rough and jerky?

Effort **or** **Performance**		**Temporal Demand** **or** **Frustration**
Temporal Demand **or** **Effort**		**Physical Demand** **or** **Frustration**
Performance **or** **Frustration**		**Physical Demand** **or** **Temporal Demand**
Physical Demand **or** **Performance**		**Temporal Demand** **or** **Mental Demand**

Frustration **or** **Effort**		**Performance** **or** **Mental Demand**
Performance **or** **Temporal Demand**		**Mental Demand** **or** **Effort**
Mental Demand **or** **Physical Demand**		**Effort** **or** **Physical Demand**
Frustration **or** **Mental Demand**		

Table C.2: Shape identification - percent correct

	Direction	Shape
Phantom	96.40%	82.43%
Passive - coupling	82.26%	49.19%
Passive - closed loop	84.44%	50.37%
Passive - dynamic compensating	83.46%	47.24%

Table C.3: Shape identification - distribution of incorrect answers (%)

	- Rect	- Tri	- Circle	V. Wall	+ Rect	+ Tri	+ Circle
- Rect		31.03	37.93	6.90	6.90	17.24	
- Triangle	26.92		38.46	15.38	7.68	3.85	7.69
- Circle	35.14	51.35		2.07			10.81
Wall	16.67	25.00	16.67			25.00	16.67
+ Rect	5.56	5.56	11.11	5.56		33.33	38.89
+ Triangle	3.13	3.13	3.13	21.88	6.25		62.50
+ Circle	5.26	7.89	2.63	5.26	42.11	36.84	

C.2 Complete Results

Table C.4: Obstacle avoidance - normalized time

	$\frac{TrialTime}{PHANTOMTime}$	Standard Dev.
Phantom	1	0.331
Passive - coupling	1.254	0.330
Passive - closed loop	1.163	0.306
Passive - dynamic compensating	1.122	0.302
Passive - no control	1.199	0.421

Table C.5: Guided motion - normalized time

	$\frac{TrialTime}{PHANTOMTime}$	Standard Dev.
Phantom	1	0.235
Passive - coupling	1.390	0.242
Passive - closed loop	1.310	0.229
Passive - dynamic compensating	1.188	0.173
Passive - no control	1.178	0.231

Table C.6: NASA-TLX Sub-Category Workload for MR PTER

	Average Workload	Standard Dev.
Mental Demand	59.76	26.20
Physical Demand	38.10	28.92
Temporal Demand	60.48	21.38
Performance	57.62	20.35
Effort	56.19	25.29
Frustration	59.05	27.19
Weighted Average	63.05	17.00

Table C.7: NASA-TLX Sub-Category Workload for the PHANTOM

	Average Workload	Standard Dev.
Mental Demand	30.79	19.38
Physical Demand	23.68	14.89
Temporal Demand	28.42	18.49
Performance	24.74	13.59
Effort	32.11	16.56
Frustration	17.89	15.21
Weighted Average	30.72	13.52

REFERENCES

[1] Allin, S., Matsuoka, Y., and Klatzky, R., "Measuring just noticeable differences for haptic force feedback: Implications for rehabilitation," in *Proceedings of HAPTICS 2002*, (Orlando, Florida), March 2002.

[2] Anderson, J., *The Architecture of Cognition*. Mahwah, NJ: Lawrence Erlbaum, 1983.

[3] Anderson, R. and Spong, M., "Bilateral control of teleoperators with time delay," in *Transaction on Automatic Control*, pp. 494–501, May 1989.

[4] Bejczy, A., "Sensors, controls, and man-machine interface for advanced teleoperation," *Science*, vol. 208, pp. 1327–1335, June 1980.

[5] Black, B. and Book, W., "On-off control of a passive haptic master during teleoperation," in *ENACTIVE 2005*, (Genoa, Italy), November 2005.

[6] Black, B. and Book, W., "Passive haptic control during teleoperation," in *Proceedings of SYROCO 2006*, (Bologna, Italy), September 2006.

[7] Blnivento, C., Eusebi, A., Melchiorri, C., Montanari, M., and Vassura, G., "Wireman: A portable wire manipulator for touch-rendering of bas-relief virtual surfaces," in *ICRA '97 Proceedings*, (Monterey, Ca), pp. 13–18, July 1997.

[8] Boschetti, G., Rosati, G., and Rossi, A., "A haptic system for robotic assisted spine surgery," in *Proceedings of the IEEE Confernce on Control Applications*, (Toronto, Canada), pp. 7–12, August 2005.

[9] Boukhnifer, M., Ferreira, A., and Fontaine, J., "Scaled teleoperation controller design for micromanipulation over internet," in *Prodeedings of 2004 IEEE ICRA*, (New Orleans, La), pp. 4577–4583, April 2004.

[10] Breese, D. and Gordaninejad, F., "Semi-active field-controllable magneto-rheological fluid dampers for mountain bikes," in *Smart Structures and Materials 2002*, pp. 283–293, 2000.

[11] Brodie, E. and Ross, H., "Sensorimotor mechanisms in weight discrimination," *Percept Psychophys*, vol. 36, pp. 477–481, 1984.

[12] Byrne, M., "Act-r/pm and menu selection: applying cognitive architecture to hci," *Journal of Human-Computer Studies*, vol. 55, pp. 41–84, 2001.

[13] Card, S., Morgan, T., and Newell, A., *The Psychology of the Human-Computer Interaction*. Hillsdale, NJ: Erlbaum, 1983.

[14] Champion, G., Gosline, A., and Hayward, V., "Initial results using eddy current brakes as fast turn-on, programmable physical dampers for haptic rendering," in *Proceedings of Symposium on Haptic Interfaces for Virtual Environment and Teleoperator Systems 2006*, (Alexandria, VA), pp. 73–74, March 2006.

[15] Ching, H. and Book, W., "Internet-based bilateral teleoperation based on wave variable with semi-adaptive predictor and direct drift control," in *Proceedings of IMECE 2005*, (Orlando, Florida), November 2005.

[16] Cho, C., Song, J., and Kim, M., "Design and control of a planar haptic device with passive actuators based on passive force manipulability ellipsoid (fme) analysis," *Journal of Robotic Systems*, vol. 22, no. 9, pp. 475–486, 2005.

[17] Cho, C., Song, J.-B., and Kim, M., "Energy-based control of a haptic device using brakes," *IEEE Trans. Syst. Man Cybern. B, Cybern*, vol. 37, pp. 341–349, Apr 2007.

[18] Clanton, S., Wang, D., Matsuoka, Y., Shelton, D., and Stetten, G., "A novel machine interface for scaled telesurgery," in *Proceedings of SPIE; Medical Imaging 2004*, (Bellingham, WA), pp. 697–704, February 2004.

[19] Davis, H. and Book, W., "Torque control of a redundently actuated passive manipulator," in *Proceedings of the American Control Conference*, (Albuquerque, Nm), pp. 959–963, June 1997.

[20] Dyke, S., *Acceleration Feedback Control Strategies for Active and Semi-Active Control Systems*. Ph.d. thesis, The University of Notre Dame, Department of Civil Engineering and Geological Sciences, 1996.

[21] Dyke, S., Spencer, B., Sain, M., and Carlson, J., "An experimental study of mr dampers for seismic protection," *Smart Materials and Structures*, 1998.

[22] Elhajj, I., Fung, W., and Liu, Y., "Real-time bilateral control of internet-based teleoperation," in *Proceedings of the 3rd World Congress on Intelligent Control and Automation*, (Hefei, China), pp. 3761–3766, June 2000.

[23] Elhajj, I., Xi, N., Fung, W., Liu, Y., Li, W., Kaga, T., and Fukuda, T., "Haptic information in internet-based teleoperation," *Transactions on Mechatronics*, vol. 6, pp. 295–304, September 2001.

[24] Ellis, R., Ismaeil, O., and Lipsett, M., "Design and evaluation of a high-performance haptic interface," *Robotica*, vol. 4, pp. 321–327, 1996.

[25] Fitts, P., "The information capacity of the human motor system in controlling the amplitude of movement," *Journal of Psychology*, vol. 47, pp. 381–391, June 1954.

[26] Fitts, P. and Seeger, C., "Compatibility: Spatial characteristics of stimulus and response codes," *Journal of Experimental Psychology*, vol. 26, pp. 199–210, 1953.

[27] Furusho, J., Sakaguchi, M., Takesue, N., and Koyanagi, K., "Development of er brake and its application to passive force display," *Journal of Intelligent Material Systems and Structures*, vol. 13, pp. 425–429, July/August 2002.

[28] Gandevia, S. and Kilbreath, S., "Accuracy of weight estimation for weights lifted by proximal and distal muscles of the human upper limb," *Journal of Physiology*, vol. 423, pp. 299–310, 1990.

[29] Gao, D., *Control Limitation Analysis for Dissipative Passive Haptic Interfaces*. Ph.d. thesis, Georgia Institute of Technology, Department of Mechanical Engineering, 2005.

[30] Gao, D. and Book, W., "Principles of steerability for dissipative passive haptic interfaces," in *Proceedings of the ASME-IMECE*, (Orlando, Florida), November 2005.

[31] Goertz, R., "Mechanical master-slave manipulator," *Nucleonics*, vol. 12, November 1954.

[32] Goertz, R. and Thompson, W., "Electronically controlled manipulator," *Nucleonics*, vol. 12, pp. 46–47, Nov 1954.

[33] Gomes, M. and Book, W., "Control approaches for a dissipative passive trajectory enhancing robot," in *International Conference on Advanced Intelligent Mechatronics*, p. 92, April 1997.

[34] Grad, P., "Against the flow," *Engineering and Technology*, pp. 34–37, December 2006.

[35] Hannaford, B. and Ryu, J., "Time domain passivity control of haptic interfaces," in *Proceedings of the 2001 IEEE ICRA*, (Seoul, Korea), pp. 1863–1869, May 2001.

[36] Hayward, V., Astley, O., Crus-Hernandez, M., Grant, D., and Robles-De-La-Torre, G., "Hatpic interfaces and devices," *Emerald Insight*, vol. 24, no. 1, pp. 16–29, 2004.

[37] Hogan, N., "Controlling impedance at the man/machine interface," in *Proc. Intl. Conf. Robotics and Automation*, (Scottsdale, AZ), pp. 1626–1631, May 1989.

[38] Howell, L. and Tripp, A., "Heavy-duty hydraulic manipulator," *Nucleonics*, vol. 12, pp. 48–49, Nov 1954.

[39] Hurmuzulu, Y., Ephanov, A., and Stoianovici, D., "Effect of pneumatically driven haptic interface on perceptional capabilities of human operators," *Presence*, vol. 7, pp. 290–307, June 1998.

[40] Jansen, L. and Dyke, S., "Semi-active control strategies for mr dampers: A comparative study," *ASCE Journal of Engineering Mechanics*, vol. 126, no. 8, pp. 795–803, 2000.

[41] Jones, L., "Perception of force and weight: Theory and research," *Psychological Bulletin*, vol. 100, no. 1, pp. 19–42, 1986.

[42] Jones, L., "Matching forces: constant errors and differential thresholds," *Perception*, vol. 18, no. 5, pp. 681–687, 1989.

[43] Kanaoka, K. and Yoshikawa, T., "Passivity monitor and software limiter which guarantee asymptotic stability of robot control systems," in *Proceedings of IEEE-ICRA 2003*, (Taipei, Taiwan), pp. 4366–4373, September 2003.

[44] Kieras, D., Wood, S., and Meyer, D., "Predictive engineering models based on the epic architecture for a multimodal high-performance human-computer interaction task," *ACM Transactions on Computer-Human Interaction*, vol. 4, pp. 230–275, September 1997.

[45] Klatzky, R., Bajcsy, R., and Lederman, S., "Object exploration in one and two fingered robots," in *Proceedings of 1987 ICRA*, (Raleigh, NC), pp. 1806–1809, March 1987.

[46] Klatzky, R., Lederman, S., and Balakrishnan, J., "Task-driven extraction of object contour by human haptics," *Robotica*, vol. 9, pp. 43–51, March 1991.

[47] Kontz, M. E., *Haptic Enhancement of Operator Capabilities in Hydraulic Equipment*. MS thesis, The Georgia Institute of Technology, G.W. Woodruff School of Mechanical Engineering, 2002.

[48] Kosuge, K., Fujisawa, Y., and Fukuda, T., "Mechanical system control with man-machine-environment interaction," in *Proc. Intl. Conf. Robotics and Automation*, (Atlanta, GA), pp. 143–148, May 1993.

[49] Kosugu, K. and Y. Fujisawa, T. F., "Control of mechanical systems with man-machine interactions," in *International Conference on Intelligent Robots and Systems*, (Raleigh, NC), na 1992.

[50] Krebs, H., Hogan, N., Aisen, M., and Volpe, B., "Robot-aided neurorehabilitation," *Transaction on Rehabilitation Engineering*, vol. 6, pp. 75–87, March 1998.

[51] Kuchenbecker, K. J., Fiene, J., and Niemeyer, G., "Improving contact realsim through event-based haptic feedback," *IEEE Trans. Visualization and Computer Graphics*, vol. 12, pp. 219–229, Mar 2006.

[52] Lee, D. and Li, P., "Passive control of bilateral teleoperated manipulators: Robust control and experiments," in *Proceedings of the American Control Conference*, (Arlington, Va), pp. 4612–4618, June 2001.

[53] Lee, D. and Li, P., "Passive coordination control of nonlinear bilateral teleoperated manipulators," in *Proceedings of the 2002 IEEE International Conference on Robotics and Automation*, (Washington, DC), pp. 3278–3283, May 2002.

[54] Lee, D. and Li, P., "Toward robust passivity: A passive control implementation structure for mechanical teleoperators," in *Proceedings of the 11th Symposium on Haptic Interfaces for Virtual Environments and Teleoperator Systems*, March 2003.

[55] Li, P., "Passive control of bilateral teleoperated manipulators," in *Proceedings of the American Control Conference*, (Philadelphia, Penn), pp. 3838–3842, June 1998.

[56] Lockhart, R. and Murdock, B., "Memory and the theory of signal detection," *Psychological Bulletin*, vol. 74, no. 2, pp. 100–109, 1970.

[57] Loomis, J. and Lederman, S., "Tactual perception," *Handbook of Human Perception*, vol. 2, pp. 1–41, 1986.

[58] Love, L. J., *Adaptive Impedance Control*. Ph.d. thesis, The Georgia Institute of Technology, G.W. Woodruff School of Mechanical Engineering, 1995.

[59] Mahvash, M. and Hayward, V., "Passivity-based high-fidelity haptic rendering of contact," in *Proceedings of 2003 ICRA*, (Taipei, Taiwan), pp. 3722–3728, September 2003.

[60] Matsuoka, Y. and Townsend, W., "Design of life-sized haptic environments," *Experimental Robotics VII*, 2001.

[61] Melchiorri, C., Montanari, M., and Vassura, G., "Control strategies for a defective, wire-based haptic interface," in *Proceedings of IROS 1997*, pp. 181–187, August 1997.

[62] Melchiorri, C. and Vassura, G., "Development and application of wire-actuated haptic interfaces," *Journal of Robotic Systems*, vol. 18, no. 12, pp. 755–768, 2001.

[63] Moore, C., *Continuously Variable Transmission for Serial Link Cobot Architectures*. MS thesis, Northwestern University, Department of Mechanical Engineering, 1997.

[64] Moore, C., Peshkin, M., and Colgate, J., "Design of a 3r cobot using continuously variable transmissions," in *Proceedings of the IEEE International Conference on Robotics and Automation*, (Detroit, MI), May 1989.

[65] Moore, C., Peshkin, M., and Colgate, J., "Cobot implementation of virtual pahts and 3-d virtual surfaces," *Transaction on Robotics and Automation*, vol. 19, pp. 347–351, April 2003.

[66] Munir, S., *Internet-Based Teleoperation*. MS thesis, Georgia Institute of Technology, Department of Mechanical Engineering, 2001.

[67] Niemeyer, G. and Slotine, J., "Stable adaptive teleoperation," *Journal of Oceanic Engineering*, vol. 16, pp. 152–162, January 1991.

[68] Niemeyer, G. and Slotine, J.-J. E., "Using wave variables for system analysis and robot control," in *Proc. Intl. Conf. Robotics and Automation*, (Albuquerque, NM), pp. 1619–1625, Apr 1997.

[69] Park, Y., Kang, H., Ewing, T., Faulring, E., Colgate, J., and Peshkin, M., "Enhanced teleoperation for d-and-d," in *Proceedings of the 2004 ICRA*, (New Orleans, La), pp. 3702–3707, April 2004.

[70] Peshkin, M. and Colgate, J., "Cobots," *Industrial Robot*, vol. 26, no. 5, pp. 335–341, 1999.

[71] Peshkin, M., Colgate, J., Wannasuphoprasit, W., and Moore, C., "Cobot architecture," *Transaction on Robotics and Automation*, vol. 17, pp. 377–390, August 2001.

[72] Quaid, A., "Bone machine: Hapic guided sculpting in the operating room," in *Proceedings of Haptics 2004*, March 2004.

[73] Reed, M., *Development of an Improved Dissipative Passive Haptic Display*. MS thesis, Georgia Institute of Technology, Department of Mechanical Engineering, 2003.

[74] Reed, M. and Book, W., "Modeling and control of an improved dissipative passive haptic display," in *Proceedings of the 2004 IEEE ICRA*, (New Orleans, La), pp. 311–318, April 2004.

[75] Ross, H. and Murray, D., *Webber: the sense of touch*. New York, NY: Academic Press, 1978.

[76] Rossi, A., Trevisani, A., and Zanotto, V., "Design and implementation of a mechatronic device for robot-assisted neurosurgery," in *Proceedings of the IEEE Confernce on Control Applications*, (Toronto, Canada), pp. 7–12, August 2005.

[77] Ryu, J., Preusche, C., Hannaford, B., and Hirzinger, G., "Time domain passivity control with reference energy following," *Transaction on Control Systems Technology*, vol. 13, pp. 737–742, September 2005.

[78] Ryu, J.-H., Kwon, D.-S., and Hannaford, B., "Stability guaranteed control: Time domain passivity approach," in *Proc. Intl. Conf. Intelligent Robots and Systems*, (Lausanna, Switzerland), pp. 2115–2121, Oct 2002.

[79] Sakaguchi, M., Furusho, J., and Takesue, N., "Passive force display using er brakes and its control experiments," in *Proceedings of the Virtual Reality 2001 Conference*, pp. 2–7, March 2001.

[80] Sgambelluri, N., Risso, R., Scilingo, E., Raugi, M., and Bicchi, A., "Free hand haptic interfaces based on magnetorheological fluids," in *Haptics 2006*, (Alexandria, VA), pp. 367–371, March 2006.

[81] Swanson, D., *Implementation of Arbitrary Path Constraints Using Dissipative Passive Haptic Displays*. Ph.d. thesis, Georgia Institute of Technology, Department of Mechanical Engineering, 2003.

[82] Tan, H., Barbagli, F., Salisbury, K., Ho, C., and Spence, C., "Force direction discrimination is not influenced by reference force direction," *Haptics-e*, vol. 4, February 2006.

[83] Tognetti, L. J., *Improved Design and Performance of Haptic Two-Port Networks through Force Feedback and Passive Actuators*. Ph.d. thesis, The Georgia Institute of Technology, G.W. Woodruff School of Mechanical Engineering, 2005.

[84] Wannasuphoprasit, W. and Chanphat, S., "A novel fluid haptic interface," in *IEEE ICIT*, (Bankok, Thailand), pp. 359–364, December 2002.

[85] Wannasuphorprasit, W., Gillespie, R., Colgate, J., and Peshkin, M., "Cobot control," in *Proceedings of the 1997 IEEE ICRA*, (Albuquerque, Nm), pp. 3571–3576, April 1997.

[86] Weghe, M., Dellon, B., Kelly, S., Juchniewicz, R., and Matsuoka, Y., "Demonstration of a large dissipative haptic environment," in *Proceedings of Symposium on Haptic Interfaces for Virtual Environment and Teleoperator Systems 2006*, (Alexandria, VA), pp. 329–330, March 2006.

[87] Yao, H., Hayward, V., and Ellis, R., "A tactile magnification instrument for minimally invasive surgery," *MICCAI 2004, LNCS*, vol. 3217, pp. 89–96, 2004.

[88] Zhu, H. and Book, W., "Practical structure design and control for digital clay," in *Proceedings of the ASME Dynamics and Control Division*, (Anaheim, California), pp. 1051–1058, November 2004.

VITA

Born and raised in Dallas, Texas, Benjamin A. Black graduated valedictorian of Jesuit College Preparatory School of Dallas. The High School cross-country athlete continued his academic and running career at Rice University in Houston, Texas. After four years at Rice, Ben finished his Bachelors of Science in Mechanical Engineering as well as a Masters of Mechanical Engineering (MME) focused in biomechanics with a minor in system dynamics and controls. While technically not a research-based degree, the MME allowed Ben the opportunity to pursue various small research projects under the guidance of Professor Marcia O'Malley in the Mehcatronics and Haptic Interfaces (MAHI) Lab. The projects including work with NASA's Robonaut and a multi-semester project with Professor Aladin Boriek of Baylor College of Medicine investigating the material properties as well as the kinematics and dynamics of the canine diaphragm during breathing. The joint research at Baylor College of Medicine led to the presentation of multiple conference posters as well as a publication in the *Journal of Applied Physiology*.

In the fall of 2003 Ben matriculated at Georgia Institute of Technology and joined the Intelligent Machine Dynamics Laboratory working with Professor Wayne Book who had a position open to pursue research using haptic devices. Ben promptly applied for and was awarded a National Instruments Academic Grant for hardware, software and support that continued through his 4 years of research.

In addition to his research and classroom duties at Georgia Tech, Ben participated in multiple teaching opportunities including the Student Teacher Enhancement Partnership (STEP) program as well as the development of a robotics program at a local

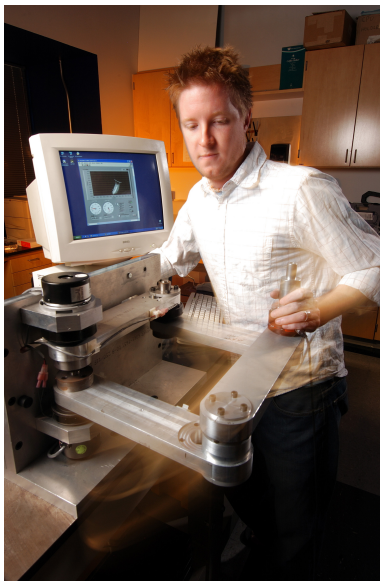

Figure 3.1: Photograph of author and MR PTER

middle school. Designed to partner Georgia Tech graduate and undergraduate students with local Atlanta High Schools, the STEP program sends students to help teach in science, math and technology classrooms. Working at Tech High (no official relation to Georgia Tech), Ben taught in an Algebra classroom and started an after-school robotics club that competed in the FIRST Vex Challenge. Also as part of the STEP program, Ben and another STEP Fellow designed, constructed and hosted an entry-level robotics competition that brought 8 teams from local high school to Georgia Tech to play a king-of-the-mountain game. In addition to teaching opportunities provided by being a STEP Fellow, Ben started and developed an after-school robotics program at the Trinity School, working with second through fifth grade students. Starting with only 5 students, Ben grew the program in one year to two classes of 15 students with another 15 signed up on the waiting list. Ben also coached Trinity's rookie First LEGO League team and helped them to a finish of roughly thirtieth in the state of Georgia.

After his time at Georgia Tech, Ben will be taking a job at National Instruments in the small Systems Engineering Group.